
THE UNIVERSITY OF MANCHESTER
**School of Mechanical, Aerospace and Civil Engineering**

UNIVERSITA' DEGLI STUDI DI PADOVA
**Dipartimento di Ingegneria Industriale DII**
Corso di Laurea Magistrale in Ingegneria Aerospaziale

# Aeroelastic behaviour of the inverted jet spoilers

*Relatori: Prof. Ugo Galvanetto*
*Prof. Antonio Filippone*

*Studente: Francesco Scabbia*
*Matricola: 1179116*

Anno Accademico 2018/2019

# Abstract

This work reviews special types of spoilers for aircraft attitude control and focuses on the aeroelastic behaviour of a new design concept conceived by Filippone, the inverted jet spoiler. Aerodynamic and structural analyses highlighted not only the low possibility of damaging or fracturing the material, but also the high probability of aeroelastic vibration occurrence because of the device large deformation due to the low stiffness of the spoiler panel. Free-stream velocity increases the loads applied to the spoiler, while the most critical aerodynamic configuration for the structure involves an angle of attack of 4°. In order to reduce spoiler deformation, stiffer material can be employed since the device displacements stand in inverse proportion to the modulus of elasticity. On the other hand, it was demonstrated that spoiler stiffness increases by shortening the chord-wise length, thickening the panel and lengthening the span-wise dimension.

# Index

# Chapter 1
# Introduction

The flight procedures have become so common that one tends to forget how complex it is to maintain the aircraft equilibrium and stability through the control system. Structure shape and weight are only two of the variables that affect the attitude of a flying vehicle. The propulsion system provides the adaptable thrust in order to both accomplish the take off and sustain the cruise flight speed. By doing this, however, engines also create a force inconstant field which perturbates the rotational motion of the vehicle. Another influencing factor is the atmospheric environment which surrounds the aircraft.

In a generic aerospace vehicle, propulsion system and airframe are designed to carry the payload and to meet the mission requirements, as illustrated in Figure 1.1. Nevertheless, the control system is the only one that can operate during the mission changing the aerodynamic geometry exposed to the flow. In this sense, the group of movable devices which constitutes the flight control system, modifies the flight dynamics in order to reach the desired performances achieving the stability of the vehicle in every instant.

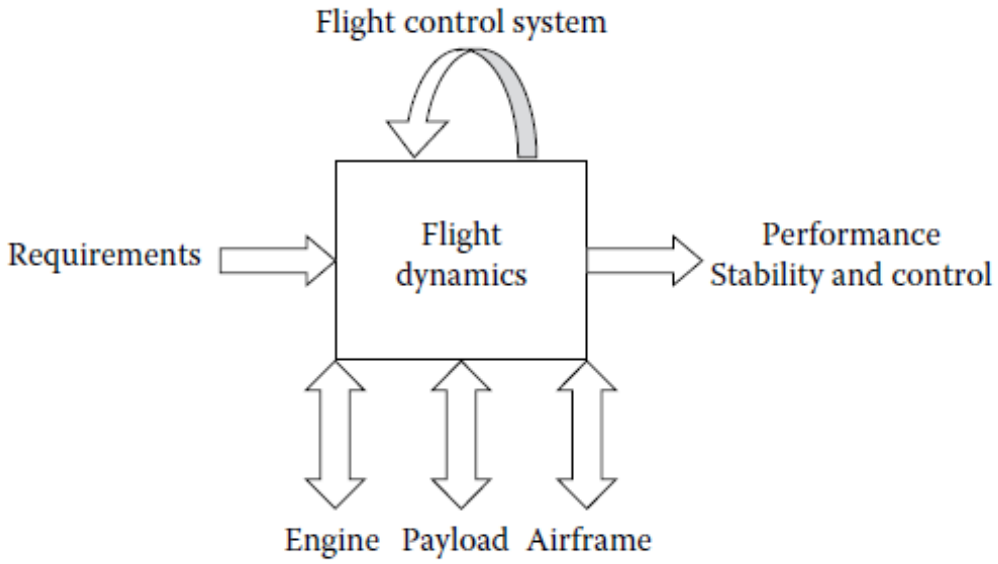


**Figure 1.1.** *The flight dynamics scheme for a generic aerospace vehicle [1]. The control system plays a fundamental role because it rules the flight dynamics and allows to reach the desired performances and stability.*

## 1.1 Definition of aircraft motion and attitude

Conventionally two systems of reference are used to determine the aircraft attitude: the body-fixed axis system $X^BY^BZ^B$ and the Earth-fixed axis system $X^EY^EZ^E$. The former, as its name suggests, follows the motion (translations and rotations) of the aircraft body and its origin $O^B$ coincides with the centre of mass of the vehicle. In a commercial transport aircraft, the shift of the centre of mass due to the fuel mass ejection can be preliminary neglected, so that the origin of the body-fixed axis system is considered motionless. $X^B$ axis is chosen to point toward the aircraft nose, $Z^B$ axis is directed downwards and perpendicular to $X^B$ such that the $X^BZ^B$ plane defines the plane of symmetry of the aircraft and $Y^B$ axis completes the triad to obtain a right-handed orthogonal axis system, as shown in Figure 1.2*a*. The latter system of reference is inertial and fixed with respect to the non-rotating Earth. Its origin $O^E$ is located on the surface of the sphere, $X^EY^E$ plane is locally tangent to the surface and $Z^E$ axis is taken to point toward the centre of the Earth, as represented in Figure 1.2*b*.

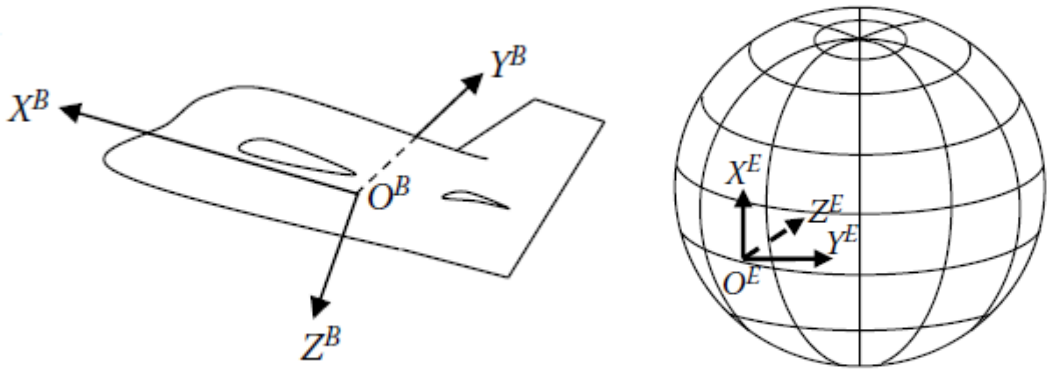


**Figure 1.2.** *(a) Body-fixed axis system and (b) Earth-fixed axis system [1].*

Furthermore, the aircraft is considered a rigid body neglecting the structural deformations due to bending and torsion loads. Due to this hypothesis, airplane position and orientation are completely determined by six degrees of freedom. The aircraft motion and attitude are described by the body-fixed coordinate system translations and rotations in the inertial Earth-fixed system. Figure 1.3 depicts the vector **R**, called the position vector, which links the origins of the body-fixed and Earth-fixed systems and represents the position of the aircraft centre of mass with respect to the inertial system of reference. The temporal variation of **R**

is described by the velocity vector **V**, which characterizes the speed of the centre of mass. **V** can be decomposed in three components along the body-fixed axes:

$$\mathbf{V} = \begin{Bmatrix} u \\ v \\ w \end{Bmatrix}^B . \tag{1.1}$$

In Figure 1.3 the angular velocity **ω** is represented as well and the decomposition along the body-fixed axes conduces to the following formula:

$$\boldsymbol{\omega} = \begin{Bmatrix} p \\ q \\ r \end{Bmatrix}^B . \tag{1.2}$$

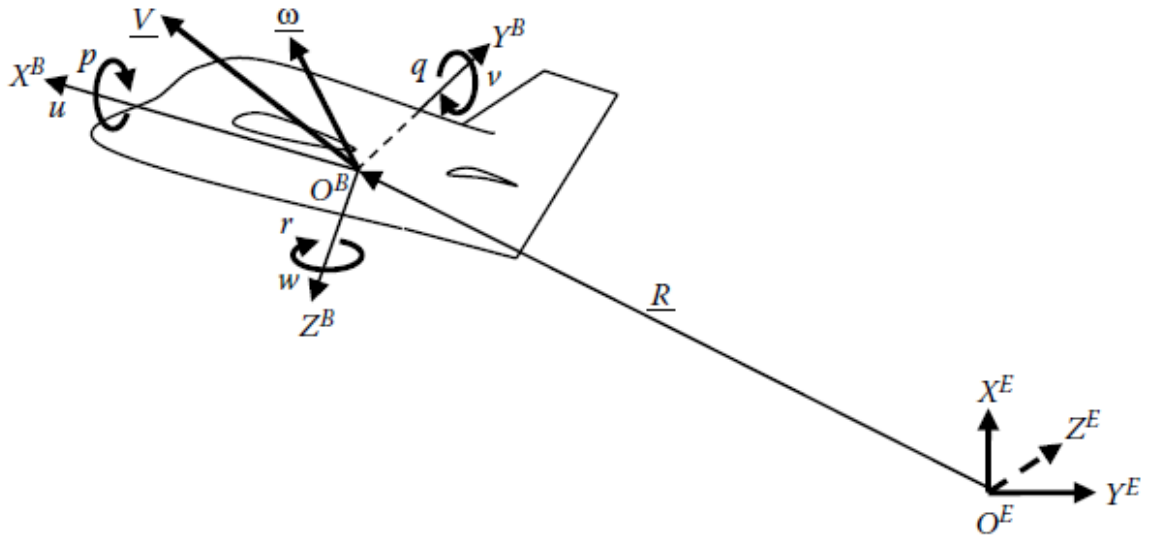


**Figure 1.3.** *Representation of the body-fixed axis system with respect to the Earth-fixed axis system [1]. The position vector* **R** *connects* $O^E$ *to* $O^B$, **V** *is the velocity of the centre of mass and* **ω** *is the angular velocity around the centre of mass. u, v, w and p, q, r are the three components of* **V** *and* **ω** *respectively in the body-fixed system of reference.*

The aircraft orientation with respect to the Earth-fixed coordinate system is usually described by a triad of angles (φ,θ,ψ), known as Euler angles. In airplane flight dynamics, φ, θ and ψ are conventionally determined with a 3-2-1 sequence of rotations (the first around Z axis, the second around Y axis and the around X axis), as shown in Figure 1.4, to take the $X^EY^EZ^E$ system to coincide with the $X^BY^BZ^B$ one. The rotation φ around $X^B$ is denominated roll angle and coincides with the inclination angle of the wings. The rotation θ around $Y^B$ is defined pitch angle and characterizes the nose-up or nose-down angle with respect to the horizon. The rotation ψ around $Z^B$ is called yaw angle and represents the rotation to the right or to the

left of the airplane nose. The derivatives of the Euler angles can be linked to *p*, *q* and *r* which, for this reason, are called roll rate, pitch rate and yaw rate respectively.

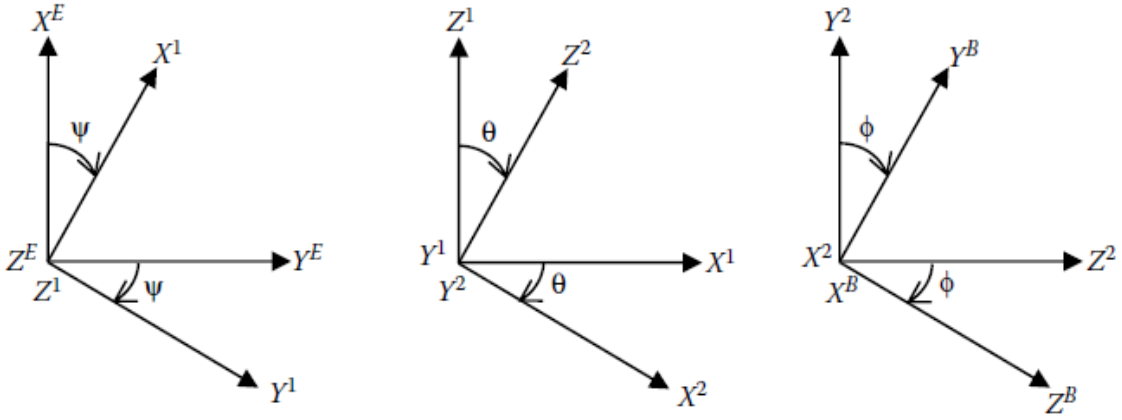


**Figure 1.4.** *The three rotations sequence to determine the Euler angles triad [1].*

According to the second law of Newton, the temporal derivative of **V** is connected to the external forces (gravitational, aerodynamic, buoyancy and propulsive forces) through the vehicle mass, which can be considered constant in first approximation. Centrifugal and Coriolis forces have small effect on aircraft position and orientation and in this discussion are neglected (flat-Earth assumption). The components *u*, *v* and *w* are determined by resolving the three equations resulting from the vector equality. Similarly, *p*, *q* and *r* can be found through the angular momentum theorem and transformed in $\dot{\varphi}$, $\dot{\theta}$ and $\dot{\psi}$. By integrating the found components, the position vector and the Euler angles are obtained in every desired instant.

## 1.2 Aircraft components

Aircrafts have many elements which are designed with a trade-off between costs and reliability to satisfy some functional requirements, so that the vehicle is able to perform every task needed for all the mission operations. Most aircrafts have wings to generate aerodynamic lift, a fuselage to carry the payload, propulsive engines to produce the thrust to overcome the vehicle aerodynamic drag and undercarriage for take-off and landing operations. The propulsion modulation is employed along with the attitude control system

to stabilize the aircraft orientation. In modern aviation, the presence of some movable components capable of generating aerodynamic reactions and affecting attitude control, greatly influences the aircraft motion. An example of airplane components and control effectors, such as flap, aileron, rudder and elevator, is given in Figure 1.5.

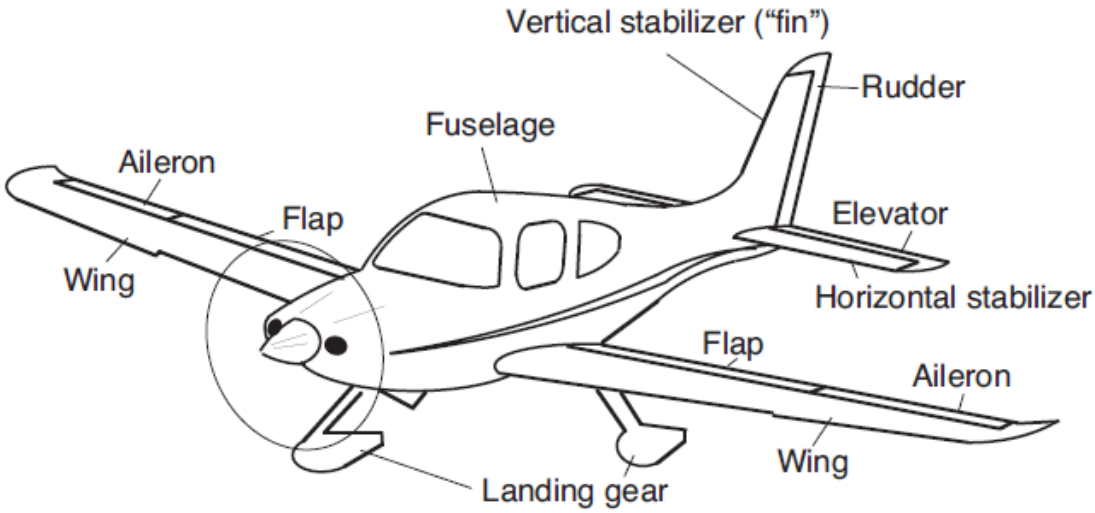


**Figure 1.5.** *Main components which are usually present in a common aircraft [2].*

Flaps and ailerons are movable surfaces mounted on trailing edges of wings and their shape is manufactured similarly. However, flaps are typically positioned symmetrically in the internal side of wings and they can move only downwards. These devices are activated simultaneously, and their deflection causes an increment in both lift and drag, which is exploited in take-off operations. If flaps are deflected by an angle around 60°, the drag increase is useful in landing phase to slow down the airplane. On the contrary, ailerons, mounted frequently near the wing tips, are used differentially (one is deflected up while the other one is deflected down) to generate a rolling torque and bank the airplane. Regularly, ailerons are employed along with flaps to brake the aircraft during landing.

The empennage is the set of tail surfaces manufactured in the fuselage aft. The vertical tail acts like a small wing generating a lift force which tends to align the airplane $X^B$ axis to the relative wind direction. The rudder is a movable panel, mounted on the trailing edge of the vertical tail, capable of generating a yawing torque for the attitude control. Similarly, the horizontal tail is designed to produce an amount of force, smaller than lift generated by wings, such as to compensate the pitching moment due to the external forces. For instance, if the aerodynamic centre does not coincide with the centre of mass, a spurious moment

around $Y^B$ axis is created and a restoring pitching torque given by the rear tail is required. Moreover, movable surfaces, called elevators, can be mounted on the trailing edges of the horizontal tail in order to modulate the lift produced. The pitch rotation control is fundamental to obtain the desired angle of attack for wing leading edges.

However, the control system performances can be furtherly improved by the exploitation of devices, named spoilers. A spoiler is defined as a panel which can be deployed from any airplane surface and its primary effect is to increase drag by a great amount and decrease lift. Conventional spoilers are generally installed on wings upper-surface and their opening deflection can reach angles of $90^{\circ}$. Depending on spoilers' position with respect to the centre of mass, these devices can provide a pitching-up or pitching-down moment with symmetric deployment. When spoilers are used differentially, yawing and rolling torques for attitude control are generated as well. Moreover, other spoiler can be mounted on fuselage and, together with all the wing devices, they act as brakes during landing phase.

**Figure 1.6.** *Conventional spoilers in action during landing brake on the ground: the large deflection increases drag force which is useful to help the undercarriage brakes.*

Spoilers application allows to lower fuel consumption in flight maneuvers and reduce stress in brakes of the landing gear. Furthermore, a steep-descent maneuver of airliners is achievable only with an increase in drag and is used to lower the distance travelled during descent, to decrease landing time and to reduce noise emission near airport residential zones [3]. Thus, spoilers have become inevitable components in modern aircrafts.

## 1.3 Special types of spoilers

Recently, research has been carried out about the flight control by means of spoiler devices on wings. Improving efficiency and effectiveness is a major concern in modern aviation because even small fuel savings produce considerably higher earnings in the long term.
Tailless aircrafts offer the advantage of reducing vehicle weight and radar detectability, but the control system loses some fundamental components, especially the rudder which provides most of the yawing control moment. This means that other devices on the wing must be able to impart the necessary yawing torque. In Figure 1.7, the split ailerons at the trailing edge are represented. The control device provides the desired yawing moment when the hingedly-mounted panels are open symmetrically in just one wing, but it also generates spurious rolling torques which have to be compensated by other tools. The moments to keep the split ailerons open are quite elevated and, as a result, the associated mechanism, which provides the forces for the surfaces deflection, is relatively heavy. Furthermore, spoilers are effective only if they emerge from the boundary layer, so frequently their nominal deflection is greater than zero to have a quicker response. Consequently, wing drag is augmented, and fuel consumption efficiency becomes lower.

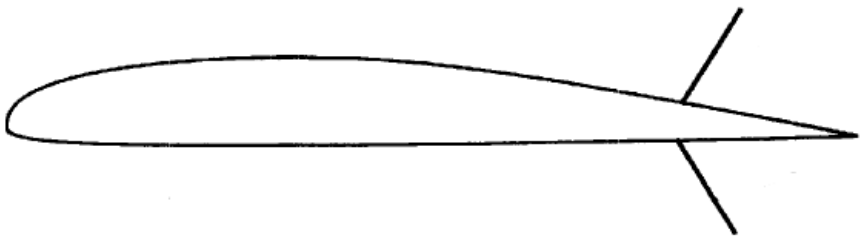

**Figure 1.7.** *Split ailerons at the wing trailing edge [4].*

Blake [4] proposed a new spoiler concept to improve the performances of split ailerons. The upper-surface spoiler is similar to a conventional one, while in the wing lower surface an inverted spoiler is installed, as shown in Figures 1.8*a* and 1.8*b*. The deployment mechanism opens the spoilers simultaneously and requires little energy to keep them in position because the closing tendency of the upper-surface spoiler is almost completely balanced by the opening tendency of the inverted spoiler. For the same reason, the spurious rolling moments cancel each other, and the net effect is a pure yawing control torque.

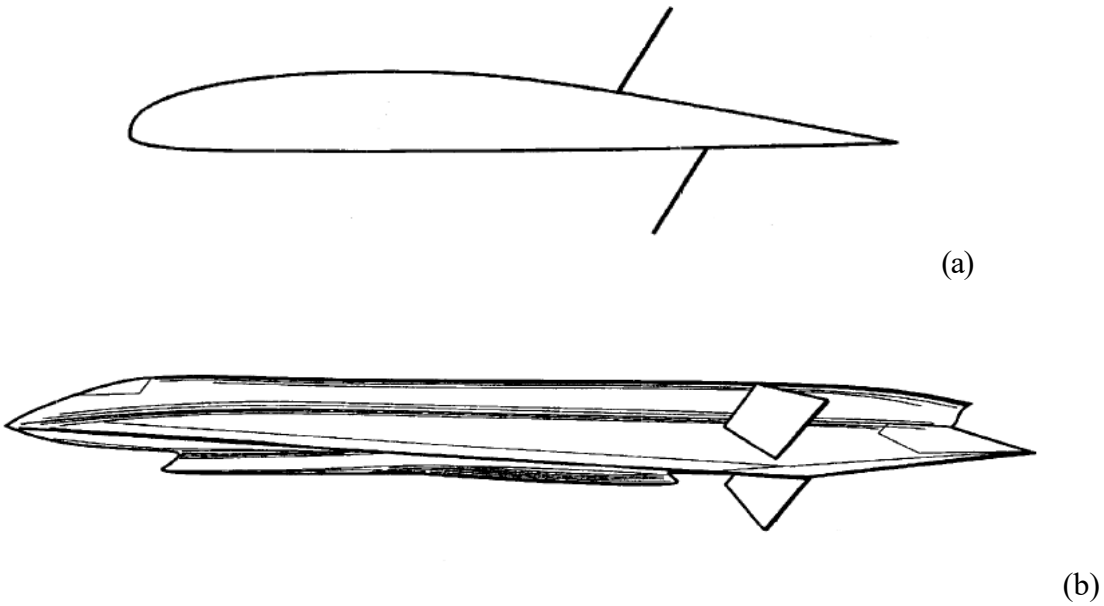


**Figure 1.8.** *Device with lower-surface inverted spoiler proposed by Blake [4].*

The forward opening inlay spoiler, proposed by Clark [5], allows to deflect the air flow outwards generating a yaw moment without loss in lift. These attitude control tools do not include any openings for the air passage. The key in the claimed device is the hinge inclinations of the inverted spoilers mounted on the top surfaces of the wings, which are depicted as $\theta_1$ and $\theta_2$ in Figure 1.9*a*. In Figure 1.9*b* the outer deflection of air flow is shown, and it is clear that an additional drag force is produced. In order to cancel the down force created by the upper-surface devices, some lower-surface spoilers are generally required. Clark claims that the correct differential deflections between the left-wing and right-wing devices can bring to zero the loss in lift.

Other devices that are worth to mention are the jet blowing apparatuses. A lot of blowing schemes were studied because they do not comprehend deflecting surfaces, thus simplifying all the problems of structural instability and damage. The opening mechanism is not required and, therefore, the device reliability is higher with respect to the conventional control surfaces. For instance, it is possible to move outwards the tip wing vortices with a high intensity jet blowing device in the spanwise direction. Consequently, the lift is sensibly incremented because the effect on the flow is similar to the one achievable with a longer wing. However, the complex aerodynamics of the wings is furtherly complicated by the jet perturbations. Another disadvantage is that there must be a source of compressed air inside the vehicle. The most straightforward solution is to tap the needed fluid after some compressor stages of the aircraft engines, despite the inevitable drop in efficiency of the

propulsion system. Otherwise, an external auxiliary power unit is required for the generation of the compressed air.

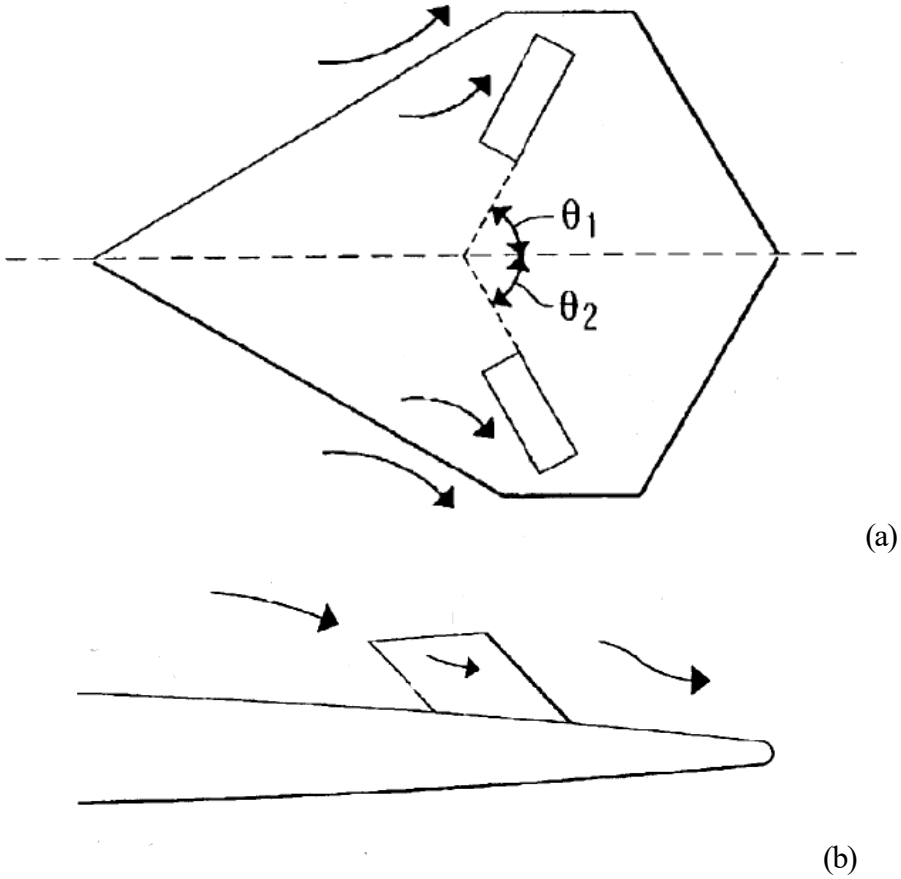


**Figure 1.9.** *Delta-wing aircraft with forward opening inlay spoilers [5]. The arrows show the approximated flow direction in the proximity of the device.*

The lateral blowing jet spoilers developed by Tavella *et al.* [6, 7], shown in Figure 1.10, generates a flow in a form of thin sheet which increases the lift. Even with a low flow mass rate, the modulation of vertical and lateral forces and rolling torques would permit to substitute flaps and ailerons with this new design concept.

If the blowing jets are positioned on the upper or lower side of the wing, these devices take the name of jet spoilers. The one-sided jet spoiler consists of only one device on the upper surface of the wing, while the two-sided jet spoiler has two blowing jets on both sides and is illustrated in Figure 1.11. The jet spoilers have no movable panels, but the blowing jet acts like a solid surface displacing the flow away from the wing surface. The consequence is the flow separation because the boundary layer is blown away from the wing surface. The

vortices created behind the jet spoiler are produced by the wing stall and the lift is penalised. The main effect of the jet spoilers is to increase the wing drag, because there is a pressure increment upstream and a pressure decrement downstream.

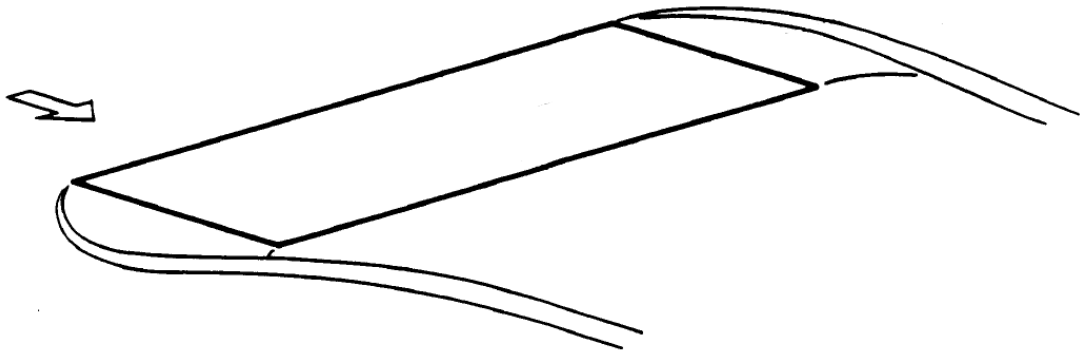

**Figure 1.10.** *Lateral blowing jet spoilers installed on the wing tip [6].*

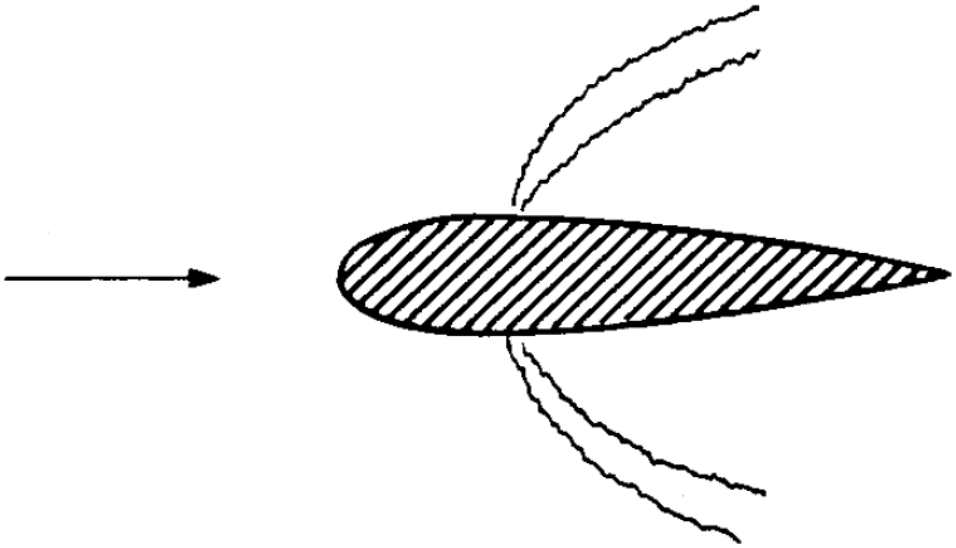

**Figure 1.11.** *Two-sided jet spoilers developed by Tavella et al. [7].*

The thicker the airfoil is, the larger the drag effect is expected to be, since the pressure can lean against a higher projected surface normal to undisturbed flow. By the same token, the optimal position appears to be where there is the airfoil maximum thickness, so that the increased-pressure and the decreased-pressure act on the higher area possible. Through the drag generated, a yawing torque can be generated with a moderate spurious rolling moment. When the two-sided jet spoilers are blowing, the flow separation also occurs in the lower side of the wings and the lift is less influenced by the stall.

By the same token, Cook *et al.* [8] proposed a circulation control actuator capable of substituting an equivalently sized flap. The flow control actuator is based on the Coanda effect, i.e. the tendency of the fluid jet to stay attached to the surfaces which is in contact with. As intuitively understandable from Figure 1.12, moving the trailing edge cylinder allows to create a modulable inclination jet which covers the same tasks of a deflectable conventional flap thanks to a feedback control system. The subsonic performances of the device are comparable with the conventional flap even with relatively moderate flow mass rate. The circulation control actuator focuses mostly on lift augmentation rather than increasing drag.

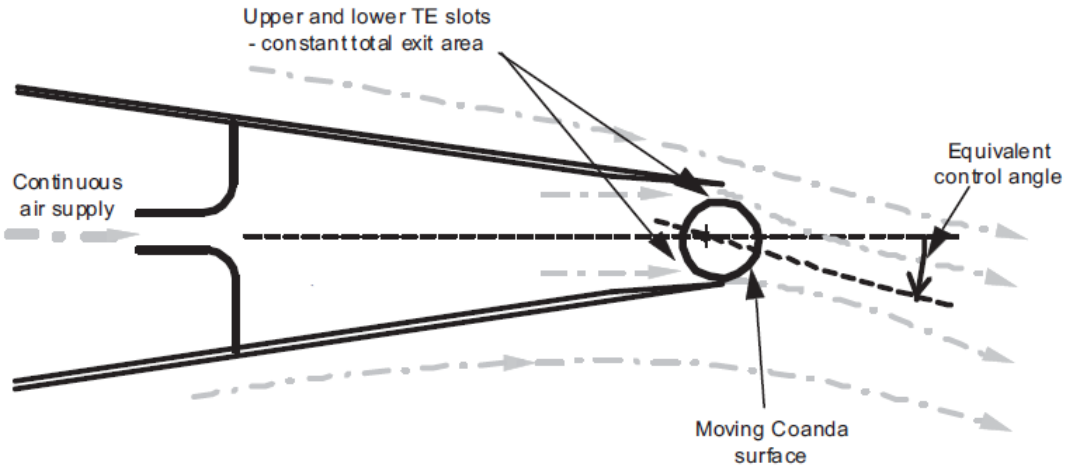


**Figure 1.12.** *Flow control actuator based on a movable Coanda surface at the trailing edge [8].*

A related design was claimed by Cyrus *et al.* [9] for a Darrieus wind turbine. The hollow blades have a section with a shape similar to the jet spoiler airfoil and the rotation permits to induce air pressure inside them. A feedback control system, which consumes a little amount of external power, is required to open correctly the outlets in order to regulate the flow separation and reduce the power generated by the turbine.

McClure [10] proposed an evolution of the jet spoilers without the need to supply the air from inside the vehicle. As depicted in Figure 1.13, there is an air inlet in the lower side of the leading edge where the pressure is relatively higher with respect to the trailing edge. Thus, the internal air tends to flow towards the two outlets which compose the jet spoilers. This device is named “passive jet spoiler” because no opening mechanism is needed. However, every opening requires a valve that can modulate the incoming and outgoing mass flow rate, so that the drag generated by the spoiler is adaptable.

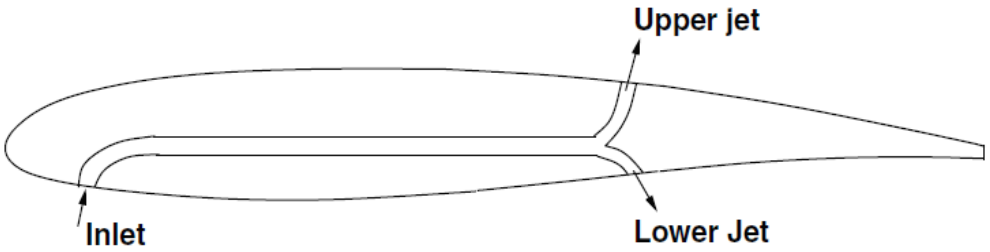


**Figure 1.13.** *Passive jet spoiler proposed by McClure [10].*

Nevertheless, the internal channel should pass through the wing spars, causing considerable problems during the manufacturing phase. Moreover, the pressure losses are significant along the channel and only weak blowing jets can be produced.

## 1.4 Inverted jet spoilers

Drag control devices, such as clam shells, have already been tested and applied to some aircraft (BAe 146 regional jet), in order to improve its steep descent capability at constrained airfields. Earlier research on a light aircraft by Olcott *et al.* [11] indicated that it is possible to increase the glide angle and landing performance with upper and lower plate spoilers.
Filippone [12, 13] focused on a particular type of spoiler, the "inverted jet spoiler", shown in Figure 1.14. During the cruise flight, the spoilers are closed and aligned to the airfoil and the wing aerodynamics is not influenced by them in this situation. However, during the phases of lift up, maneuver and landing, a mechanism (electric or based on a cam shaft) able to open the panels can be activated by a control system and in this way the cavities inside the airfoil are exposed to the flow. The air flow in the bypass is naturally generated because of the difference in pressure between the upper and lower sides of the spoiler. Indeed, the flow on the airfoil upper surface tends to accelerate and reduce the pressure with respect to the lower side.
The airfoil seems to be structurally divided in two parts, but in the 3-dimensional case the spoilers have a limited length along the wingspan and structural continuity is achieved, as illustrated in Figure 1.15. The device with the opening mechanism could be moved in the wing aft part to leave the indispensable space for the wing spar. Stagnating flow is inherently unsteady, but with this configuration there are no points where the flow velocity is null.

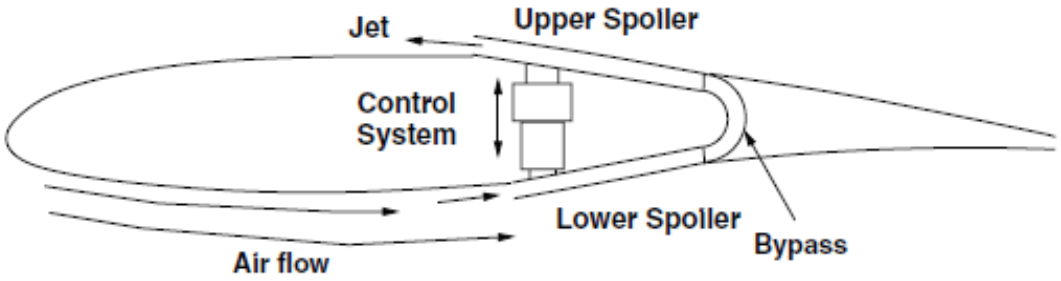


**Figure 1.14.** *Inverted jet spoiler inside an airfoil [12].*

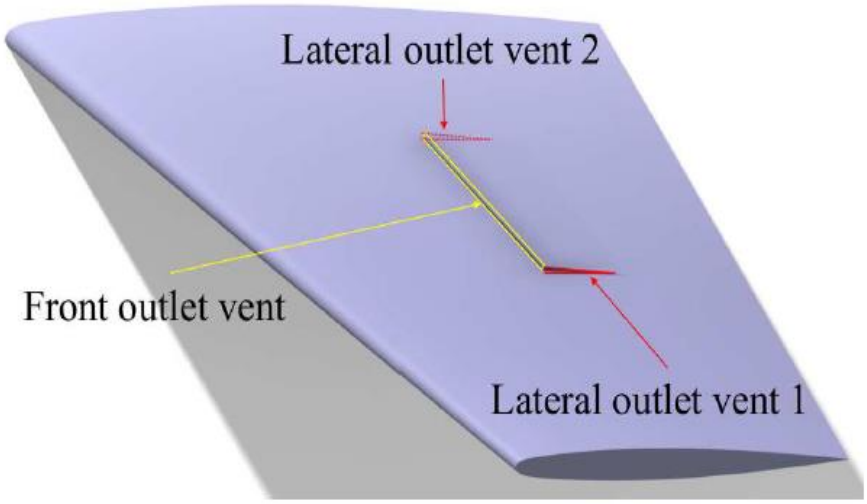


**Figure 1.15.** *3-dimensional shape of the spoilers on the wing [13].*

The mass flow inside the spoiler channel is small because of the friction dissipation between the fluid and the solid wall. The jet outlet is pointed upstream, but it tends quickly to be redirected along the airfoil aft by the external flow. A boundary layer separation bubble is often generated behind the jet, but it involves only a small part of the upper-spoiler surface because of the minor intensity of the internal flow. Tiny boundary layer detachments are also present inside the channel near the inlet and outlet vents.

Even if the bypass is not necessary for the device functioning, it creates the conditions to have a spontaneously blown jet, which will be surely weaker than the jets generated by external sources. The conduit is designed to alleviate problems such as vibrations caused by flow into the wing, although no experiments are available at this time to corroborate this hypothesis. From the analyses of Filippone [12], the drag produced by pressure forces is dominant with respect to the one generated by viscous losses. Indeed, the increment in pressure before the spoilers and the increment of aerodynamic surface will contribute to

increase the drag. By contrast, the lift may be affected by two opposite phenomena: the separation of the boundary layer at the upper surface will decrease the lift; the increment of pressure at the lower surface due to the spoiler orientation will increase it.
The drag force ΔD generated by the bypass is calculated as the difference in momentum between the outlet and inlet vent:

$$\Delta D = \mathbf{F} \cdot \mathbf{i} = \dot{m}(\mathbf{U}^{+} - \mathbf{U}^{-}) \cdot \mathbf{i}\,, \tag{1.3}$$

where **F** is the aerodynamic force produced by the bypass, **i** is the vector pointed toward $X^B$ axis, ṁ is the flow mass rate inside the channel and $\mathbf{U}^{+}$ and $\mathbf{U}^{-}$ are the mean velocity at the upper and lower spoiler extremes respectively. The deflection of the spoilers can increase the mass flow rate and subsequently the drag generated, but the panels must be positioned inside the wing during the cruise flight and therefore the largest opening is limited.
The effectiveness of the device pass through various geometric parameters. For instance, the maximum jet momentum is realised with a spoiler deflection of the 1% of the chord because for higher deflections the separation bubble dimensions increase and the speed at the outlet vent is penalised. Anyways, the jet intensity is so low that it is almost immediately dissipated by the incoming flow, which is forced to move outwards, generating the force opposite to the vehicle forward motion. Another important parameter is the length of the channel because it affects the pressure losses on the solid walls. If the air must flow for a longer distance along fixed surfaces, the dissipation becomes increasingly important, and the jet is weaker. As a result, the stall induced on the upper wing surface is less intense and the device efficiency is penalised. Thus, shorter channel is convenient to increase drag, and the spoiler length and U-bend channel shape should be carefully studied. Then, in a 3-dimensional wing configuration the spoiler spanwise extent and position influence the effectiveness of the device.
The ultimate aim of the inverted jet spoiler is to increase the drag without affecting in a substantial way the aircraft lift in order to generate control forces and torques. This device is useful during landing phases to furtherly decelerate and increase the descent rate to put the airplane on a steeper trajectory. In low-to-moderate speed maneuvers the inverted jet spoiler can be activated through the control system to provide lateral and longitudinal control. If only one between the left- and right-wing spoilers is used, a yawing moment is produced. This is fundamental, overall, for military tail-less aircrafts. pitching and rolling

moments are generated when the point of aerodynamic force application is shifted upstream or downstream with respect to the centre of mass, despite the inconvenient and undesired increment in drag. It can be noted that the inverted jet spoiler requires only small deflections to operate and this could be an advantage for some types of aircrafts. For instance, military airplanes need low radar detectability and that is surely a characteristic of this device.

## 1.5 Aeroservoelasticity

Aeroelasticity is the branch of physics and engineering which deals with the interaction of aerodynamic, inertial and structural forces. Aeroelastic phenomena occur when any deformable body is exposed to a fluid flow and there is a non-negligible coupling between the aerodynamic pressures and the displacements induced thereby in the structure. The wings are typical instances of structures that undergo deformation because of the aerodynamic forces and the change of shape modifies the fluid flow itself.

Several years ago, Collar suggested that aeroelasticity involves three different disciplines: dynamics, solid mechanics and aerodynamics. This could be visualized in a scheme called the "Collar's triangle" in Figure 1.16. If the structure can be modelled as a rigid body moving in a fluid flow neglecting the elastic behaviour, the reciprocal interaction between the aerodynamic forces and the inertial forces involves the field of the flight dynamics. If the aerodynamic forces can be neglected, vibrational mechanics is concerned with the coupling of elastic and inertial forces. Aeroelastic phenomenon is either static if there is equilibrium between aerodynamic forces and elastic reactions, or dynamic if the structure keeps vibrating because no static equilibrium between aerodynamic pressures and elastic response of the structure is achieved, and inertial forces comes into play. The dynamic aeroelasticity of a wing is called "flutter" and it causes vibrations of the body in the direction perpendicular to the air flow.

Usually aeroelastic phenomena are undesired in the structures of flight vehicles. Indeed, static aeroelasticity could change the aerodynamical properties of the wing and dynamic aeroelasticity could reduce considerably the fatigue life of the structures because the vibrations induce more loading cycles than expected. In both cases, the most dangerous event is the catastrophic failure of the wing, an eventuality which must be definitely avoided.

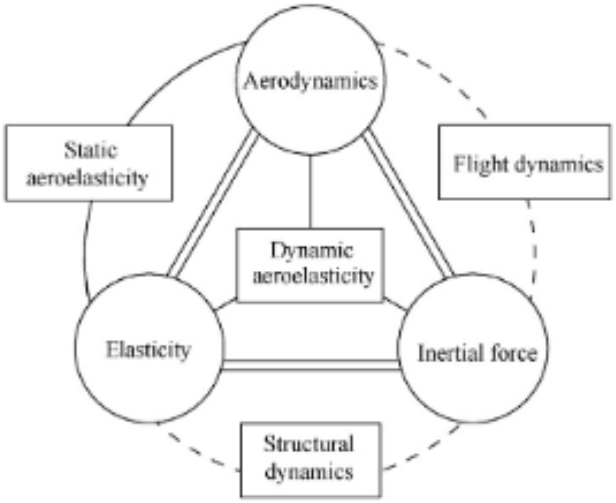


**Figure 1.16.** *Collar's triangle [14].*

Even though there is a growing interest in aeroelastic phenomena in civil engineering (flows about bridges and tall buildings) and mechanical engineering (flows around turbomachinery blades and inside flexible pipes), the theoretical progress has always been mainly developed in aerospace field of study. In modern aerospace applications, the problem could be also more complicated since the dynamics of the control devices affect significantly the aeroelastic phenomenon. Thus, the new term "aeroservoelasticity" was coined [15].
Modern airframes are designed to be lightweight for better performances, although deflections and distortions under air load of wings, fuselage and tail are significant due to structural flexibility. Moreover, the dominant natural frequencies tend to be low enough to excite dangerous vibrational modes. Even though body flexibility practically does not affect aircraft net position and velocity, vibrations disturb during the mission maneuvers, promote poor ride quality for passengers and crew and reduce structure fatigue life.

## 1.6 Work aim and presentation

The inverted jet spoiler seems to be a very promising auxiliary device for aircraft attitude control. Aerodynamic studies have been conducting by Filippone, who focused on the optimisation of the most influencing geometric parameters. However, his work could be meaningless if the aerodynamic pressures involving the spoiler panels are too intense to bear for the structure itself. Indeed, spoiler surfaces are considerably thin and flexible: this could

bring to substantial deformations of the device and, eventually, to fracture. As discussed previously, structural deformations of the spoiler modify the device shape and, thereby, the attitude control performances.

Since the inverted jet spoiler is a quite new concept, no studies on the structural and vibrational behaviour of the system have been carried out yet. This work proposes to preliminary study the interaction between fluid flow and solid surfaces of the device through well-known pieces of software, such as ABAQUS (based on Finite Element Method) for structural analyses and ANSYS (Computational Fluid Dynamics) for aerodynamic analyses. In Chapter 2, preliminary structural static and dynamic analyses of the 3-dimensional are carried out to verify the no-exceedance of material yield strength. In Chapter 3 the 2-dimensional aerodynamic analyses accuracy is proved through a mesh independency test and the comparison with reference case of study by Filippone. Moreover, a parametric study on the angle of attack for a typical low speed maneuver at low altitude and in cruise flight, is conducted transferring the flow pressures in the structural solver. Because of large tip spoiler displacements and probable risk of aeroelastic phenomena, in Chapter 4 some methods to reduce spoiler motion amplitude are revised in the wind conditions worst-case scenario for the low speed maneuver. In Chapter 5, the conclusions of this work are reported.

# Chapter 2
# Preliminary structural analyses

Filippone carried out some 2-dimensional and 3-dimensional aerodynamic simulations of the airfoil and of the wing respectively [12,13]. The analyses demonstrated that the spoilers tend to open up as a result of the difference between internal and external flow pressure, but still the hinge moments required to maintain the desired device deflection are lower than the conventional spoiler ones. Since the inverted jet spoiler is a quite new concept, no studies on the structural and vibrational behaviour of the system have been conducted yet. That is why a static analysis needs to be implemented in order to check whether the structure can resist to the aerodynamic loads generated by the air flow around the wing and inside the bypass. Furthermore, it is possible that some aeroelastic vibrations could be originated from the interaction between the fluid and the structure. In particular, the most dangerous situation occurs when the time-variant loads synchronise with the natural frequencies of the body, since the resonance phenomenon amplifies the deformations and, consequently, the stresses throughout the structure. For this reason, a modal analysis is carried out to obtain as a result the resonance frequencies and the normal modes of the wing with the open spoilers. Subsequently, a dynamical analysis is conducted with time-variant loads which follow a harmonic function to achieve the resonance condition.

## 2.1 Computational model

In order to investigate the structural behaviour of the inverted jet spoilers, the analyses are executed with the FEM software ABAQUS. This work focuses on the case in which the spoilers are completely open (the possible deflections are in the order of 1% of the chord). The baseline geometry of the ONERA M6 wing is imported from a NASA study [16] and the implemented configuration for the spoilers is shown in Figure 2.1. The coordinate system is set with the X axis aligned with the chord $c$, the Y axis parallel to the spanwise direction

and the Z axis that completes the right-handed coordinate system. Thus, axes directions are identical to body-fixed axes, but the origin is placed on the leading edge of the root wing cross-section. The length of the spoilers lays between X/*c*=0.5 and X/*c*=0.7, while the span of the device is between Y/*b*=0.3 and Y/*b*=0.6, where *b* is the total span of the wing.

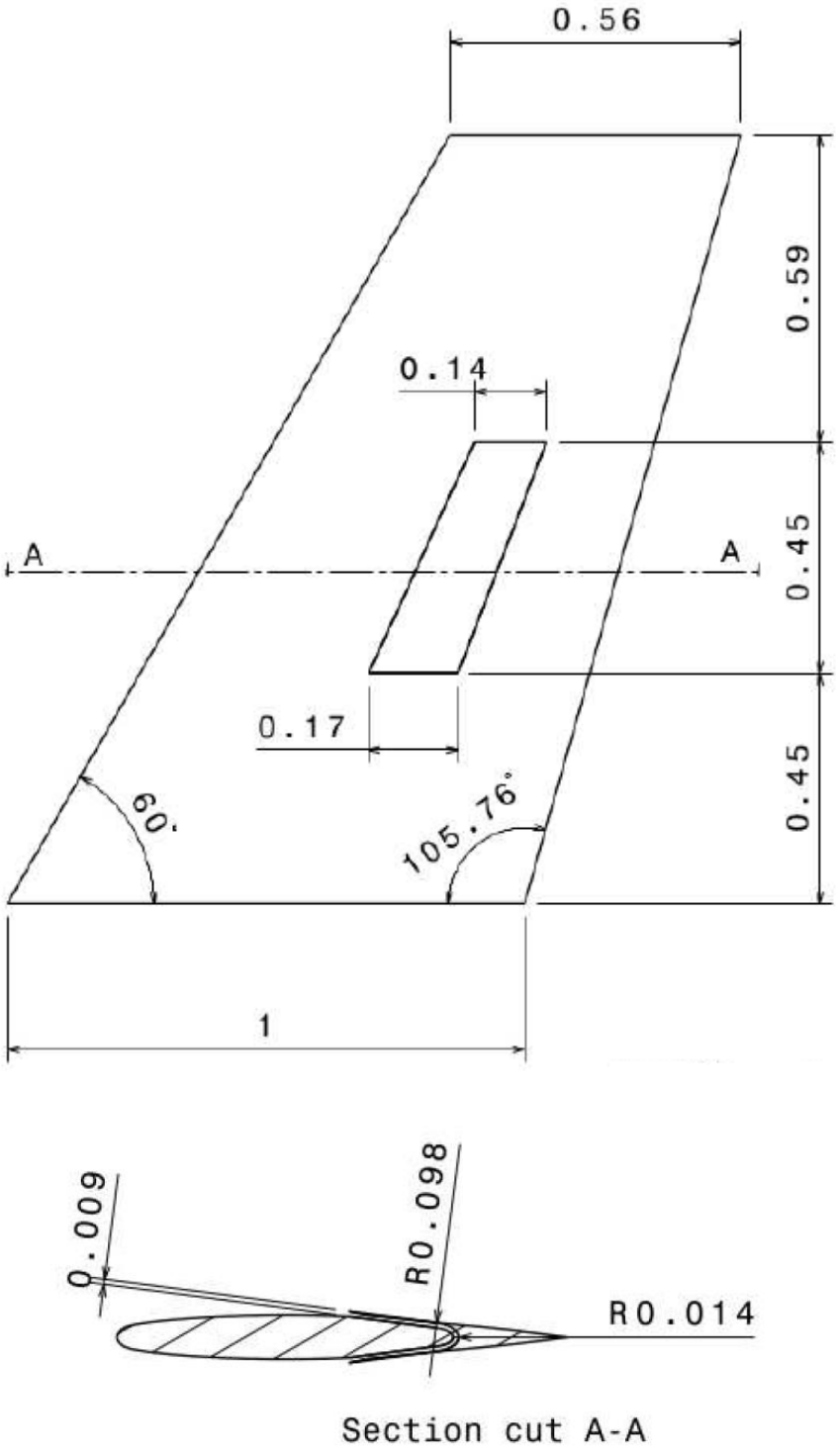


**Figure 2.1.** *Geometry used for the ABAQUS model adimensionalized with respect to the root chord length [13].*

To date, most of the wing components have been built with aluminium alloys because of the elevated specific strength (strength/weight ratio) and the relatively low costs. In particular, the chemical composition and the temper of AA7075-T6 allow this material to have one of the highest combinations of strength and fracture toughness among the other aluminium alloys [17]. The properties of this aluminium alloy, displayed in Table 2.1, are used in the model.

**Table 2.1.** *Properties of AA7075-T6 [17].*

| Density [kg/m$^3$] | Elastic modulus [GPa] | Poisson ratio | Yield strength [MPa] |
|---|---|---|---|
| 2800 | 71.0 | 0.33 | 505 |

The aerodynamic coefficients are calculated with the wind conditions of a number of Reynolds $Re = 10^6$ and a number of Mach $M = 0.25$, at an altitude of $h = 500$ m. With reference to the International Standard Atmosphere [2], the thermodynamic variables are displayed in Table 2.2. The pressure, the density and the velocity of the undisturbed flow are called $p_\infty$, $\rho_\infty$ and $U_\infty$ respectively. These variables vary with season, weather and time of day, but below 10 km of altitude the variability of density is under 1%.

**Table 2.2.** *Air properties obtained from International Standard Atmosphere table [2].*

| $h$ [m] | $p_\infty$ [Pa] | $T_\infty$ [°C] | $\rho_\infty$ [kg/m$^3$] | $a$ [m/s] |
|---|---|---|---|---|
| 500 | 95460.8 | 11.75 | 1.167 | 338.37 |

The velocity $U_\infty$ of the undisturbed air flow can be easily calculated as:

$$U_\infty = a \cdot M = 84.59\, m/s \ . \tag{2.1}$$

Therefore, the absolute pressure $p$ around the wing is obtained from the well-known formula:

$$p = p_\infty + \frac{1}{2}\rho_\infty U_\infty^2 \cdot C_p \ . \tag{2.2}$$

The values of the pressure coefficient $C_p$ around the wing with an angle of attack $\alpha$ equal to 4°, are taken from the study of Filippone [13] in Figure 2.2.

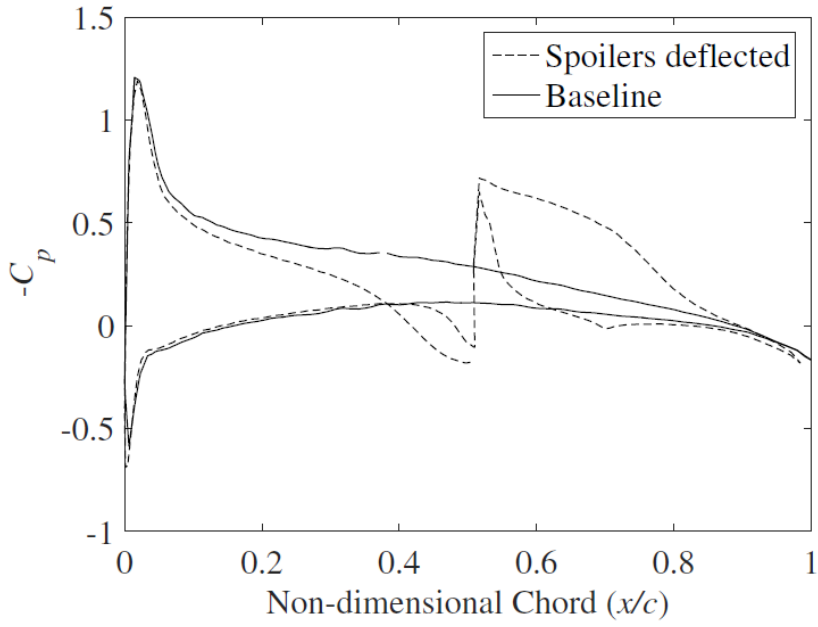


(a)

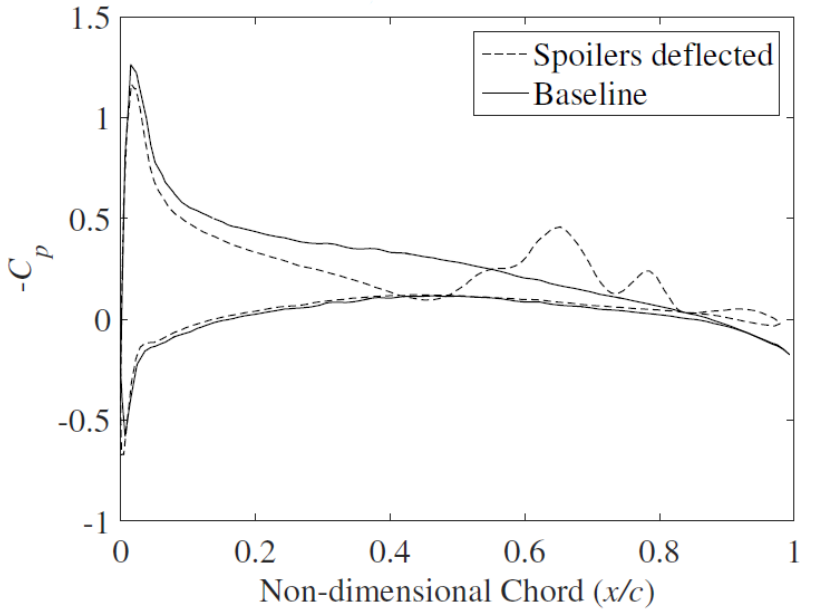


(b)

**Figure 2.2.** *$C_p$ distribution along the wing chord at two spanwise positions. (a) is a wing section with the spoiler, and (b) is a wing section without the spoiler [13].*

The pressure inside the bypass of the spoiler is collected from the first study of Filippone [12] shown in Figure 2.3, even though the simulation of the phenomenon was carried out only in a 2-dimensional case with a different position of the spoiler and with some differences in the air flow variables ($M = 0.3$, $Re = 1.9 \cdot 10^6$, $\alpha = 0°$). There are little pressure gradients in the inlet, in the outlet and in the U-bend of the spoiler, but it can be assumed

that the pressure distribution is constant inside the device. In order to get the pressure from the pressure coefficient $C_p$, the same procedure already seen is applicable.

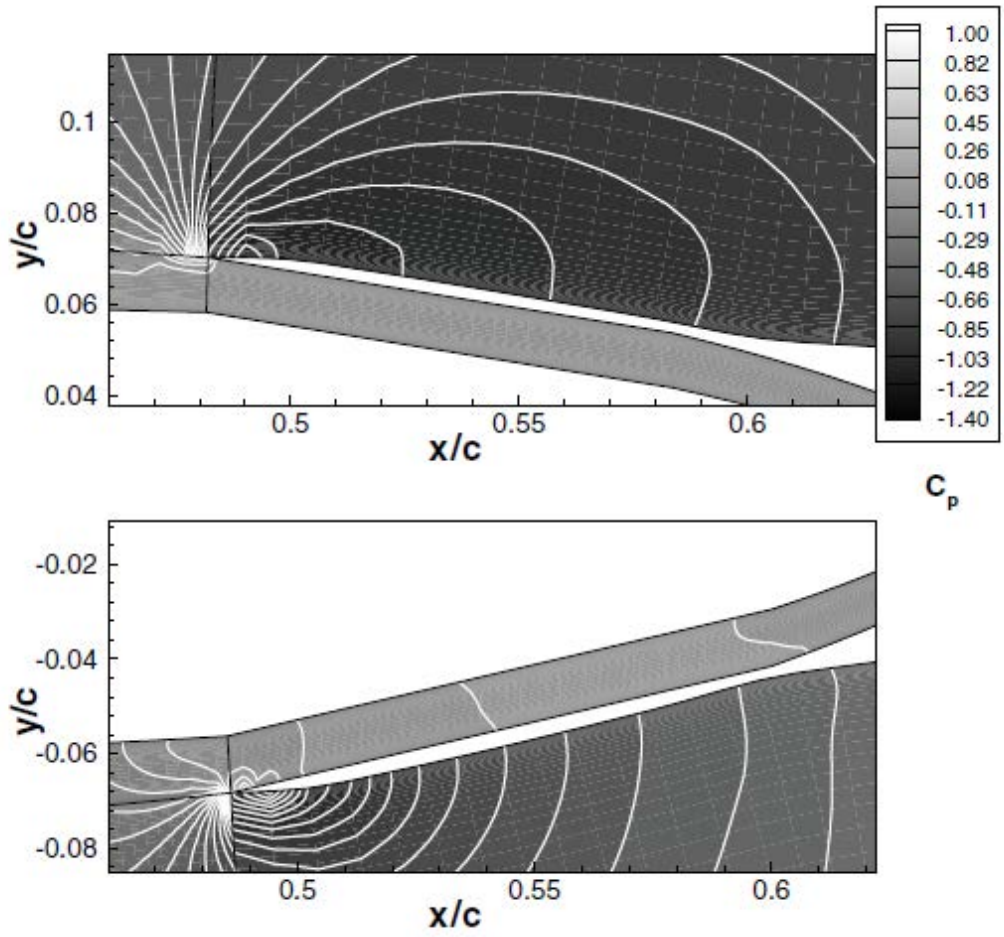


**Figure 2.3.** *$C_p$ distribution at the outlet and at the inlet of the spoiler [12].*

Since the available data is not sufficient to cover the whole external surface of the 3-dimensional wing, some approximations have to be done. The wing is partitioned in 5 parts with planes parallel to the XZ plane, as shown in Figure 2.4, and in each part the loads are set to be uniform in Y direction. The central part contains the inverted jet spoiler and the pressure is calculated with the dotted line in Figure 2.2*a*. Near the spoiler, other two parts were generated, and the loads are consequently defined by the pressure coefficient represented by the dotted line in Figure 2.2*b*. It is assumed that in the last two parts, which are the farther ones from the device, the aerodynamic flow of the airfoils is not influenced by the presence of the spoiler, thus in this case the pressure coefficient is considered to be the continuous line in Figure 2.2.

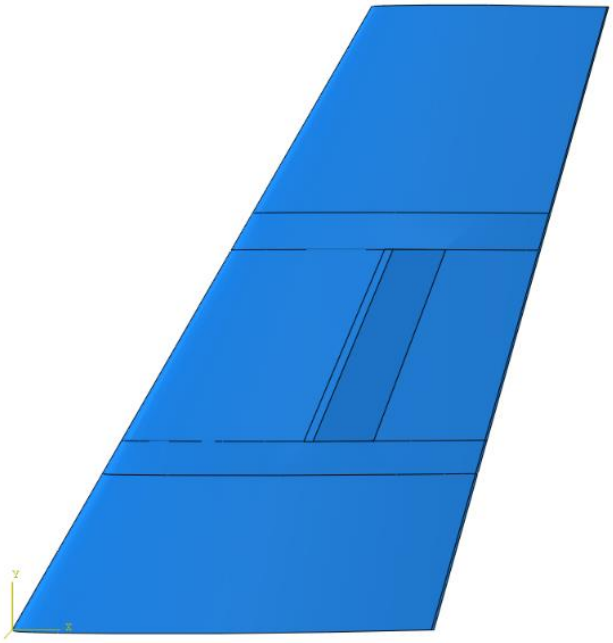

**Figure 2.4.** *Partitions of the wing.*

At this point, the pressures are applied on the parts creating a field by means of a high order polynomial expression obtained with a MATLAB script, that finds the best fit among some points of the graphs in Figure 2.2. The only necessary boundary condition is an encastre in the root section of the wing and it represents the junction of the structure to the fuselage. Then, the body is meshed with about 35000 tetrahedral elements and a static analysis is set up.

## 2.2 Static analysis

The displacements to which the structure is subjected in the static analysis, are shown in Figures 2.5 and 2.6, while the stresses generated by the static loads can be observed in Figures 2.7-9.

It can be easily noticed that the upper and the lower spoiler withstand the biggest displacements, because they are thin plates exposed to the pressures generated by the air flow. Since the device is the less stiff part of the wing, it is very important to study its structural behaviour and its resistance to loads. Nonetheless, the maximum displacement is 0.0348 mm and it is practically negligible compared to the dimensions of the device.

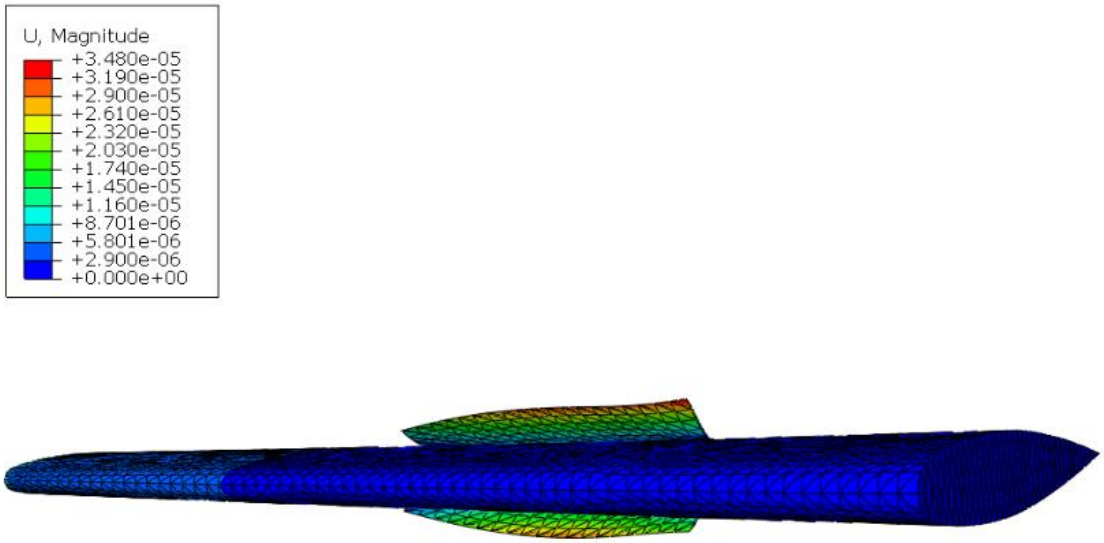


(a)

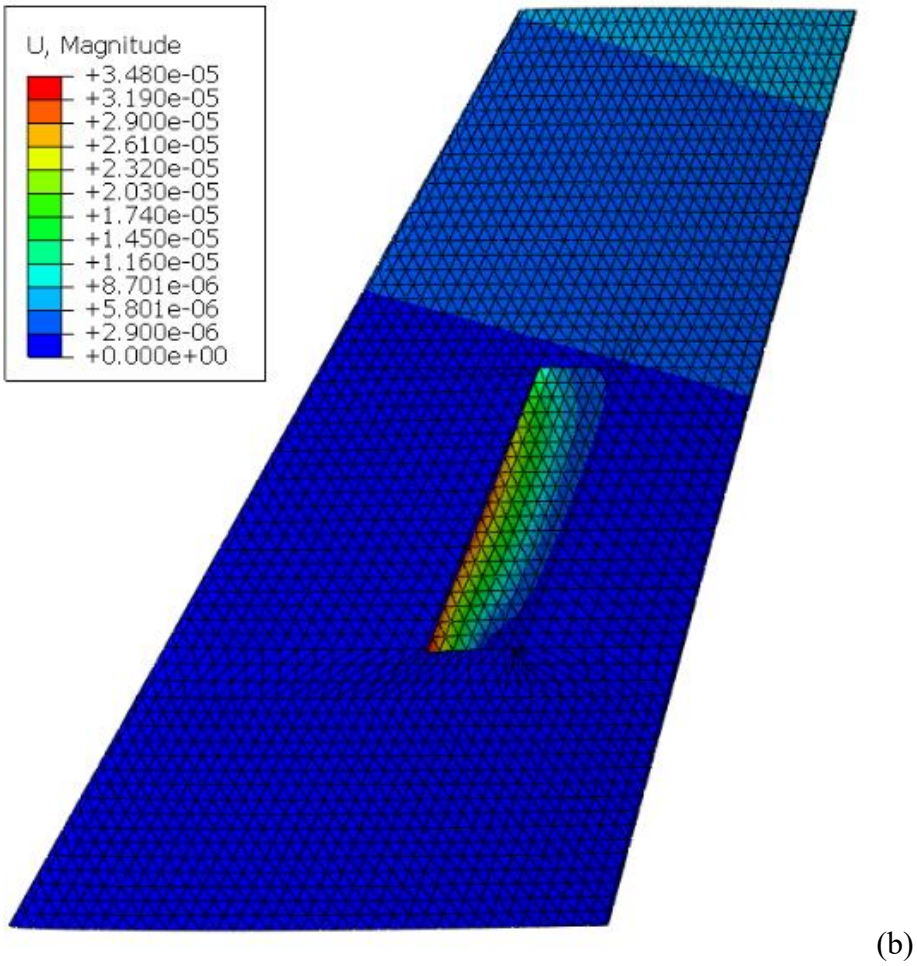


(b)

**Figure 2.5.** *Two visualisations of the displacements of the structure amplified by a scale factor of $10^3$.*

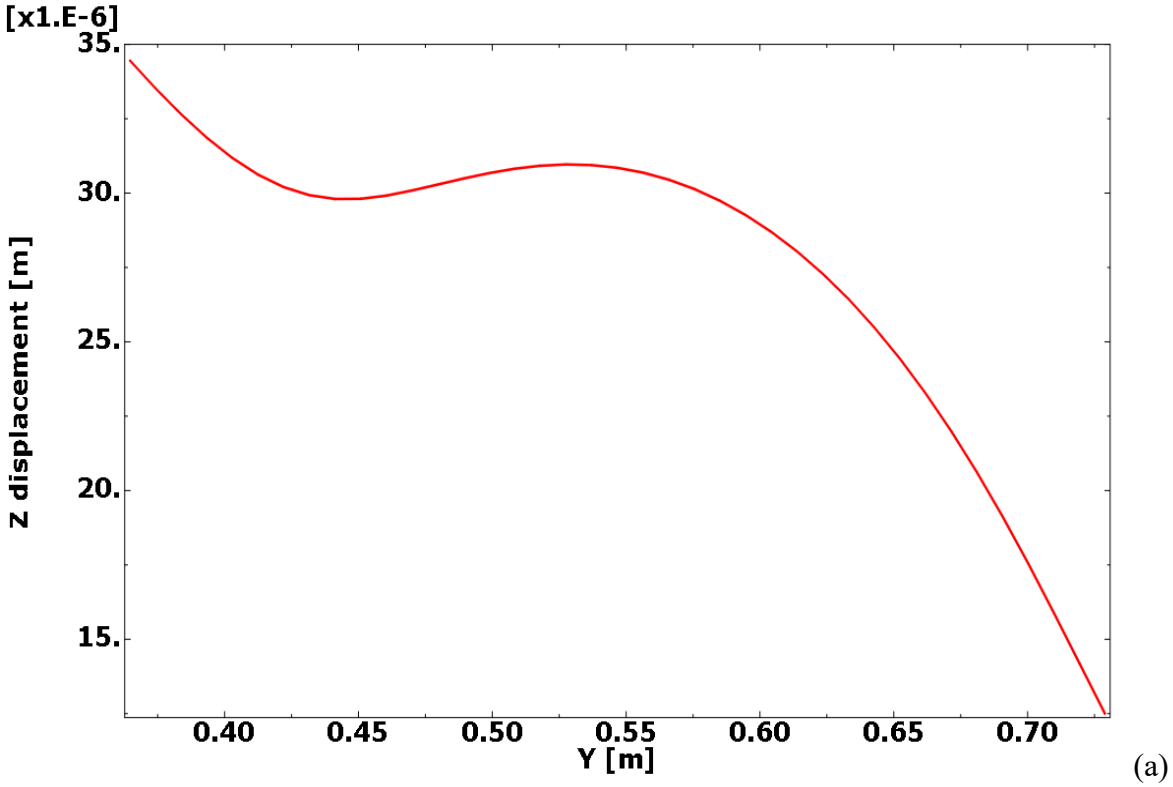


(a)

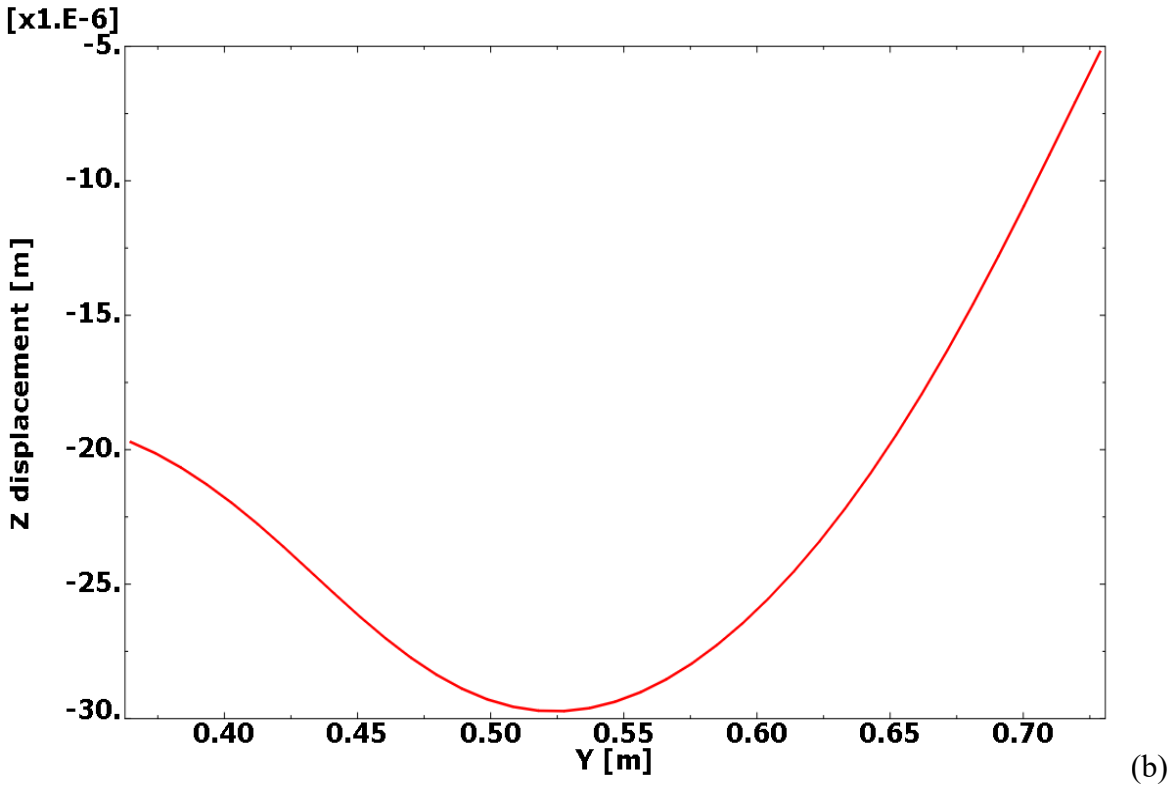


(b)

**Figure 2.6.** *Graphs in function of Y coordinate which represent the displacement in direction Z of the upper spoiler edge (a) and of the lower spoiler edge (b).*

As Figure 2.7 points out, the parts of the structure which have to withstand greatest stresses are the lateral edges of the spoiler. The tensile and compressive stresses due to the bending moments reach their maximum in the points where the edges of the device are connected to the main structure of the wing, as shown in Figures 2.8 and 2.9. Despite the thin thickness of the upper and lower spoilers, the stresses generated by the aerodynamic pressures are very low in comparison with the yield strength of the material of the wing. Indeed, the maximum stress in the structure (3.529 MPa) occurs in the node in which the lower spoiler is attached to the wing, while the aluminium alloy can bear more than 100 times of the stress before yielding (505 MPa), so the structure should resist very well to the static loads.

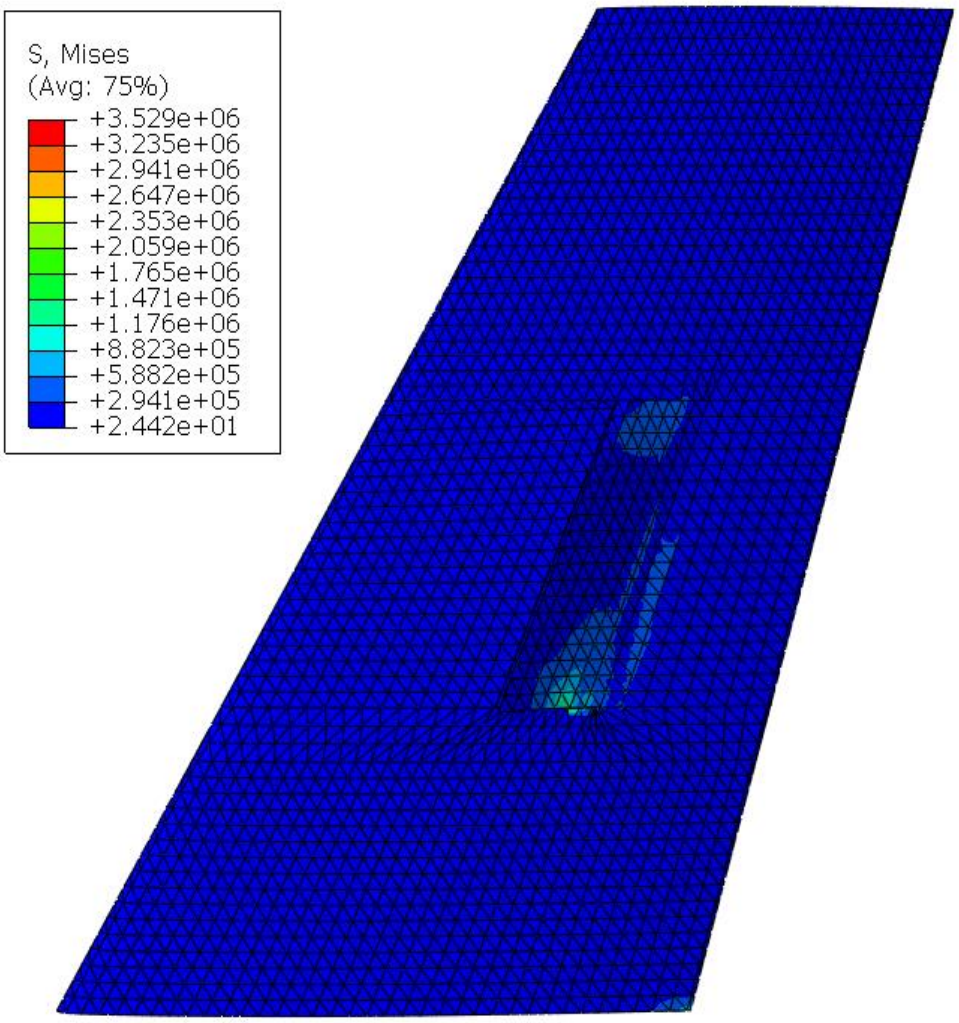


**Figure 2.7.** *Visualisation of the Von Mises stresses in the structure.*

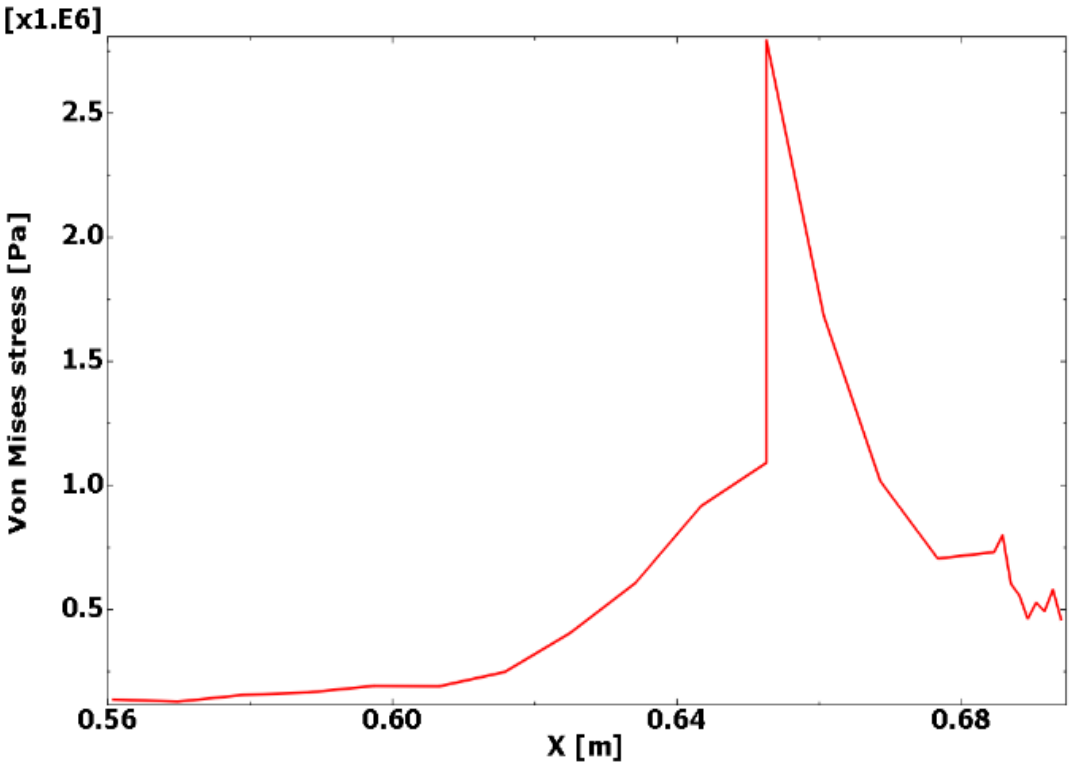


(a)

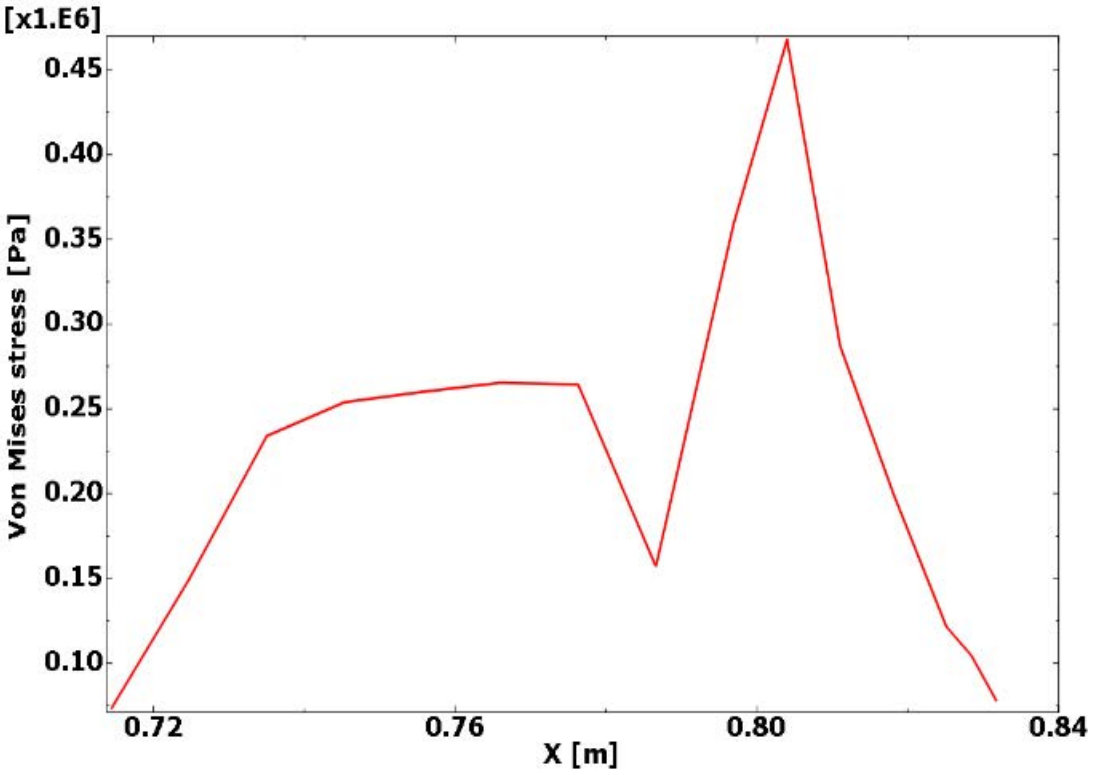


(b)

**Figure 2.8.** *Von Mises stresses in the lateral internal edges of the spoiler along X coordinate. (a) represents the stresses in the upper spoiler edges closer to the root section, instead (b) represents the stresses in the upper and spoiler edges farther from the root section.*

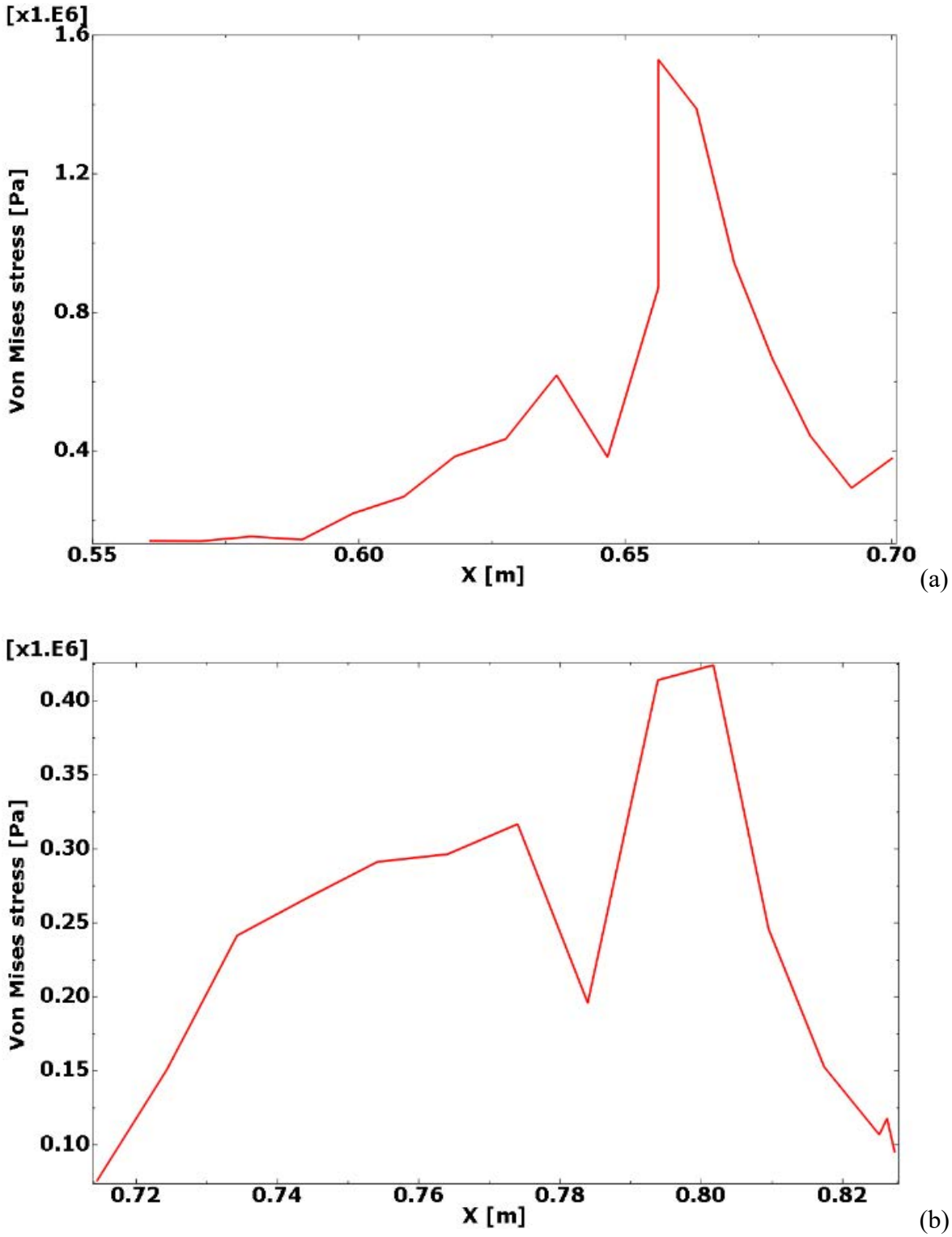


**Figure 2.9.** *Von Mises stresses in the lateral internal edges of the spoiler along X coordinate. (a) represents the stresses in the lower spoiler edges closer to the root section, instead (b) represents the stresses in the lower spoiler edges farther from the root section.*

The structure appears to be safely dimensioned, but the structural stresses could be intensified by vibrations. Therefore, the static analysis is not sufficient to assess the worst-case scenario and further analyses are required.

## 2.3 Modal analysis

First of all, a modal analysis was carried out to find the natural frequencies and the normal modes of the wing with the open spoiler. The modal analysis allows to foresee the most critical frequencies for the body and to understand the deformed shape of each normal mode. The first natural frequency, i.e. the lower natural frequency, belongs to the flexural mode of the wing, as depicted in Figure 2.10. However, the normal mode, which is worth studying in this work, is the second mode, because it involves mainly the inverted jet spoiler, as shown in Figure 2.11. The other modes are neglected, because they are unlikely to happen in physic reality. Furthermore, usually the mode harmonics with lower natural frequency contain most of the total energy of the system and it is easier to excite them since at the beginning the aeroelastic phenomenon involves vibrational motions with greater natural periods.

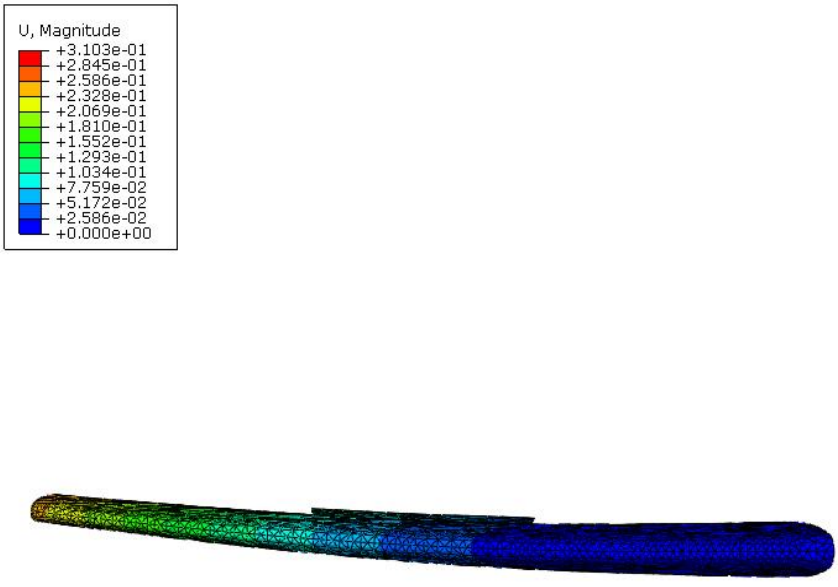


**Figure 2.10.** *The first normal mode which involves mainly the bending of the entire wing.*

The second vibrational mode is depicted in Figure 2.11. It can be noted that the movement of the upper and lower spoiler panels is antisymmetric with respect to XY plane, in spite of the symmetry of geometry. The central part along the spoiler span extent appears to be less stiff than the lateral ones, although the spoiler thickness remains constant.

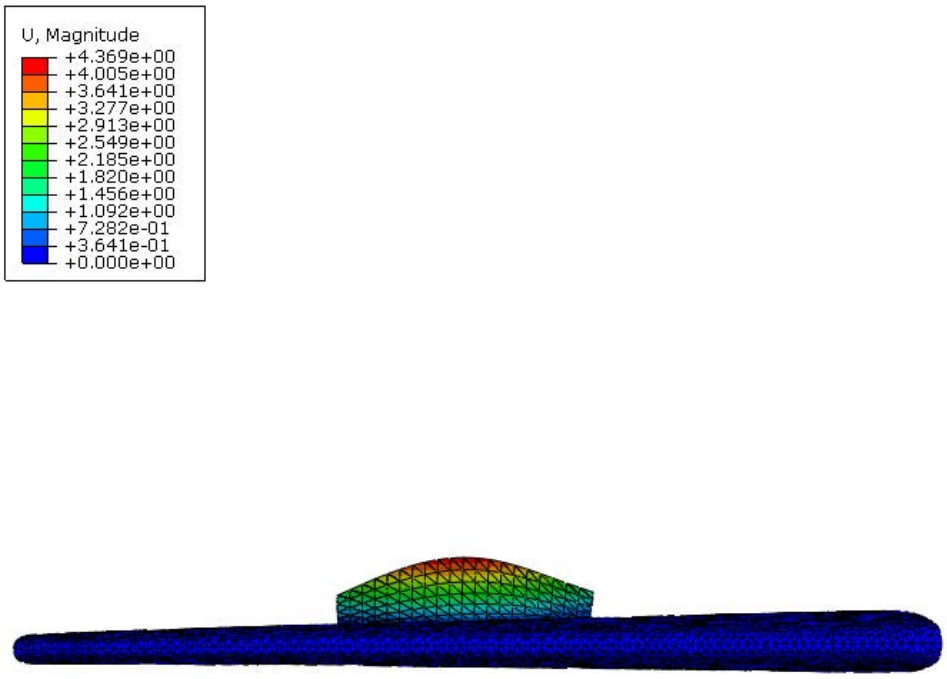


**Figure 2.11.** *The first normal mode (a) involves mainly the bending of the entire wing, the second normal mode (b) involves mainly the spoiler.*

Once the natural frequency of the second mode was found (161.57 Hz), it is used as frequency of the harmonic load for the dynamic analysis. Since the modal analysis is conducted without any partition of the body, there are some differences between the meshes of the two analyses and, consequently, the natural frequency and the frequency of the loads in the dynamic analyses are slightly different.

## 2.4 Dynamic analysis

A procedure similar to the static analysis is used for the dynamic analysis, but the loads are implemented to be the most dangerous ones for the structure. Through the modal analysis, it is possible to understand which part of the structure is more involved in each mode from the visualization of the normalized displacements of the modes. Thanks to that, the mode in which the spoiler is more stressed could be individuated and the condition of resonance was studied. Indeed, the dynamic loads are set to vary in time with a sinusoidal function in which the frequency is equal to one of the natural frequencies of the spoilers and the amplitude is equal to the static loads in the first case studied. The phenomenon is simulated for a total time of 1 s and a uniform time steps of 0.0006 s is used to compute the solution in at least 10 instants for every period of the harmonic function. Furthermore, comparing the boundary conditions of this work with the studies of Colakoglu [18], the critical damping factor is defined equivalent to 0.02% in the model. This value takes into account only the internal damping of the aluminium alloy, and not the damping due to the interaction between the structure and the air. This method analyses the worst-case scenario, because the lower the damping is, the higher the peak of resonance is.

As expected, the results highlight superior displacements and stresses in the body than in the static analysis, but the most critical parts of the structure are in the same position. The motion in Z direction of the central point of the upper and lower spoiler is shown respectively in Figure 2.12 and 2.13, and it can be noticed that the displacements follow the frequency of the harmonic load. Both spoilers also vibrate with a major frequency slightly above 3 Hz. Even if they are two of the nodes with the biggest displacements, the magnitude never overcomes 1.063 mm. One of the hypotheses standing behind the FEM static analysis is that the model is considered linear, and this assumption is verified because the displacements are very small in comparison with the dimensions of the wing.

The stresses due to the dynamic loads, in the node which connects the lower spoiler to the wing, are represented in Figure 2.14, and they follow the frequency of the external forces as well. Among all the nodes and all the instants, the maximum of the stresses does not overcome 73.33 MPa, so the structure should resist also in this case. Nevertheless, the fatigue life of the wing can have a great reduction as the frequency of the forced vibrations is quite high.

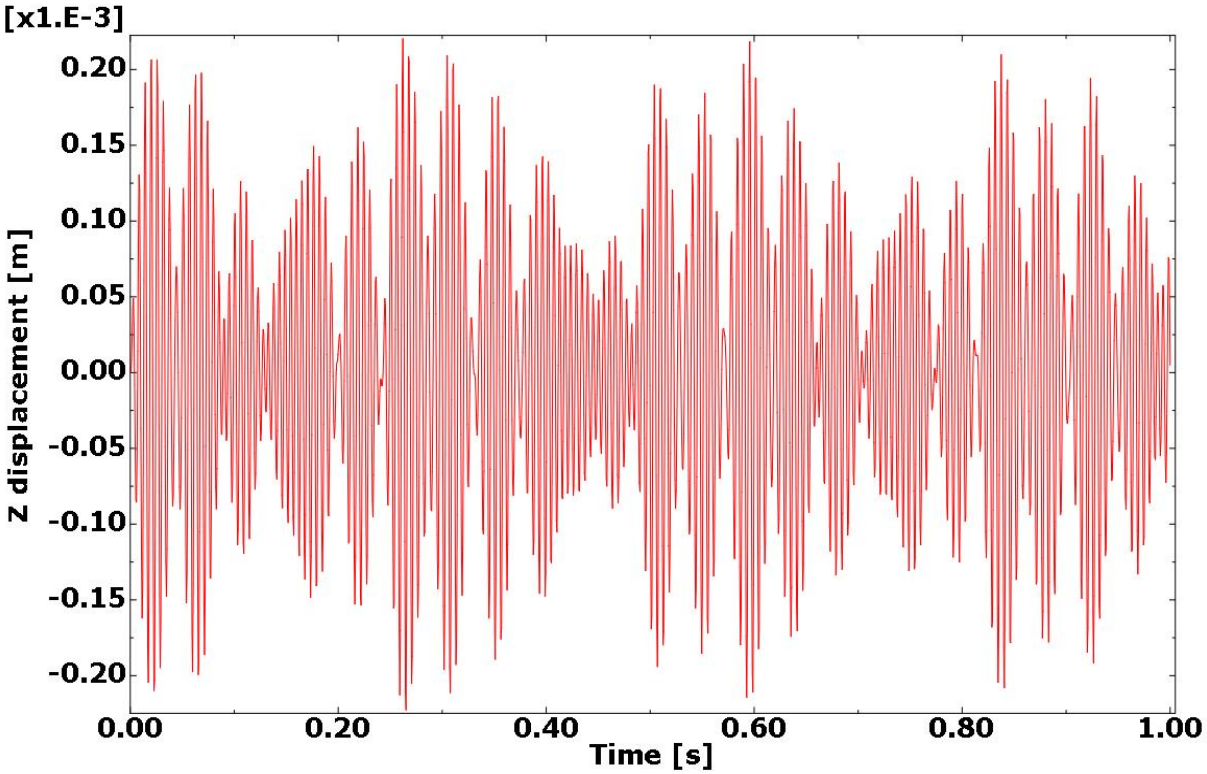


**Figure 2.12.** *Displacements in Z direction of the central node of the upper side of the spoiler as a function of time.*

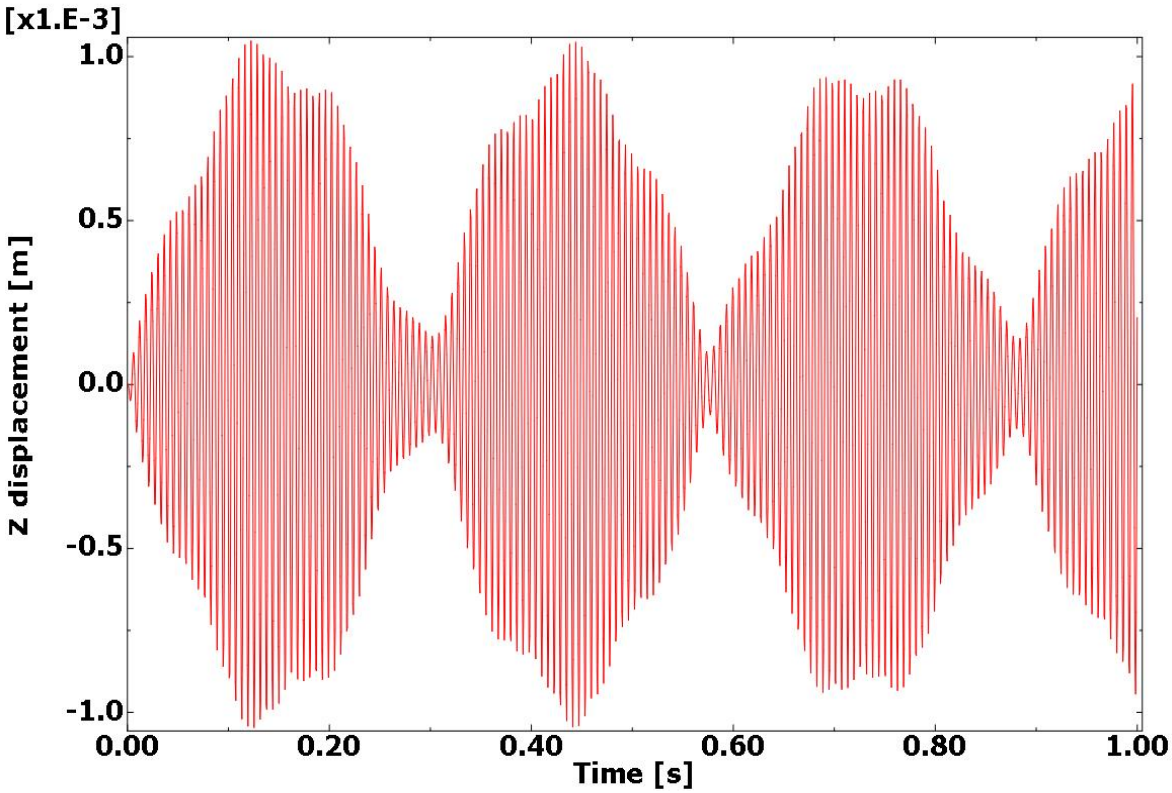


**Figure 2.13.** *Displacements in Z direction of the central node of the lower side of the spoiler as a function of time.*

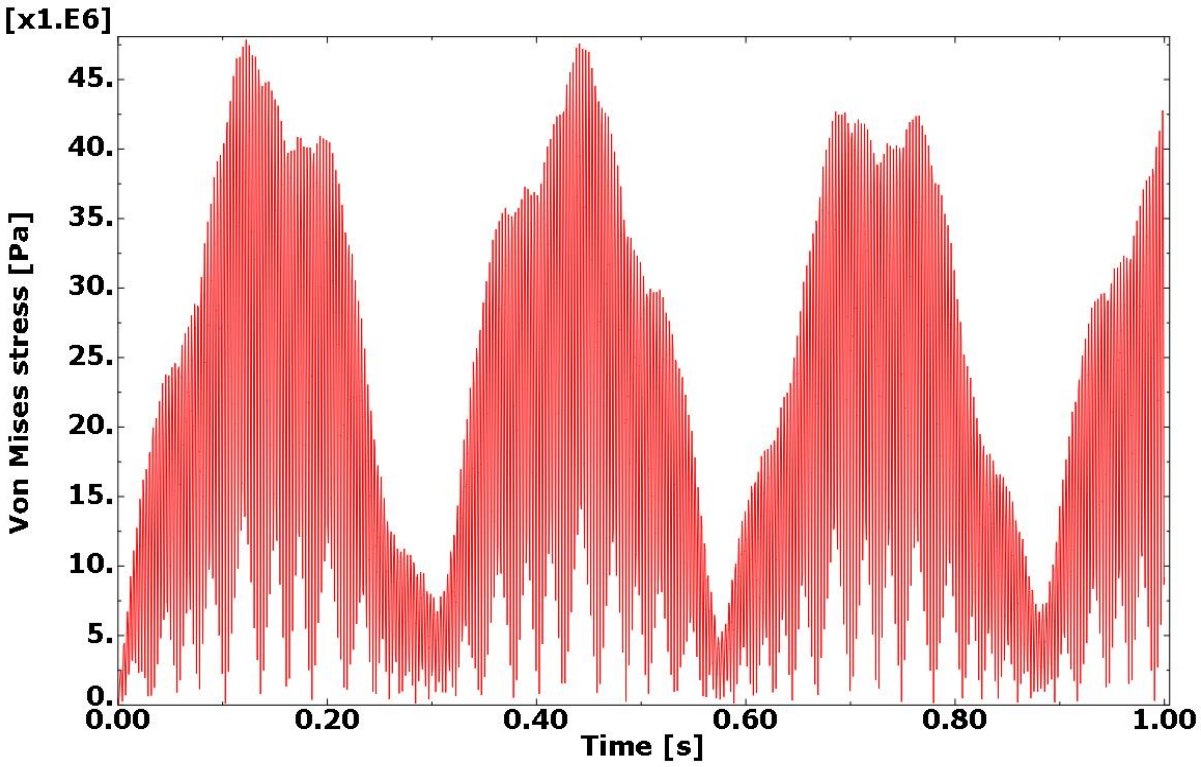


**Figure 2.14.** *Von Mises stress in function of time of the node closer to the fuselage which connects the lower side of the spoiler to the wing.*

The resonance condition amplifies about 30 times the displacements and about 15 times the stresses because of the low damping factor. However, it is highly improbable that the variation of the aerodynamic field synchronizes with the elevated natural frequency of the inverted jet spoiler.

## 2.5 Discussion of the results

The structural behaviour of the inverted jet spoiler was studied in some particular boundary conditions, and the stresses in the device never overcame the yield strength of the material, not even in the most critical dynamical case. However, the loads are quite heavily approximated because they were obtained from 2-dimensional data graphs and the pressure in the spoiler bypass was taken from a simulation with different wind conditions. In order to have more precise results, a new CFD simulation on the wing should be carried out so that the pressures can be imported in the structural model.

In this work, the forced vibrations of the structure were generated by loads which vary in time with a simple sinusoidal law. In physical reality, the vibrations of a body exposed to an air flow are created by the interaction between the fluid and the structure itself. De facto, the flow imposes some pressures on the surface of the wing and changes the deformation of the body, but the new deformed shape of the body modifies the fluid flow and the pressure distribution. This phenomenon is known as "aeroelasticity" because it involves the reciprocal interaction between the aerodynamic forces and the elasticity of the structure. The most important parameter is definitely the velocity of the air flow, and without the possibility to execute some experimental tests, the most accurate way to study this phenomenon is combining CFD and FEM simulations. Thus, some other analyses should be conducted to study more accurately the aeroelastic behaviour of the inverted jet spoiler varying the velocity and the angle of attack of the undisturbed flow.

# Chapter 3
# 2-dimensional aeroelastic analyses

In order to start studying the complex phenomenon of the inverted jet spoiler aeroservoelasticity, some 2-dimensional simulation are carried out, which are useful to verify the numerical results with the results obtained in the papers of Filippone [12,13] and to identify the worst loading case for the device. The preliminary case studied in ABAQUS had the heavy approximation of the definition of the loads from the graphs in [13], which implies inevitable errors in the data extrapolation. On the contrary, the coupling of the two programmes ANSYS and ABAQUS allows to transfer the static pressures which stand on the airfoil, calculated with the CFD programme, into the load case in the structural software ABAQUS. In this way, the method used is devoid of any human error and inaccuracy, and the results confidence is expected to be higher.
First, the consistency and robustness of the method is proved and the influence of the air flow velocity surrounding the inverted jet spoilers is studied. By the same token, the angle of attack and the inlet velocity were modified to have a preliminary idea of the aerodynamic and structural behaviour of the device in different flight phases.

## 3.1 Aerodynamic computational model

First, a 2-dimensional analysis of the airfoil with completely deployed spoilers was carried out to verify the numerical results with the ones obtained by Filippone [12,13]. The geometry is imported from the model of the 3-dimensional ONERA M3 wing, previously studied in ABAQUS, and the section in the middle of the spoiler is extracted, as shown in Figure 3.1. Even if the symmetric airfoil seems to be structurally divided in two parts, in the 3-dimensional case the spoilers have a limited length along the wing and structural continuity is achieved.

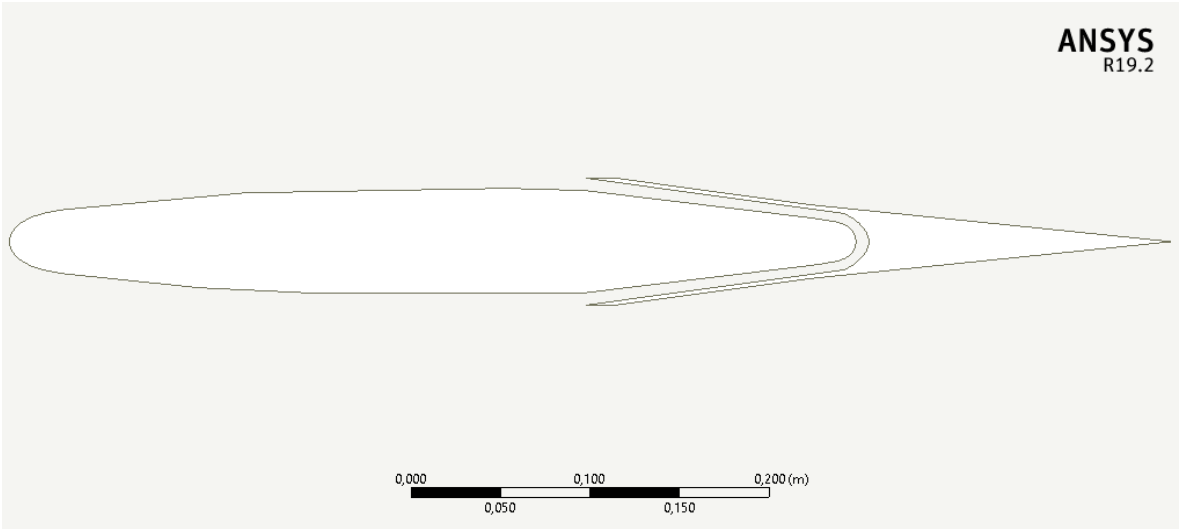


**Figure 3.1.** *Geometry implemented in ANSYS model.*

According to the study of Filippone [12], there is a suction peak behind the two spoiler leading edges and, as a result, the deflected panels tend to open further because of the aerodynamic forces. As shown in Figure 3.2, the worst-case scenario for the device from the structural point of view is the situation in which the spoiler hinge is located at a coordinate normalized with the chord length X/*c* =0.7. For this reason, the leading edge of the spoilers is positioned at X/*c* = 0.5 and the hinge at X/*c* = 0.7. The chord length is 0.65 m, meanwhile the channel height is 7.5 mm. The contour of the U-bend between the upper and lower spoilers is generated by using cubic splines because, in general, it is not possible to connect the spoilers with circular arcs. Nonetheless, the most critical parts of the structure are definitely the deployed panels thanks to which the configuration with the open channel is achieved, because their constant thickness is only 2.37 mm. The low stiffness of the spoilers is the reason why some structural simulations have to be carried out.

The 2-dimensional analyses of the spoiler aerodynamics are performed with a Reynolds-averaged Navier-Stokes (RANS) code with appropriate turbulence closures in ANSYS FLUENT. As the study [19] suggests, the far-field is placed at least at a distance 10 chords upstream and 15 chords downstream from the airfoil to obtain results acceptably accurate from the analysis.

The wall presence considerably affects turbulent flows because the mean velocity field must be equal to zero at the wall surfaces (no-slip condition). Furthermore, viscous damping decreases the tangential velocity fluctuations close to walls, while turbulence and mean vorticity are rapidly amplified toward the near-wall region because of large gradients in

mean velocity. Therefore, the near-wall modelling significantly impacts the fidelity of numerical simulations and an accurate description of the flow in the near-wall region determines successful aerodynamic predictions [20].

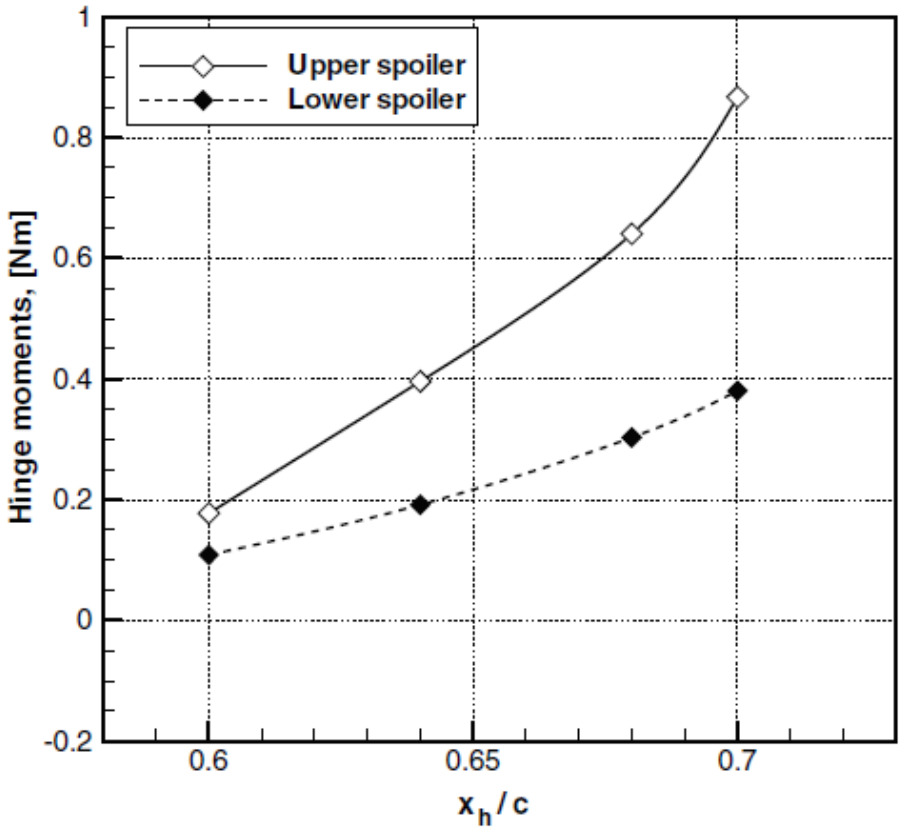


**Figure 3.2.** *Hinge moments for different hinge positions with α = 0° in the study of Filippone [12].*

The near-wall region can be essentially subdivided into three layers, as illustrated in Figure 3.3. In the zone closest to the wall, called "viscous sublayer", the molecular viscosity covers a dominant role and the flow is almost laminar. Turbulence begins to play a major role in the outer layer, called the “fully-turbulent layer”. Finally, there is an interim region between the viscous sublayer and the fully-turbulent layer, called “buffer layer”, where the effects of molecular viscosity and turbulence are equally important.

A fundamental parameter to distinguish the regions is the “dimensionless wall distance”, which can be defined as:

$$y^+ = \frac{y}{\delta_\nu} , \tag{3.1}$$

where $y$ is the distance from the wall and $\delta_v$ is the viscous length scale. $\delta_v$ is a measure of the viscosity of the fluid and is calculated with the following formula:

$$\delta_v = \frac{\nu}{U_\tau} \ . \tag{3.2}$$

$v$ is the kinematic viscosity, i.e. the ratio between the dynamic viscosity $\mu$ and the density of the fluid $\rho$, and $U_\tau$ is the shear velocity or friction velocity, which can be defined as:

$$U_\tau = \sqrt{\frac{\tau_w}{\rho}} \ , \tag{3.3}$$

where $\tau_w$ is the shear stress at the wall. Eventually, $y^+$ can be rewritten as:

$$y^+ = \frac{\rho \cdot U_\tau \cdot y}{\mu} \ . \tag{3.4}$$

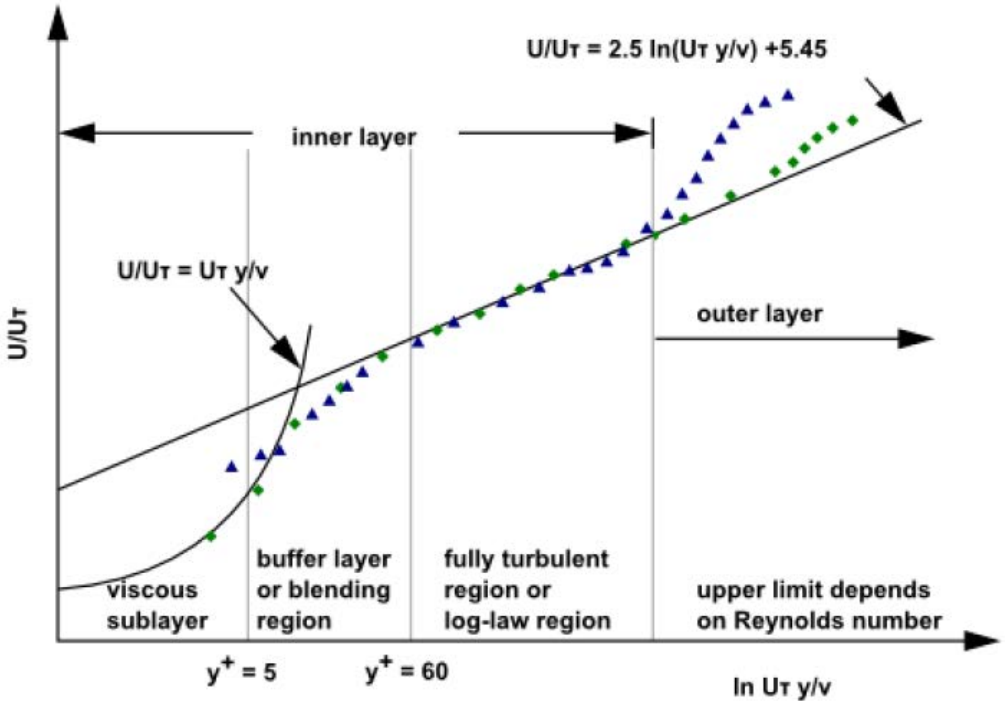


**Figure 3.3.** *Subdivisions of near-wall region plotted in semi-logarithmic coordinates [20].*

The sublayers in the near-wall region are conventionally classified depending on the $y^+$ value:

$y^+ < 5$ → viscous sublayer,

$5 < y^+ < 30$ → buffer layer,

$y^+ > 30$ → fully-turbulent layer.

In order to model the near-wall region, there are traditionally two approaches, as illustrated in Figure 3.4. In the first approach, the inner region which is influenced by viscosity, i.e. the viscous sublayer and the buffer layer, is not resolved, but semi-empirical formulas, denominated "wall functions", are used to link the region between the wall and the fully-turbulent region. The use of wall functions prevents the necessity to modify the turbulence models to account for the wall presence [20]. Nevertheless, the accuracy of numerical results decays if the first node near the wall lays inside the buffer layer. In other words, $y^+$ must be superior to 30 if a wall function is used. However, a more accurate approach, the "near-wall modelling" approach, involves the modification of the turbulence models to enable the viscosity-affected region to be resolved with a mesh all the way to the wall, including the viscous sublayer [20]. In this case, $y^+$ has to be near the value of 1 in all the surfaces exposed to the flow.

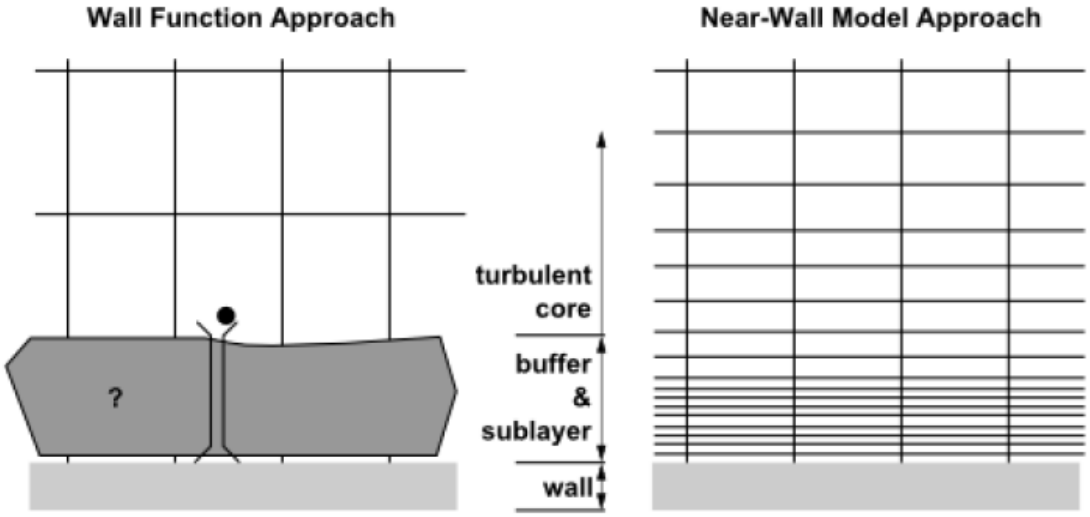


**Figure 3.4.** *Two approaches for the near-wall treatment [20].*

k-ε models are almost independent on the inlet flow conditions, but they are less accurate evaluating the boundary layer separation near the wall. Therefore, this kind of models are principally valid for turbulent flows in the regions adequately far from walls. On the other hand, provided the proper near-wall mesh resolution, k-ω models were designed to be applied throughout the boundary layer because they describe more accurately the influence

of the pressure gradient on the boundary layer. However, these methods are very sensitive to the inlet conditions. The shear-stress transport (SST) k-ω model was developed to effectively blend the robust formulation of the k-ω model in the near-wall region with the accuracy of the free-stream representation in the k-ε model [20]. With respect to k-ω model, the formulation of k-ε model contains only an additional term, which can be multiplied by a blending function to unify the two models. The blending function is designed to be 1 in the near-wall region to activate the k-ω model, and 0 away from the surfaces, so that the k-ε model equation could be solved there. These features make the SST k-ω model more accurate and reliable for a wider class of flows, e.g. adverse pressure gradient flows, airfoils, transonic shock waves [20].

For the SST k-ω model, the $y^+$ value of the first cell height must be near 1 to accurately capture the gradients of velocity in the near-wall region, but this value cannot be known *a priori,* and this makes difficult to generate a good quality mesh. However, the $y^+$ value can be estimated from the previously given definitions:

$$y^+ = \frac{\rho \cdot y}{\mu} \cdot \sqrt{\frac{\tau_w}{\rho}} \quad . \tag{3.5}$$

The only unknown is the shear stress at the wall, but $\tau_w$ can be obtained from the skin-friction coefficient $C_f$ as:

$$\tau_w = \frac{1}{2} \cdot C_f \cdot {U_\infty}^2 \quad , \tag{3.6}$$

where $U_\infty$ is the free stream velocity. To estimate the skin-friction coefficient, some empirical formulas are used and for this work the following experimental validated rule [21] has been considered:

$$C_f = \frac{0.074}{Re^{0.2}} \quad . \tag{3.7}$$

Even though this formula is valid for turbulent flows over a flat plate, it could be a useful tool to estimate the skin-friction coefficient and, subsequently, the first cell height $\Delta y_1$. *Re* is the Reynolds number which is defined as:

$$Re = \frac{\rho \cdot U_\infty \cdot L}{\mu} \quad . \tag{3.8}$$

$L$ is the characteristic length, which can be considered the chord length $c$ for an airfoil.
The 2-dimensional analysis developed by Filippone [12], was carried out with the wind conditions of Mach number $M$ = 0.25 at an altitude of $h$ = 500 m. With reference to the International Standard Atmosphere [2], the aerodynamic variables are displayed in Table 3.1.

**Table 3.1.** *Air properties obtained from International Standard Atmosphere table [2].*

| $h$ [m] | $p_\infty$ [Pa] | $\mu$ [Pa·s] | $\rho_\infty$ [kg/m$^3$] | $a$ [m/s] |
|---|---|---|---|---|
| 500 | 95460.8 | 0.00001796 | 1.167 | 338.37 |

The velocity $U_\infty$ of the undisturbed air flow could be easily calculated from the speed of sound a and the Mach number M as:

$$U_\infty = a \cdot M = 84.59\ m/s \ . \tag{3.9}$$

With these data it is possible to estimate the first cell height which should be implemented in the mesh if the target for the $y^+$ value is 1:

$$\Delta y_1 = \frac{\mu}{\sqrt{\rho} \cdot y^+} \cdot \sqrt{\frac{1}{0.5 \cdot \frac{0.074}{Re^{0.2}} \cdot {U_\infty}^2}} = 5\ \mu m \ . \tag{3.10}$$

If the geometry and the flow modelled are quite simple, often this correlation is very accurate, but for more complex analysis a refinement in the near-wall region could be required to achieve the desired $y^+$ value.
Following the previously described design features, three unstructured meshes are generated with ICEM CFD varying the number of blocks divisions and, for instance, the mesh with the medium number of elements is shown in Figures 3.5-7. The mesh generator of the ICEM CFD programme allows to create quadrilateral cells which can follow the shape of the sharp wing trailing edge and the sharp spoilers leading edges reducing the number of required elements.

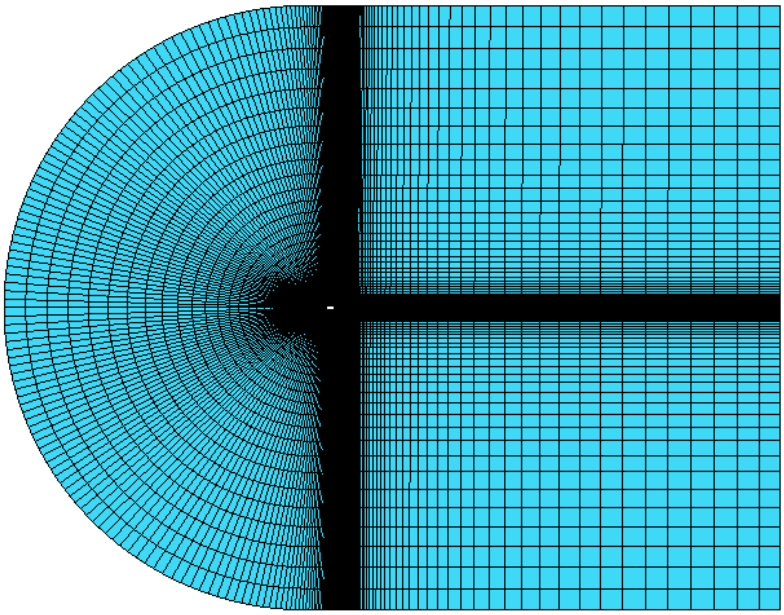

**Figure 3.5.** *Complete medium mesh generated in ICEM CFD.*

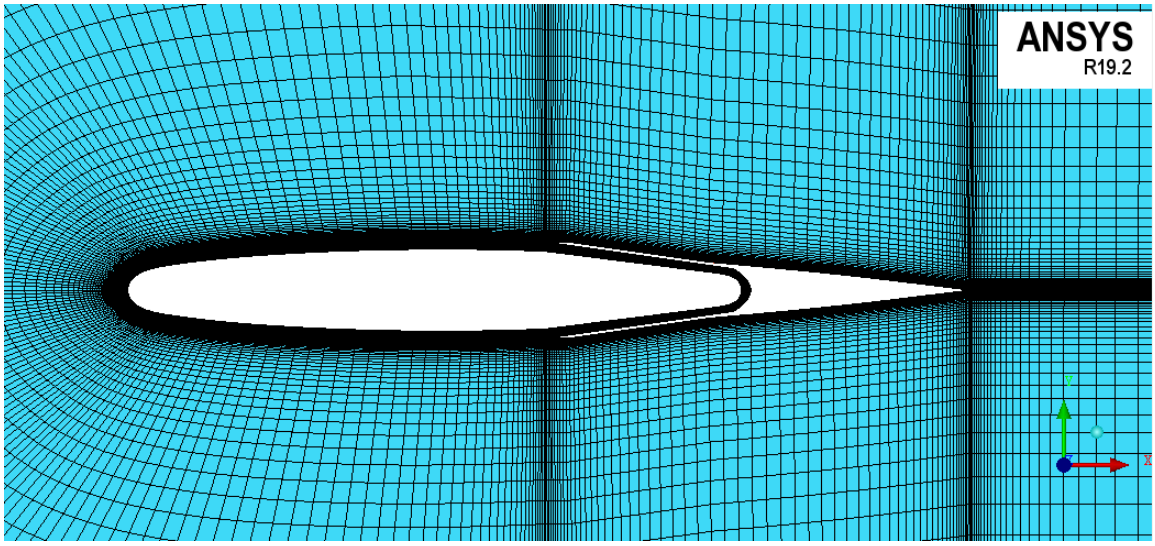


**Figure 3.6.** *Medium mesh around the airfoil generated in ICEM CFD.*

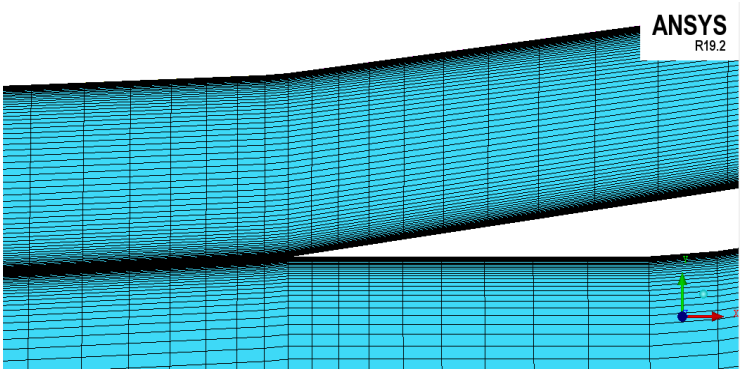


**Figure 3.7.** *Particular of the lower spoiler inlet vent of the medium mesh generated in ICEM CFD.*

The SST k-ω equations are used in the analysis presented because of their high accuracy for the kind of studied flow. The air properties at different altitudes are inserted thanks to the Standard Atmosphere data [2]. The wing surfaces are associated with a no-slip boundary condition and the inlet velocity is set up with different speed intensities and different angles of attack to study the inverted jet spoiler aerodynamic and structural behaviour. The SIMPLE algorithm allowed to obtain the pressure and velocity coupling and all equations are spatially discretised with second order upwind scheme.

## 3.2 Model verification

In order to check the consistency of the implemented model, a test of grid refinement for a given spoiler configuration is run. The drag and lift coefficients are monitored for the three different built meshes:

- Coarse mesh: 67 015 cells
- Medium mesh: 124 429 cells
- Fine mesh: 209 792 cells

The angle of attack was set to $0^o$ in order to obtain a symmetric flow and the wind conditions were set to number of Mach $M = 0.25$, so that the inlet velocity is $U_\infty = 84.59$ m/s, at an altitude of $h = 500$ m, which correspond to a low speed maneuver at low altitude for fixed wing aircraft. The drag coefficient $C_d$ and lift coefficient $C_l$ convergence history of the meshes can be observed in Figures 3.8 and 3.9 respectively.

Once 100 iterations are completed, the difference in the drag coefficient $C_d$ between the three models is considered to be negligible. The lift coefficient $C_l$ is converged to 0, as expected for a symmetric airfoil, in only 50 iterations. These results demonstrate the model mesh-independency and guarantee a good confidence in the successive analysis. In the three analyses, the wall $y^+$ never overcomes the value of 1, thus the aerodynamic variables are well represented from the model, even in the near-wall region, because the first cell height lays surely in the viscous sublayer.

In this research, the most meaningful result which can be obtained from the aerodynamic analysis is the static pressure profile throughout the surfaces of the wing and the spoiler. The pressure distribution is symmetric with respect to the X-axis because of the symmetry of the

geometry and the velocity inlet boundary conditions. As the contour in Figure 3.10 points out, the pressure distribution inside the bypass is essentially constant within the spoiler area since the pressure gradients along the length and the height of the channel are considerably lower than the ones outside the spoilers. In Figure 3.10, the suction peaks can be easily seen near the spoiler leading edges and this leads to a hinge moment that tend to open ulteriorly the panels.

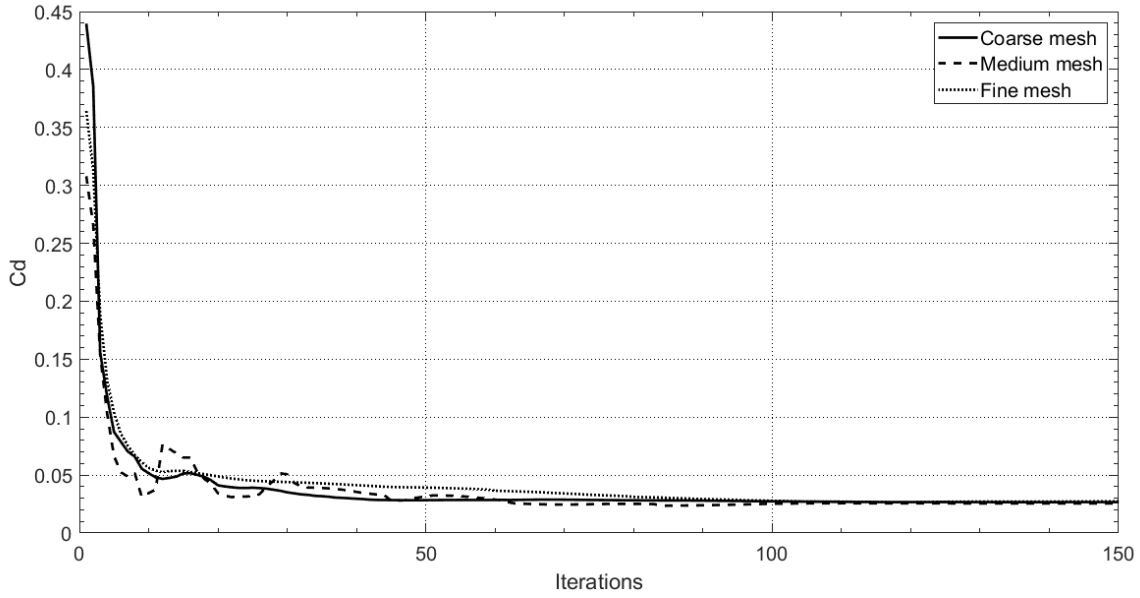


**Figure 3.8.** *Drag coefficient $C_d$ convergence history for the coarse (solid line), medium (dashed line) and fine (dotted line) meshes.*

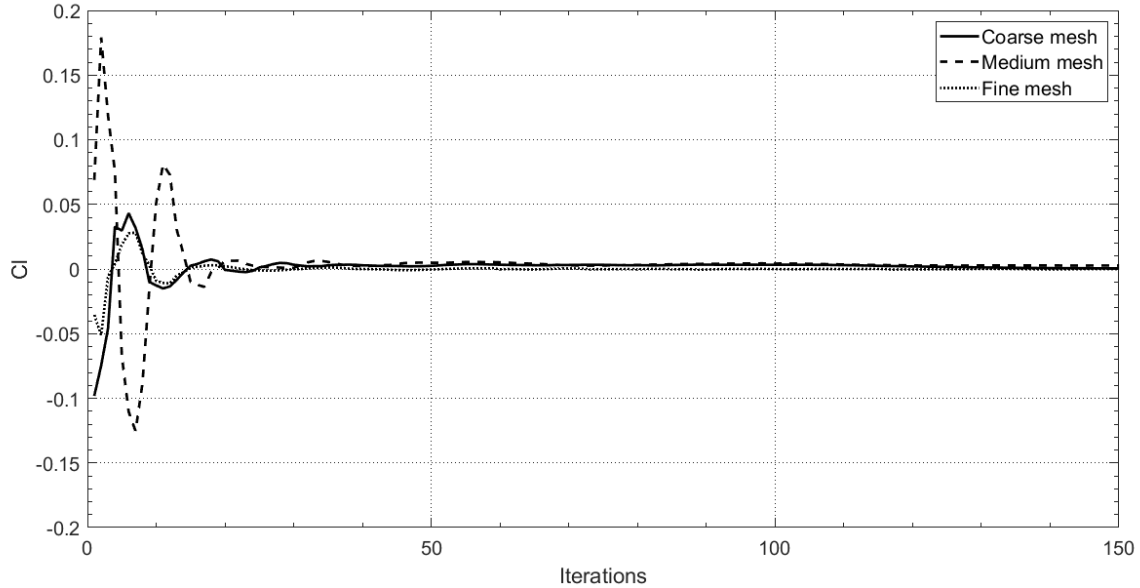


**Figure 3.9.** *Lift coefficient $C_l$ convergence history for the coarse (solid line), medium (dashed line) and fine (dotted line) meshes.*

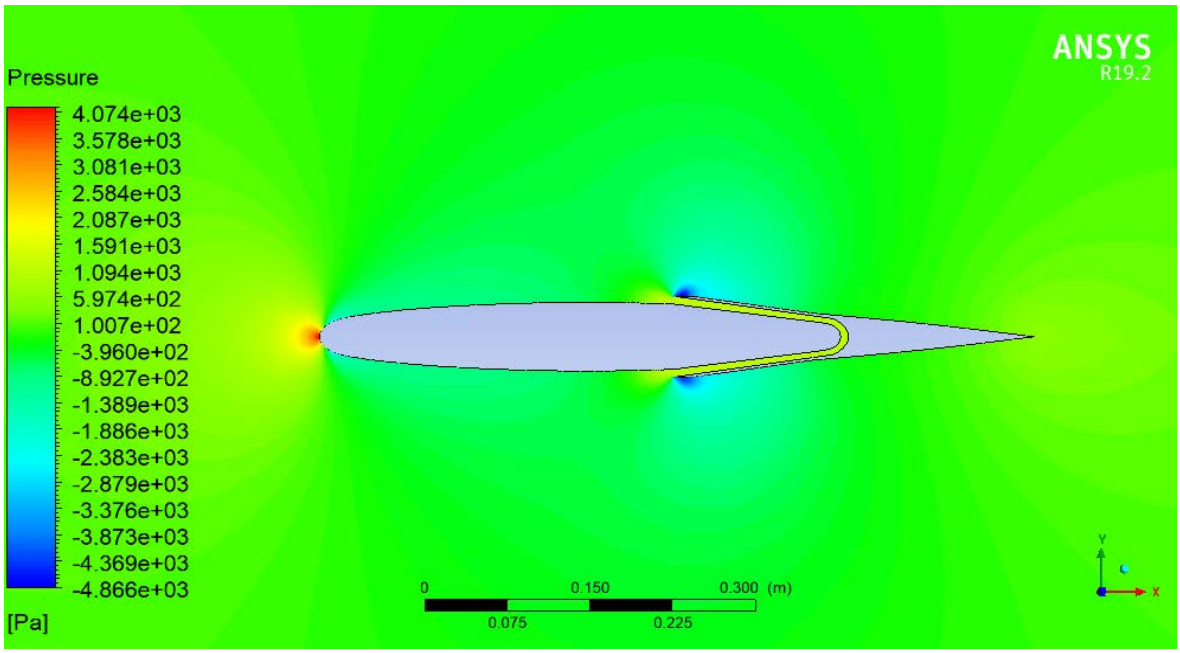


**Figure 3.10.** *Contour of static pressure for the medium mesh in the case of an angle of attack of 0°.*

In Figure 3.11 the static pressure along the chord length of the airfoil top surface is represented. Due to the model symmetry, the pressure distribution of the lower surface overlaps the plotted graph. The discontinuity caused by the presence of the spoiler is well visible in Figure 3.11 between X/*c* = 0.5 and X/*c* = 0.7.

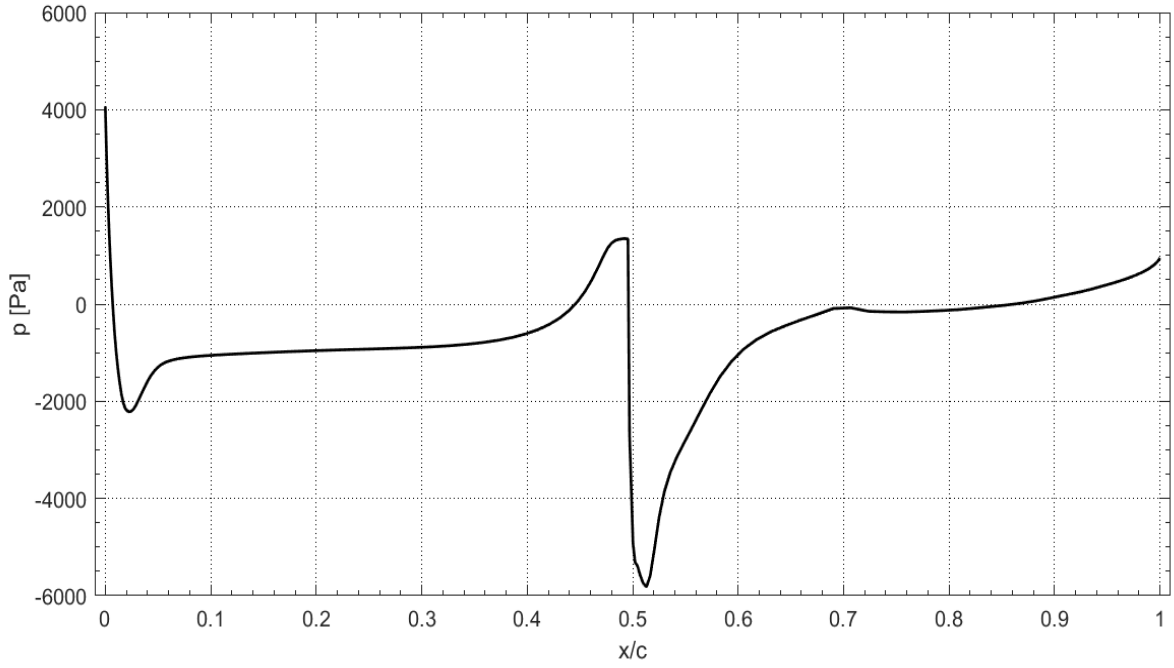


**Figure 3.11.** *Static pressure along the X-coordinate normalized with the chord length.*

The maximum static pressure (4067 Pa) is located at the airfoil leading edge, while the minimum pressure is -5820 Pa in the suction peak in the external side of the spoiler (X/*c* = 0.51). The numerical results obtained are very similar to the 2-dimensional study of Filippone [12] and the small differences can be assimilated to the different airfoil used in his study.

Subsequently, the 2-dimensional geometry and the pressure distribution are imported in ABAQUS. The preliminary analysis in ABAQUS pointed out that the displacements in the wing structure are considerably small in comparison with the spoiler panels, which are the most critical zones because of their limited thickness. Therefore, the wing spanwise flexural behaviour, which in a 2-dimensional case results in vertical displacements, and the chord-wise flexural behaviour can be safely neglected. In order to take into account only the structural behaviour of the spoilers, 4 fixed supports are set up along the axis of symmetry (X axis) as shown in Figure 3.12. This kind of boundary conditions blocks the wing movement but allows the free displacement of the device under the aerodynamic pressure forces. For this reason, a finer structural mesh is built in the spoiler area to capture more accurately the strains and the stresses that arise in that region. Furthermore, the properties of AA7075-T6 aluminium alloy, displayed in Table 2.1, are used in the model and a static analysis is carried out, similarly to what was done in Paragraph 2.2.

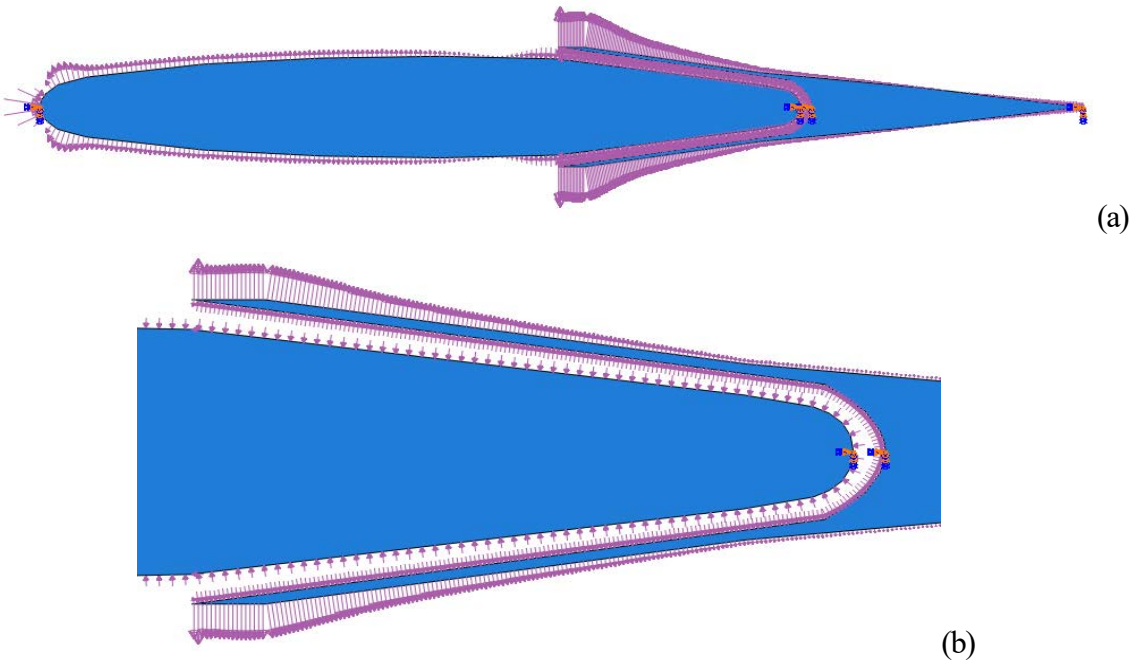


**Figure 3.12.** *Transfer of static pressure in ABAQUS (a) for the complete wing and (b) for the spoiler. The imposed encastres are visible as well.*

The structural results are symmetric as expected, but there is a great increase in displacements and, consequently, in stresses in comparison to the case previously studied in ABAQUS. This is due to an underestimation of the loads in the preliminary analysis. As shown in Figure 3.13, the spoiler leading edge undergoes a 2.37 mm displacement, which can easily cause a significant modification of the aerodynamic field and trigger the aeroservoelasticity vibrational phenomenon. However, the maximum stress does not overcome 30 MPa, which is not even close to the yield strength limit of the wing aluminium alloy.

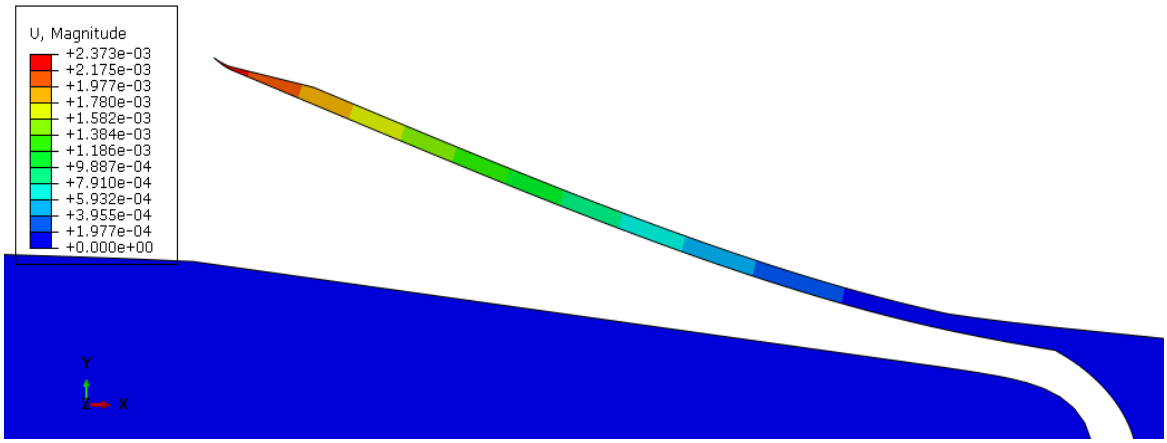


**Figure 3.13.** *Displacements in [m] of the upper spoiler amplified by a scale factor of 10. The displacements of the lower spoiler are symmetric with respect to the X axis.*

Figure 3.14 shows the tendency of the upper spoiler to open up. The spoiler load is comparable with a typical bending moment: the region in the upper side near the zone where the spoiler panel is attached to the airfoil is subjected to compressive stress, while the lower one experiences tensile stress. Therefore, if any fracture occurs, it will likely start from the point in the lower side with the maximum stress for the upper spoiler. This discussion is valid for the lower spoiler as well, given that everything is mirrored with respect to the X axis for symmetry. The vertical displacement and the Von Mises stress along the most critical zone of the device, e.g. the lower side of the upper spoiler, can be seen in the graphs of Figures 3.15 and 3.16.

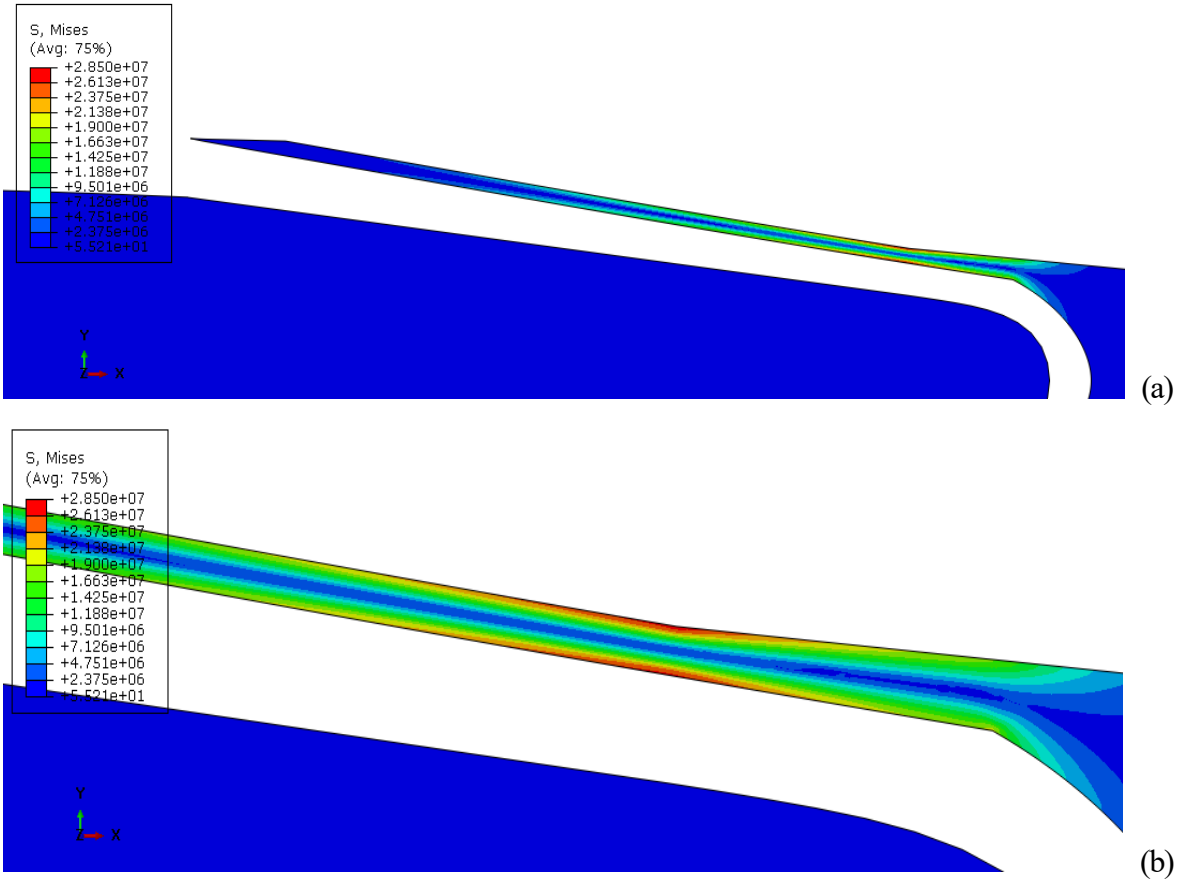


**Figure 3.14.** *Von Mises stress in [Pa] throughout the whole spoiler (a) and in the most stressed zone (b). Spoiler deformation is not scaled.*

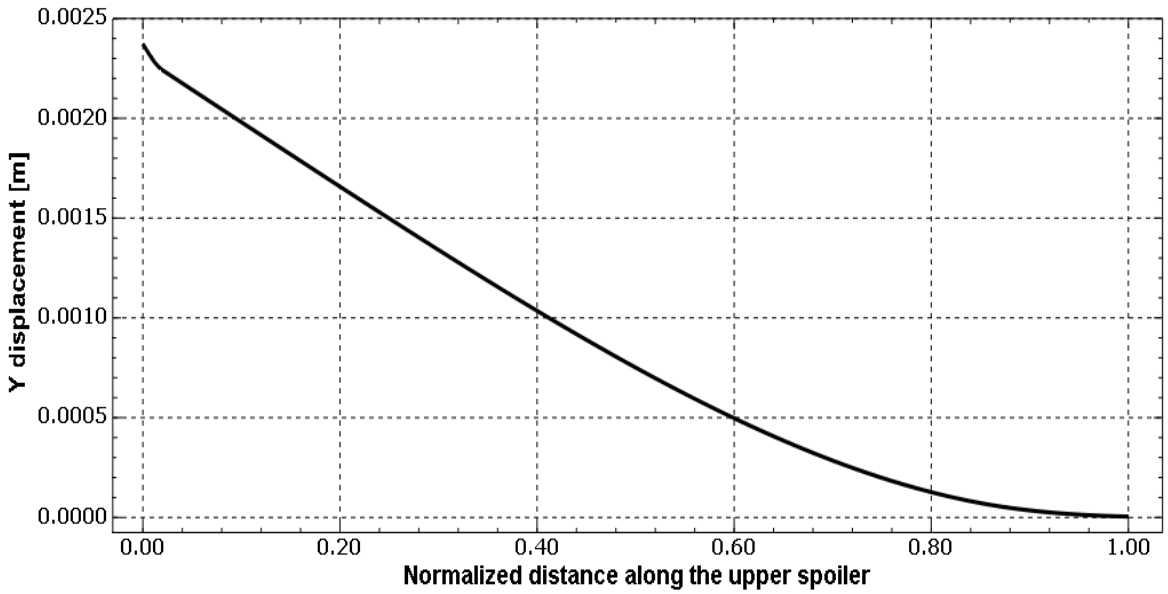


**Figure 3.15.** *Y displacement (a) and Von Mises stress (b) along the lower side of the upper spoiler.*

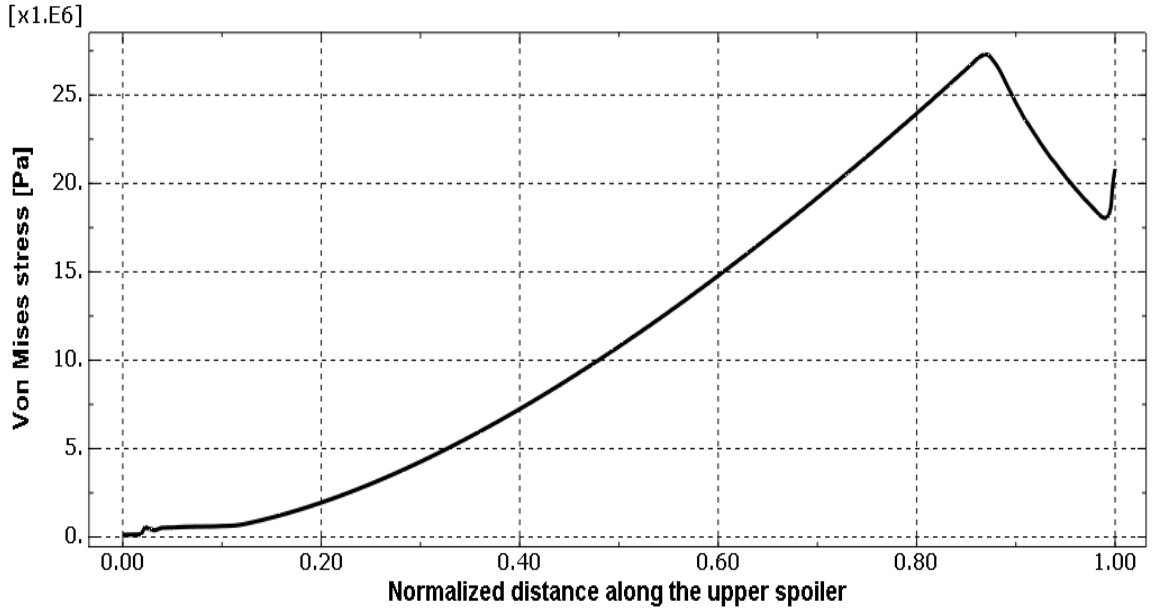


**Figure 3.16.** *Von Mises stress along the lower side of the upper spoiler.*

The underlaying hypothesis is that the opening mechanism is capable of applying perfectly the required hinge moment to maintain the desired deflection. Indeed, the spoiler maximum stress is not applied on the hinge point, but at a certain distance from it, as shown in Figure 3.16.

## 3.3 Comparison with the reference case of study

Another numerical test has been run to check the consistency of the results. In [13] Filippone studied the 3-dimensional spoiler aerodynamics in the case with an angle of attack $\alpha = 4^{o}$ and a number of Mach $M = 0.25$, which correspond to a low speed maneuver at low altitude for fixed wing aircraft. In Figure 3.17 the pressure coefficient $C_p$ along the chord length is represented at the wing section in a spanwise coordinate normalized with the span length $Z/b = 0.44$. The presence of the device significantly affects the pressure and velocity distributions, particularly in the chordwise central region where the discontinuities at $X/c = 0.5$ indicate the locations of the spoilers leading edges. Because of the increment of the surfaces exposed to the air flow, the drag increases when the inverted jet spoiler is operating with respect to the configuration with closed spoilers, while the lift and pitching moment magnitudes slightly decrease [13].

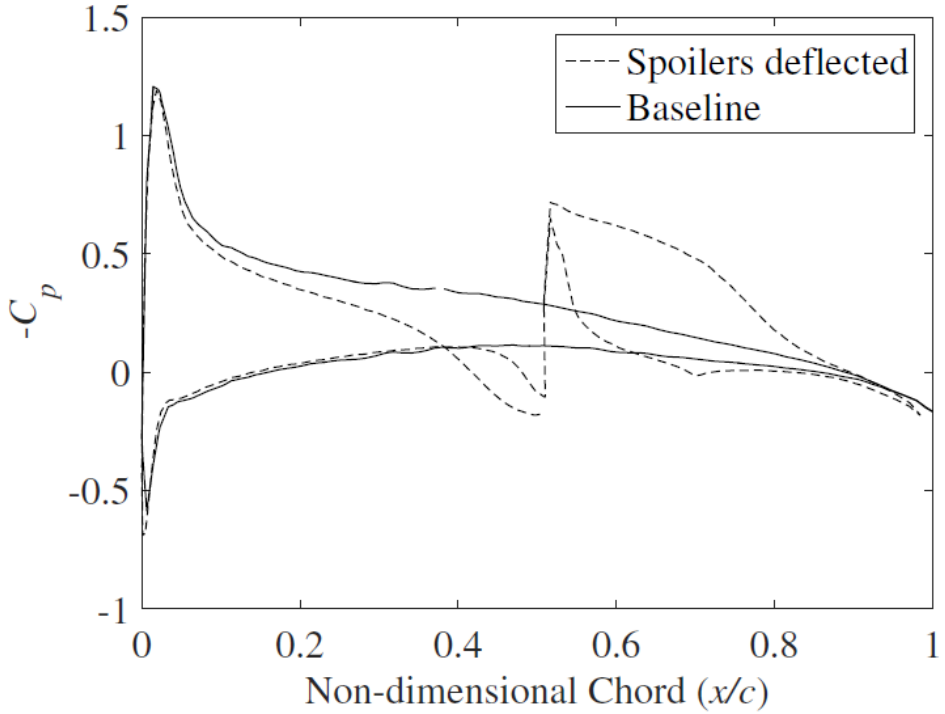


**Figure 3.17.** *$C_p$ reference distribution along the non-dimensional chord in the middle of the spoiler (Z/b = 0.44) with closed spoilers (solid line) and with deflected spoilers (dashed line) [13].*

Changing the angle of attack modifies the velocity distribution around the airfoil surfaces, especially in the suction side where the flow tends to accelerate more than the previous case studied. Subsequently, although the same mesh was used, in some regions in the upper surface of the wing the wall $y^+$ increased to 10, which is an unacceptable value for the SST k-ω model. Therefore, new meshes were built iteratively decreasing the first cell height $\Delta y_1$, in order to achieve again $y^+ \approx 1$ in all the wall surfaces. The result of this procedure is that $y^+$ does not overcome values of 1.1 if $\Delta y_1 = 1$ µm. The static pressure around the airfoil obtained with the new mesh features is showed in Figure 3.18.

The static pressure, which was exported in ABAQUS, is plotted in Figure 3.19 as well. The shape of this graph can be compared with Figure 3.17, which can be considered the reference case of study. In both the analyses, the pressure before the spoiler increases and reaches a maximum, after the spoiler, instead, the pressure jumps to a negative value and starts increasing again. There are some small differences near the channel inlet and in the suction side near the trailing edge which may be caused by the different dimensionality of the models and slightly diverse geometry, but the global similarity of the two curves guarantees a good confidence in the aerodynamic results.

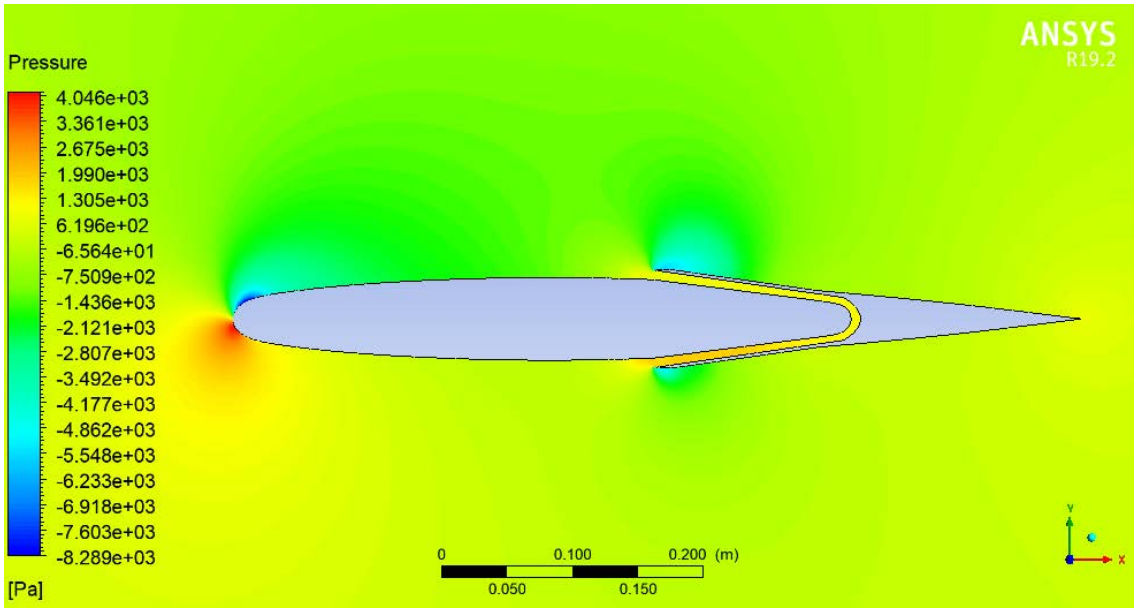


**Figure 3.18.** *Contour of static pressure with an angle of attack of 4°.*

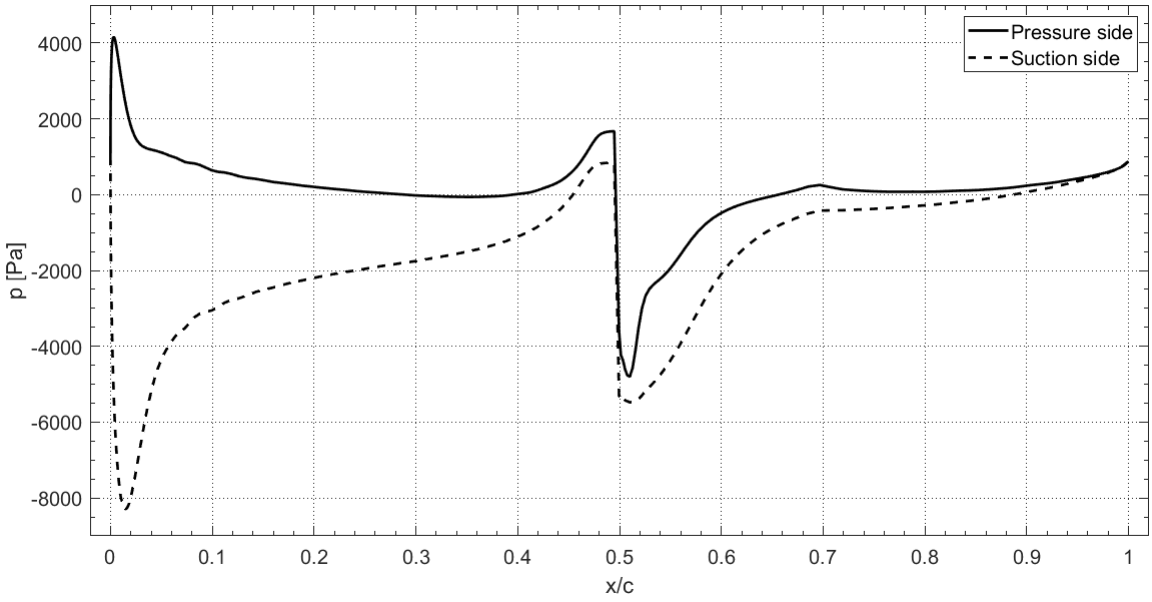


***Figure 3.19.*** *Static pressure obtained from the 2-dimensional analysis with α = 4º.*

The static analysis in the structural spoiler highlights a similar behaviour to the one previously studied, but the maximum displacement (2.886 mm) occurs in the upper spoiler tip. The maximum tensile stress increases to 32.85 MPa in the lower side of the upper spoiler. The lower spoiler is less stressed with respect to the case with angle of attack α = 0º, but the decrement in the displacement and in the stress is very small compared to the increment of the same quantities in the upper spoiler. However, the stress still does not reach the yield strength limit of the aluminium alloy.

## 3.4 Parametric study in the angle of attack for a low speed maneuver at low altitude

The 2-dimensional structural behaviour of the device has been studied at different angles of attack by using the same mesh implemented for the case of $\alpha = 4^{o}$. If the angle of attack changes, the velocity distribution is modified as well as the pressure around the airfoil and inside the spoiler channel. Since the wing geometry with the device is very complex, it is hard to predict in which way the velocity distribution changes around the body. In a simple airfoil, augmenting the angle of attack means that in the suction side the air flow tends to increase its velocity and to decrease its pressure, and vice versa for the pressure side. Thus, the upper spoiler may be exposed to an air flow with higher velocity and there the stresses should be higher. Furthermore, the displacements in the lower spoiler are expected to be smaller than the symmetric case with no angle of attack. However, there is also a contribution of the aerodynamic forces in the device internal side to the deformation of the inverted jet spoiler. Indeed, the pressure inside the channel, which stands on the spoiler panel, creates a net force that can increase or oppose to the tendency of the spoiler to open up.

In all the analyses, the wall $y^{+}$ amplifies with the increment of the angle of attack, but it never overcomes the value of 1.5 in all the wing surfaces, even in the case $\alpha = 8^{o}$. The static pressures of the new cases are represented in Figures 3.20-22.

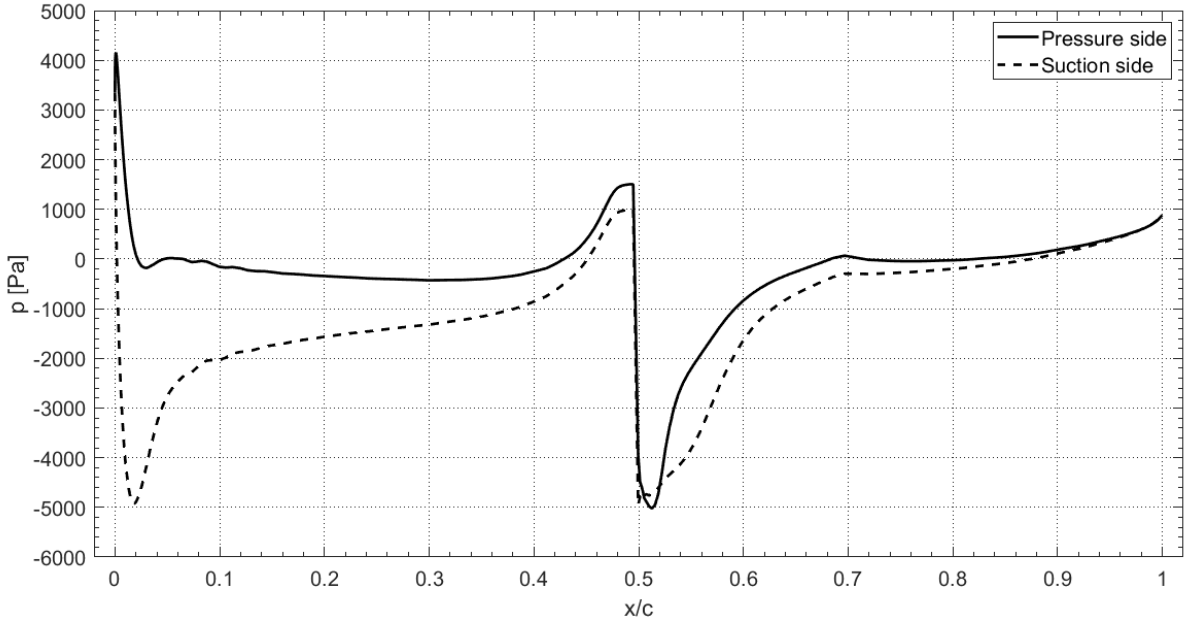


**Figure 3.20.** *Static pressure obtained from the 2-dimensional analysis with $\alpha = 2^{o}$.*

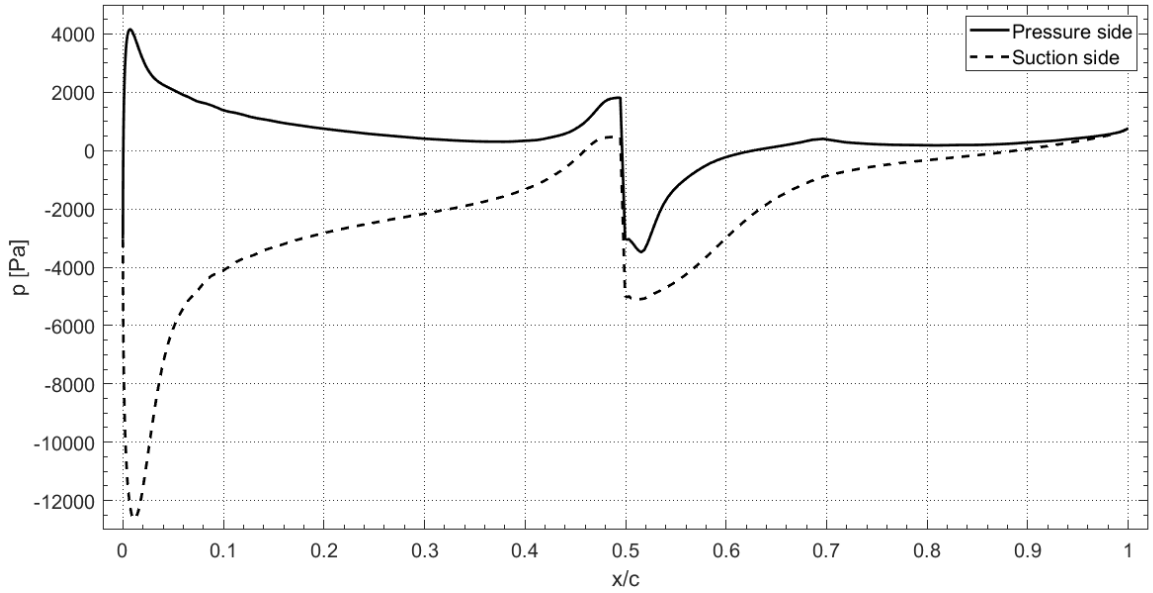


**Figure 3.21.** *Static pressure obtained from the 2-dimensional analysis with α = 6º.*

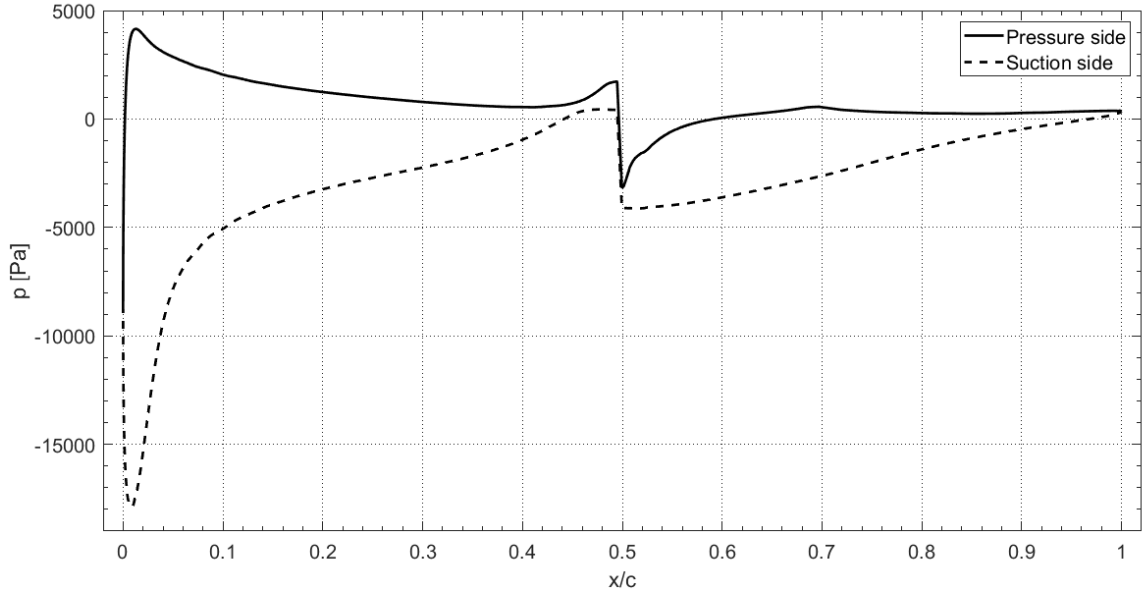


**Figure 3.22.** *Static pressure obtained from the 2-dimensional analysis with α = 8º.*

These graphs have always the same global shape, but the values of the jumps in the discontinuities at X/*c* = 0.5 tend to vary for different α. In particular, the discontinuities decrease their magnitude for angles of attack superior to 4º.

The pressures inside the spoiler channel have approximatively a constant value along the linear parts of the channel and a monotonic growing tendency in the U-bend bypass. The pressure averages in the long and short walls of the channel are reported in Table 3.2, separating the upper and lower parts of both with respect to the axis of symmetry.

**Table 3.2.** *Average pressures inside the spoiler channel for different angles of attack.*

| Angle of attack $\alpha$ | Average pressure on the upper side of the channel longest wall [Pa] | Average pressure on the upper side of the channel shortest wall [Pa] | Average pressure on the lower side of the channel longest wall [Pa] | Average pressure on the lower side of the channel shortest wall [Pa] |
|---|---|---|---|---|
| 0º | 1123 | 1122 | 1171 | 1163 |
| 2º | 1073 | 1084 | 1549 | 1543 |
| 4º | 924 | 920 | 1512 | 1463 |
| 6º | 733 | 743 | 1677 | 1619 |
| 8º | 468 | 363 | 1512 | 1303 |

The case with $\alpha = 0^o$ should have same values between the upper and lower parts of the channel because of the model symmetry and no flows inside the device should be generated. However, there is a small discrepancy between the two values which may be caused by computational approximations and low-quality mesh in that regions. The difference is, although, negligible from a structural point of view and the aerodynamic results are accurate enough to describe the fluid-structure interaction. The pressure gradient between the long and short wall of the channel is very small for small angles of attack and it increases of small amounts with the growth of the angle of attack. The only exception is the case with $\alpha = 8^o$ in which the difference in pressure between the two walls is increased considerably with respect to the previous cases. On the other hand, the gradient along the channel length leads to a significant pressure difference between the inverted jet spoiler inlet vent in the lower part of the airfoil and the outlet vent located in the suction side of the airfoil. This difference keeps growing while increasing the angle of attack since the inlet pressure decreases with growing angles of attack and, instead, the outlet pressure increases until the case with $\alpha = 6^o$.

If the pressure inside the spoiler was the only one present, increasing the air flow angle of attack would stress more the lower panel of the spoiler. Nonetheless, the global displacements of the panels are ruled not only by the aerodynamic forces inside the channel, but also by the pressures outside the inverted jet spoiler. The balance of the forces in the upper and lower side of the device gives the global behaviour of the spoiler, and it can be in contrast with the trend of the pressure inside the channel.

By varying the angle of attack, the whole aerodynamic field is modified and the different lift and drag coefficients are listed in Table 3.3. $C_l$ is very close to 0 for a null $\alpha$ because of the airfoil symmetry and it obviously increases for growing angles of attack as it should be for a generic airfoil. The effect of the aerodynamic changes in the inverted jet spoiler is to increase the effectiveness of the device itself, as depicted in Figure 3.23. The increase of the drag coefficient is also verified in the work of Filippone [12] and it is due to the separation bubble enlargement given by the jet intensification.

**Table 3.3.** *Aerodynamic coefficients for different angles of attack for a low speed maneuver at low altitude.*

| Angle of attack $\alpha$ | Lift coefficient $C_l$ | Drag coefficient $C_d$ |
|---|---|---|
| 0° | 0.001 | 0.025 |
| 2° | 0.211 | 0.027 |
| 4° | 0.415 | 0.028 |
| 6° | 0.626 | 0.034 |
| 8° | 0.850 | 0.054 |

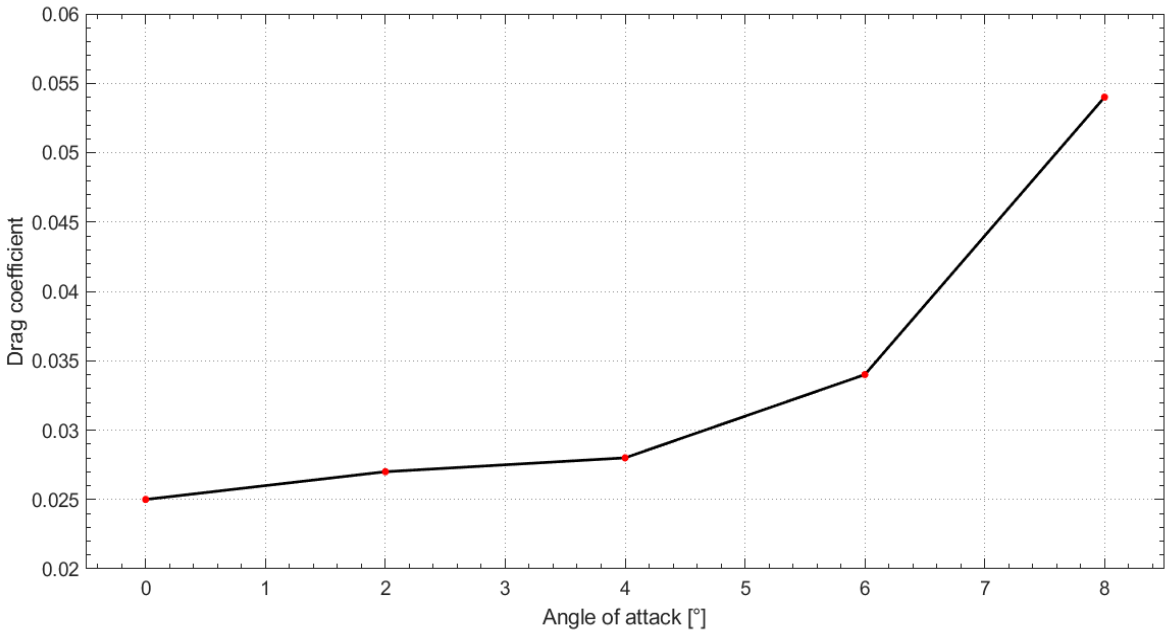


**Figure 3.23.** *Drag coefficient as a function of the angle of attack for a low speed maneuver at low altitude.*

By importing the aerodynamic results in ABAQUS, the results in Table 3.4 can be obtained, in which the displacements of the upper and lower spoiler leading edges and the maximum tensile stresses in each spoiler are reported. Since the displacements could become a non-

negligible by a geometrical point of view, a non-linear static analysis is set up. Frequently, the equilibrium configuration of a static analysis is very close to the undeformed one, enough to consider negligible the deformations which would modify the stiffness matrix. However, when the displacements are greater than a hundredth of the maximum model geometrical dimension, the results based on the initial geometry becomes more approximated. The non-linear analysis allows to increment gradually the applied loads in order to pass through equilibrium configurations close to the previous ones and calculates at every increment the updated stiffness matrix. In this case, the spoiler deflections due to aerodynamic pressures are such that non-linear analysis is required, which is conducted with 200 load increments. The results are also displayed in Figures 3.24-27.

**Table 3.4.** *Results from ABAQUS for different angles of attack with non-linear analysis.*

| Angle of attack $\alpha$ | Displacement of the upper spoiler tip [mm] | Displacement of the lower spoiler tip [mm] | Maximum tensile stress of the upper spoiler [MPa] | Maximum tensile stress of the lower spoiler [MPa] |
|---|---|---|---|---|
| 0º | 2.370 | -2.289 | 27.31 | 26.83 |
| 2º | 2.576 | -2.445 | 29.27 | 28.27 |
| 4º | 2.886 | -2.270 | 32.85 | 26.49 |
| 6º | 2.737 | -2.091 | 31.52 | 24.37 |
| 8º | 2.448 | -1.600 | 29.16 | 18.62 |

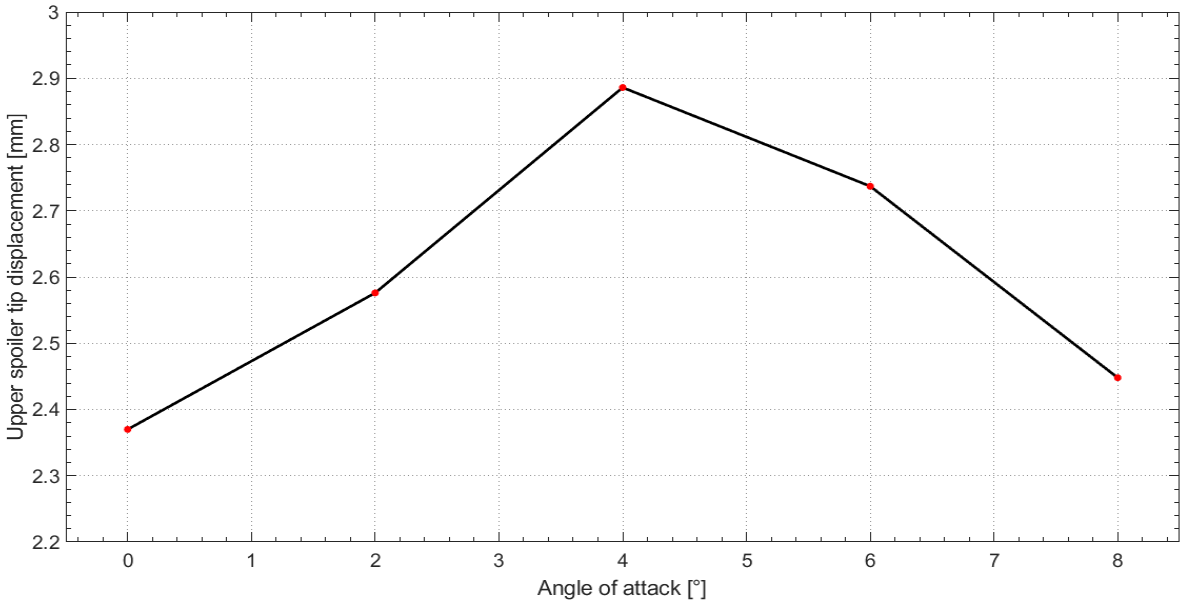


**Figure 3.24.** *Upper spoiler tip displacement as a function of the angle of attack for a low speed maneuver at low altitude.*

There is a tight correspondence between the deformations and the stresses: high tensile stress corresponds to high spoiler tip displacement. The most critical situation for the upper spoiler occurs when the free-stream velocity has an angle of attack of 4° with respect to the airfoil, while is 2° for the lower spoiler. As expected, the upper spoiler is more stressed than the lower one.

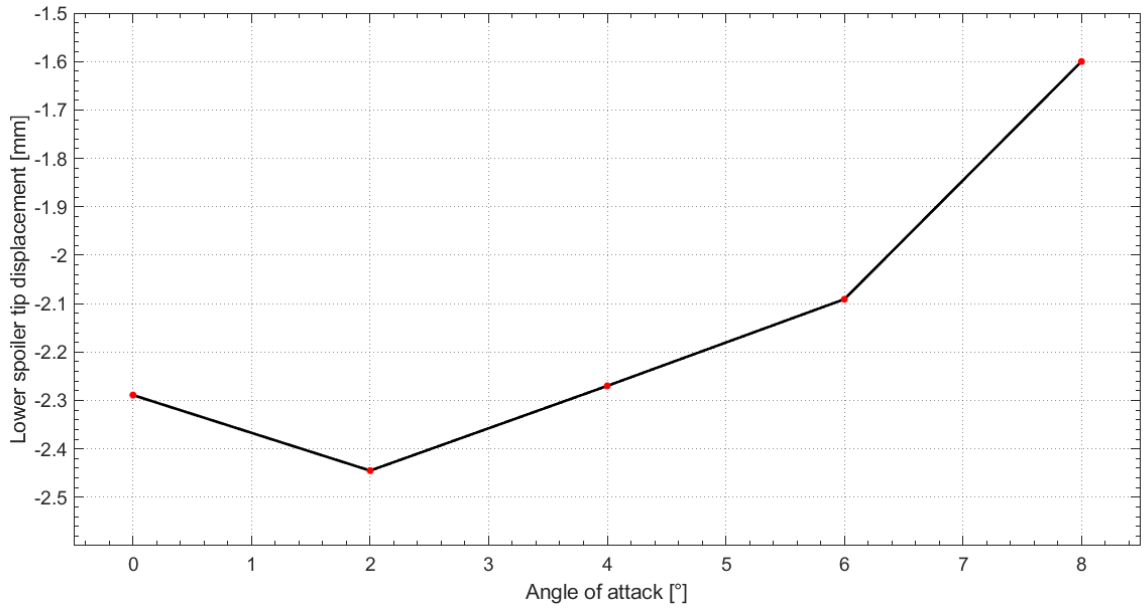


**Figure 3.25.** *Lower spoiler tip displacement as a function of the angle of attack for a low speed maneuver at low altitude.*

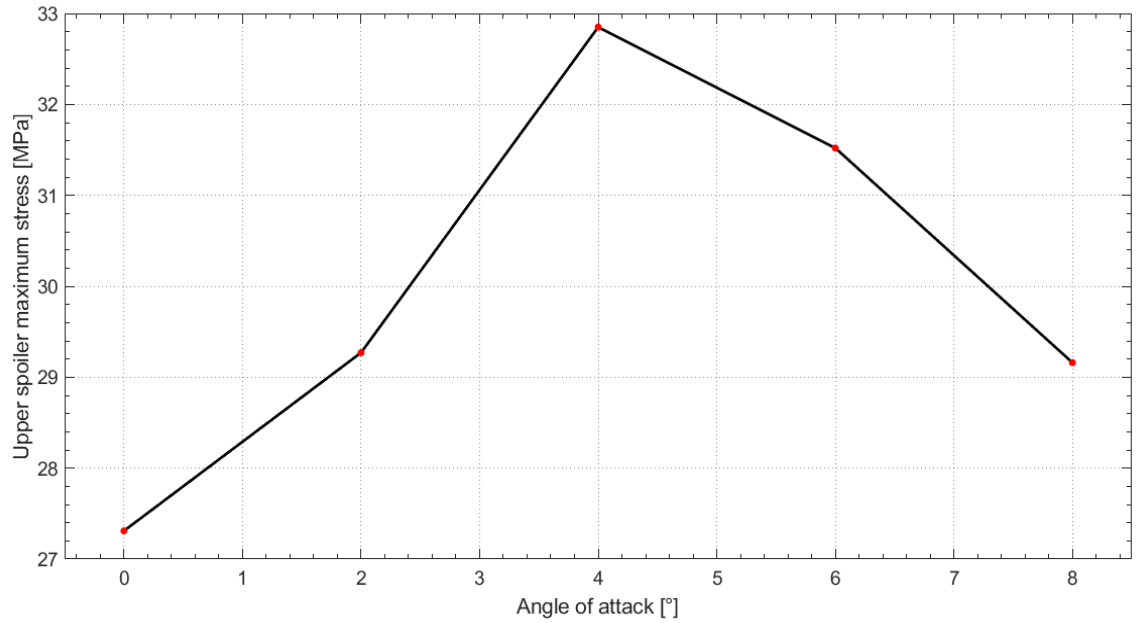


**Figure 3.26.** *Upper spoiler maximum stress as a function of the angle of attack for a low speed maneuver at low altitude.*

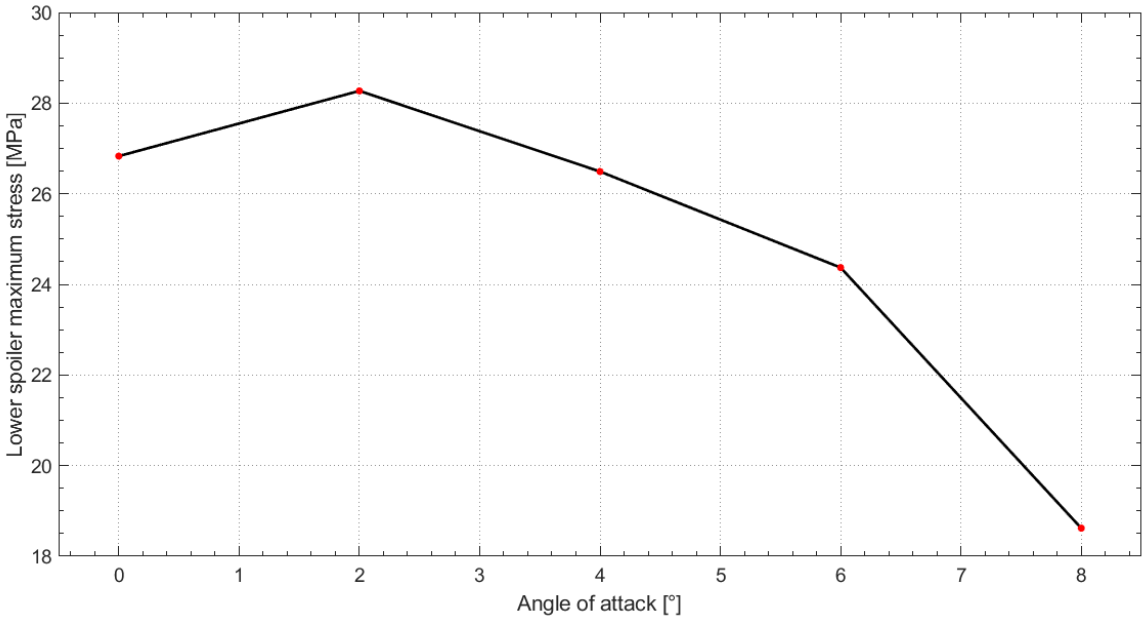


**Figure 3.27.** *Lower spoiler maximum stress as a function of the angle of attack for a low speed maneuver at low altitude.*

The velocity distribution with an angle of attack different from 0º changes differently between the suction side and the pressure side of the airfoil: in the suction side the flow tends to accelerate more than in the pressure side. For this reason, the upper spoiler is subjected to more dangerous stresses since the pressure in the upper side tends to be lower. The most critical situation appears to be the case with an angle of attack $\alpha = 4^{o}$, when the upper spoiler undergoes a displacement of 2.89 mm and a tensile stress of 32.84 MPa. The displacement increases the outlet spoiler vent width of 38.5% and this could be likely the beginning of the aeroelastic phenomenon. The stresses are still lower than the aluminium alloy yield stress limit, and the material of the device should resist to this static loading case.

## 3.5 Parametric study in the angle of attack for a maneuver in cruise flight

Flow velocity is the boundary condition parameter which affects the most the vibrational behaviour of any body immersed in a fluid. As just demonstrated with the parametric study in the angle of attack, the higher is the air velocity, the more probable is that the wing and the inverted jet spoiler could absorb energy from the fluid flow turning it into spatial fluctuations and be excited vibrationally.

Usually, the cruise flight is the longest phase in a typical commercial aircraft mission and, unfortunately for the wings and their devices, the cruise flight velocity is one of the highest speeds in the maneuvering envelope [2]. Sometimes, the large commercial aircrafts need to make some maneuvers during the cruise flight in order to stabilize its trajectory and attitude. In order to verify the usability of the device during the cruise flight, other 2-dimensional simulations are carried out with the same angles of attack used in the previous case. Since the inlet velocity is superior, the pressure around the airfoil and inside the channel are expected to be higher with respect to the case of low altitude maneuver and, thus, the stresses in the structure should be higher. Increasing the angle of attack may bring the same variations in the pressures than the previous case, but the aerodynamic behaviour is extremely difficult to predict given the geometry complexity.

The typical cruise conditions for a large commercial aircraft are number of Mach $M = 0.85$ at an average altitude $h$ = 10000 m. In Table 3.5, the data obtained from the Standard Atmosphere are reported.

**Table 3.5.** *Air properties obtained from International Standard Atmosphere table [2].*

| $h$ [m] | $p_\infty$ [Pa] | $\mu$ [Pa·s] | $\rho_\infty$ [kg/ m$^3$] | $a$ [m/s] |
|---|---|---|---|---|
| 10000 | 26436.3 | 0.00001469 | 0.413 | 299.46 |

Repeating the same calculations, the inlet velocity becomes $U_\infty$ = 254.54 m/s and the first cell height is $\Delta y_1$ = 2 μm. Although the increase in velocity should affect more the first cell height, the decrement due to the velocity is partly compensated by the reduction in air density because of the different altitude. The first cell height is still compatible with the mesh built in the previous case with $\Delta y_1$ = 1 μm, thus this mesh continues to be used for these new analyses. The wall $y^+$ increase with the increment of the angle of attack, but $y^+$ is still inferior to 2 in the case of $\alpha = 8^o$. Therefore, the aerodynamic results are acceptably accurate from the turbulence model point of view.

The static pressures of all the cases studied are represented in Figures 3.28-31. These graphs are very similar to the previous studied ones, but the scale in the Y axes is quite larger. Inside the channel, the pressure is still almost constant along the width of the device and it increases slowly in a monotonous way along the length of the device from the lower opening (inlet vent) to the upper opening (outlet vent). The average static pressures inside the channel for

the various cases are reported in Table 3.6, and their values are considerably higher than the previous case.

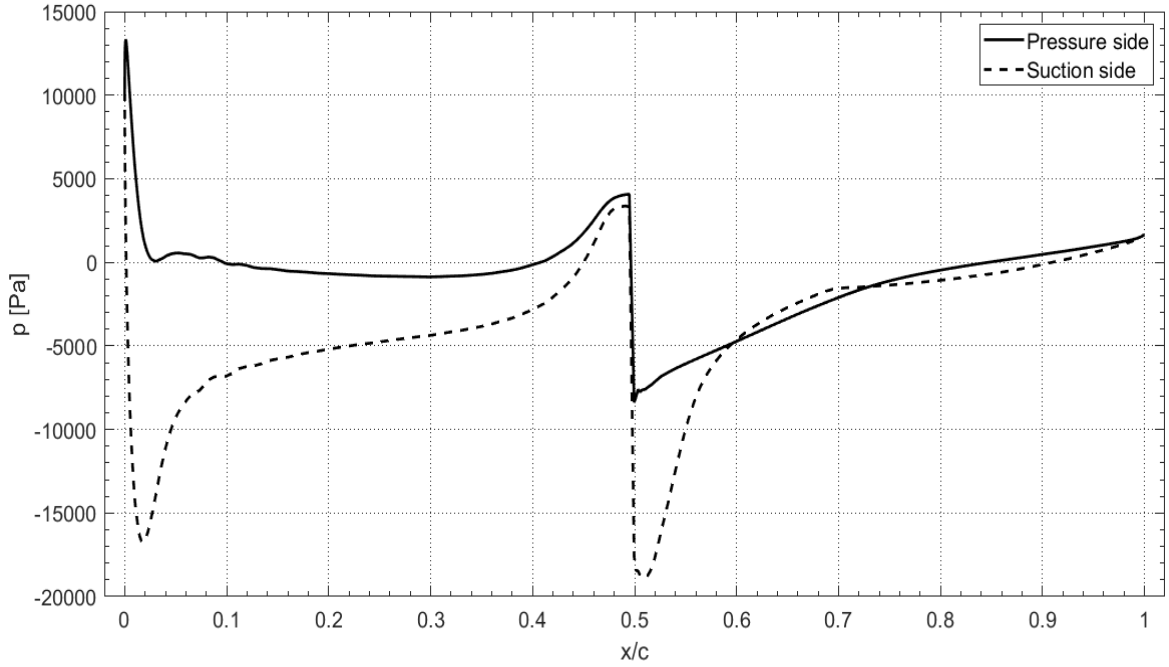


**Figure 3.28.** *Static pressure obtained from the 2-dimensional analysis with α = 2º.*

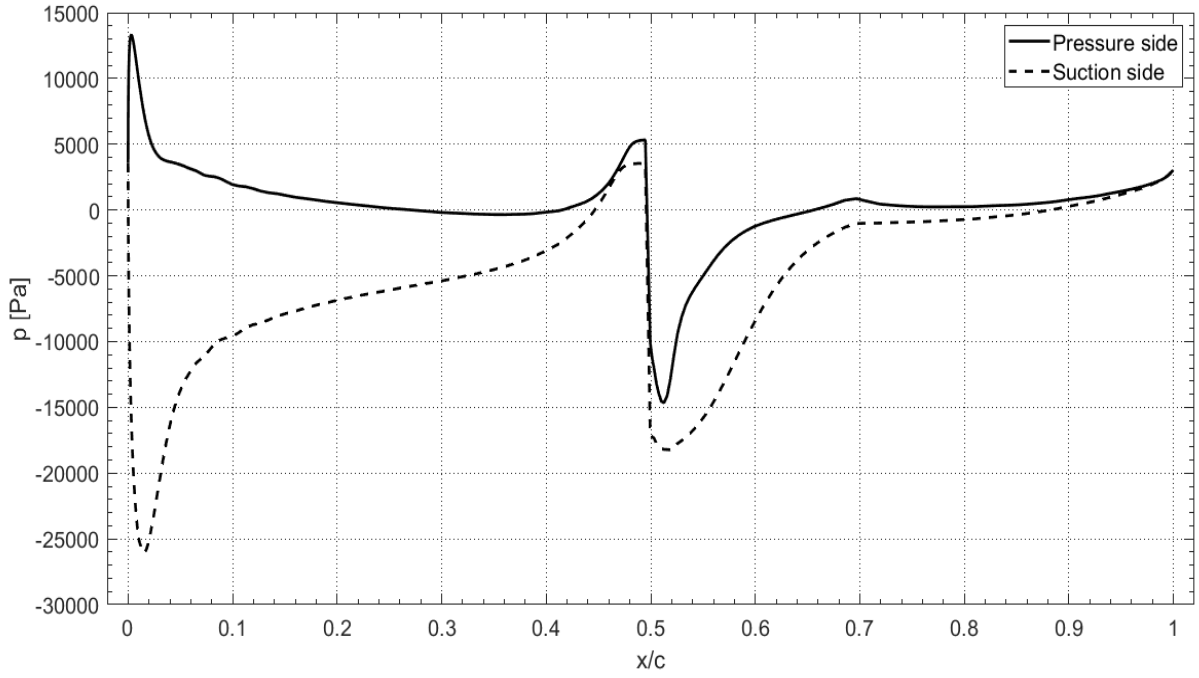


**Figure 3.29.** *Static pressure obtained from the 2-dimensional analysis with α = 4º.*

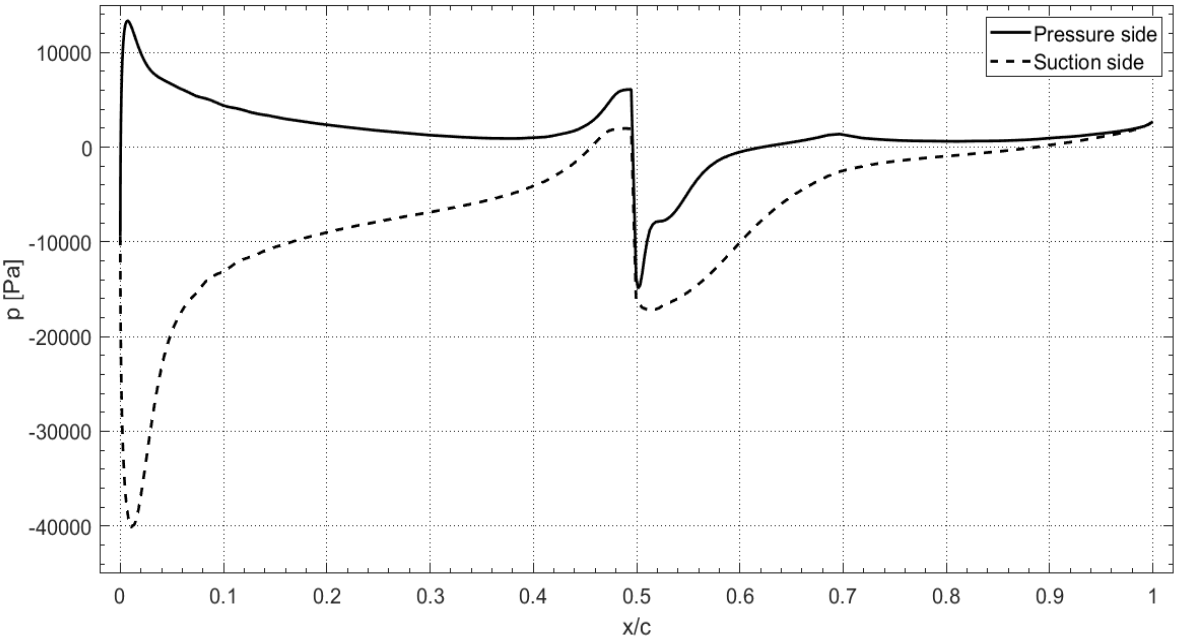


**Figure 3.30.** *Static pressure obtained from the 2-dimensional analysis with α = 6º.*

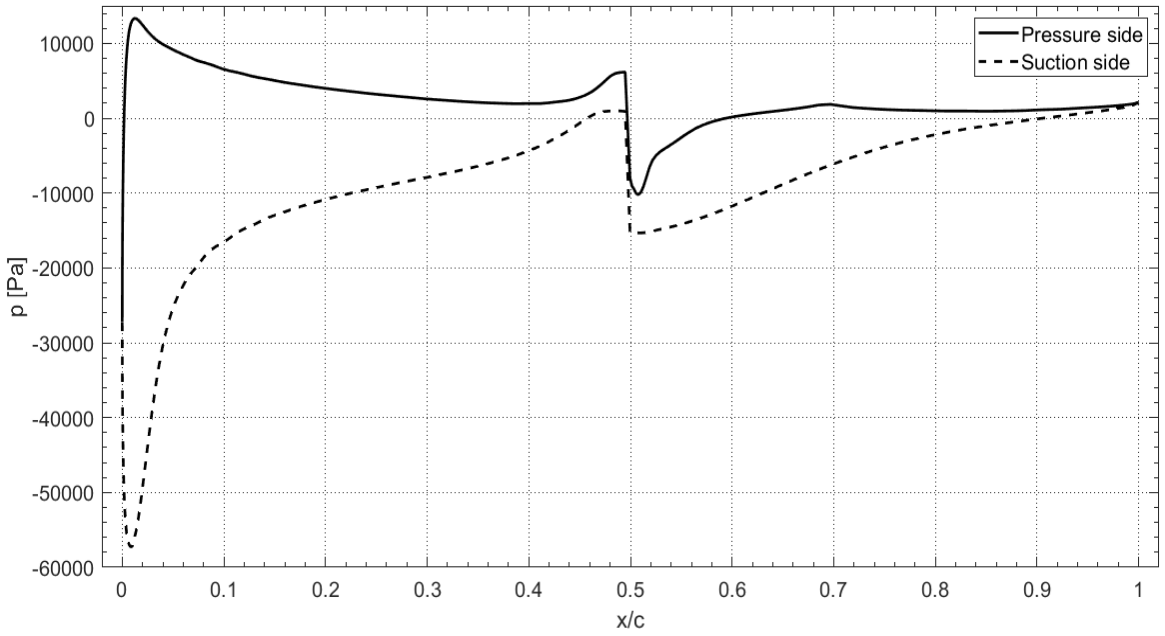


**Figure 3.31.** *Static pressure obtained from the 2-dimensional analysis with α = 8º.*

As found in the previous analyses, the lift and drag coefficients increase with the growth of the angle of attack. However, Table 3.7 and Figure 3.32 show that the device effectiveness improvement is less pronounced than in the low speed maneuver.

**Table 3.6.** *Average pressures inside the spoiler channel for different angles of attack.*

| Angle of attack $\alpha$ | Average pressure on the upper side of the channel longest wall [Pa] | Average pressure on the upper side of the channel shortest wall [Pa] | Average pressure on the lower side of the channel longest wall [Pa] | Average pressure on the lower side of the channel shortest wall [Pa] |
|---|---|---|---|---|
| 2° | 3400 | 3390 | 4043 | 3956 |
| 4° | 3787 | 3717 | 5549 | 5300 |
| 6° | 3234 | 3244 | 6314 | 6105 |
| 8° | 2885 | 2830 | 6302 | 5958 |

**Table 3.7.** *Aerodynamic coefficients for different angles of attack for a maneuver in cruise flight.*

| Angle of attack $\alpha$ | Lift coefficient $C_l$ | Drag coefficient $C_d$ |
|---|---|---|
| 2° | 0.209 | 0.029 |
| 4° | 0.411 | 0.033 |
| 6° | 0.624 | 0.037 |
| 8° | 0.840 | 0.048 |

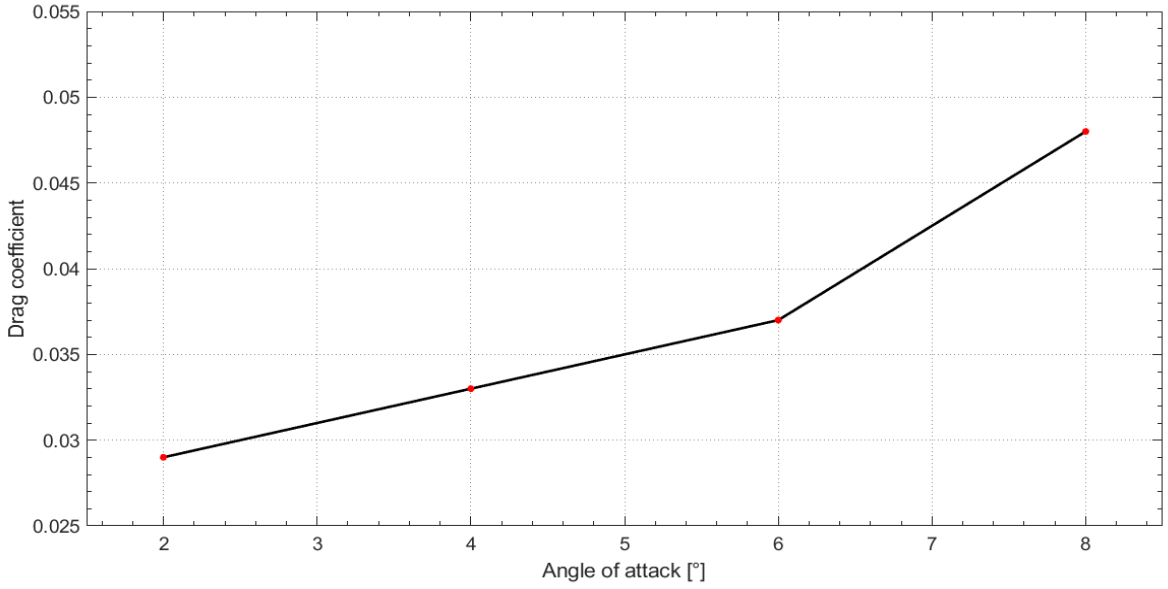


**Figure 3.32.** *Drag coefficient as a function of the angle of attack for a maneuver in cruise flight.*

In Table 3.8 are listed the results on the upper spoiler obtained from a static analysis by ABAQUS on the static pressures. The upper spoiler is still the most stressed part of the device when the angle of attack is positive. Figures 3.33 and 3.34 plot the obtained results.

**Table 3.8.** *Results from ABAQUS for different angles of attack with non-linear analysis.*

| Angle of attack $\alpha$ | Displacement of the upper spoiler tip [mm] | Maximum tensile stress of the upper spoiler [MPa] |
|---|---|---|
| 2° | 8.616 | 97.57 |
| 4° | 10.272 | 118.84 |
| 6° | 9.480 | 110.96 |
| 8° | 8.747 | 104.66 |

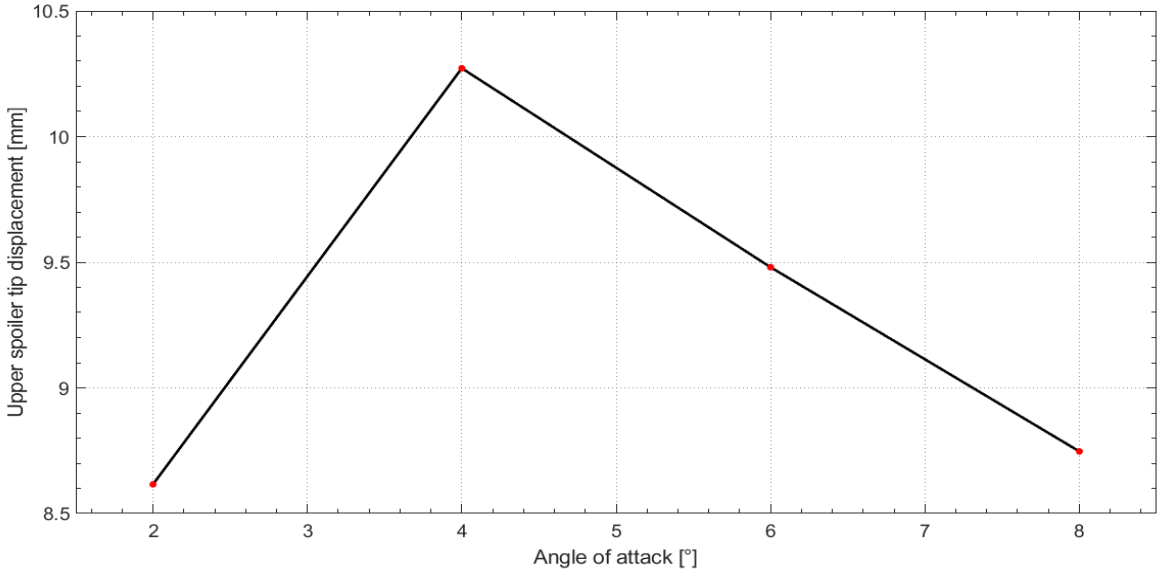


**Figure 3.33.** *Upper spoiler tip displacement as a function of the angle of attack for a maneuver in cruise flight.*

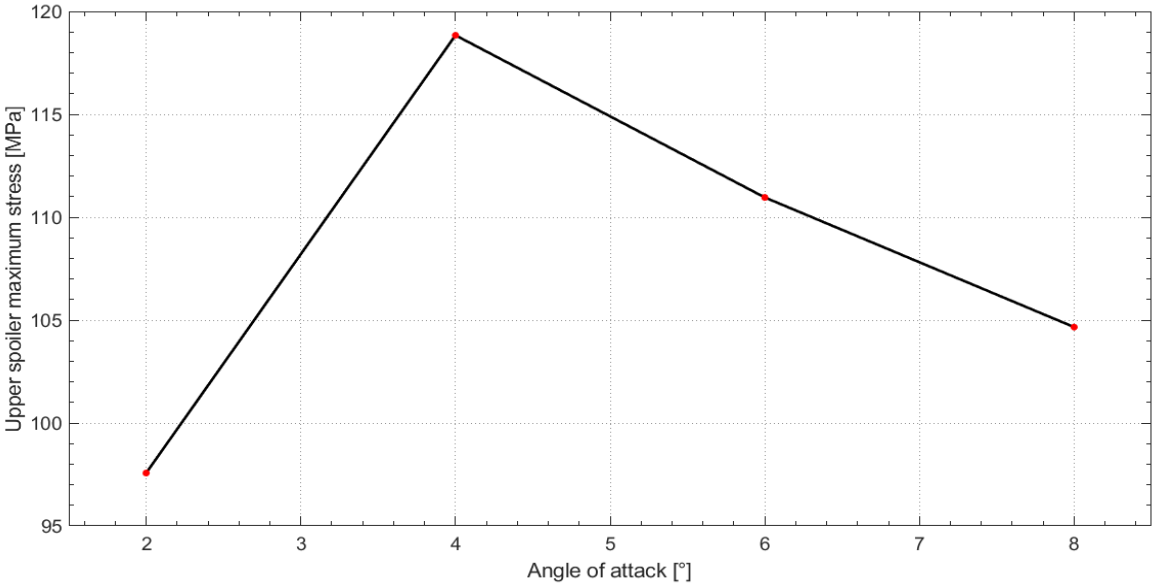


**Figure 3.34.** *Upper spoiler maximum stress as a function of the angle of attack for a maneuver in cruise flight.*

Again, the worst case is the one with an angle of attack $\alpha = 4^o$. The stresses in the spoiler are higher, but they remain under the yield strength limit of the material. However, the displacements are very big and the outlet vent of the device more than double its width. In order to study these sizes of displacements the non-linearity is added in the structural model to maintain a good model accuracy. Regardless, these results convey the idea of the spoiler panels deformation size and it is very likely that aeroelastic vibrations could be generated by this phenomenon.

## 3.6 Discussion of the results

A simplified 2-dimensional case of the inverted jet spoiler was studied in order to verify the robustness of the method used. The consistency of the results was proved by a mesh-independency test and a comparison with the results previously obtained in the work of Filippone [12,13]. The results highlight that the preliminary analysis conducted in ABAQUS underestimated the applied loads. As expected, increasing the velocity of the fluid flow surrounding the device panel causes an increment in the static pressure around the spoilers and, subsequently, in the stresses and the deformation of the spoiler. Based on the results obtained, it can be foreseen that increasing the inlet velocity will also increase the stresses inside the spoilers. Furthermore, the worst situation in both cases studied with different boundary conditions is the air flow with an angle of attack $\alpha = 4^o$.

# Chapter 4
# Reducing aeroservoelasticity

Previous analysis highlighted large displacements of the inverted jet spoiler tip, even in the less stressing case of the low speed maneuver, in which the device is meant to work properly. While the spoiler is opening up, pression gradients between pressure and suction side supposedly increase as in an airfoil with a growing angle of attack. The risk assessment of aeroelastic phenomena should be carried out experimentally, but some considerations can be made about reducing vibration amplitude by decreasing the spoiler displacements. However, even if the aeroelastic vibrations do not occur, spoiler deflection due to aerodynamic loads is an off-design condition which could deteriorate the device performances. Thereby, spoiler deformation is an undesired phenomenon and it must be avoided by increasing the stiffness of the panel. Furthermore, by diminishing the hinge moment the weight of the opening mechanism decreases.

## 4.1 Changing materials

In [17] the most common materials properties and manufacturing technologies for aerospace applications are presented. During the preliminary analysis, the AA7075-T6 aluminium alloy was supposed to be the structural material of both wing and inverted jet spoiler. From the 1920s, aluminium alloys have constituted the forming metals for fuselage, wings and empennage because of the low cost, the manufacturing simplicity and the significantly high elastic modulus to density ratio. However, except for the susceptibility to corrosion and the poor high-temperature resistance, the main drawback in aluminium alloy employment for attitude control devices is the relatively low modulus of elasticity. The direct consequences are elevated deflections in response to applied loads, deviation from the desired aerodynamic field and probable aeroelastic vibration initiation.

Despite the increasing researches and improvements of composite materials, the aluminium alloys will not be replaced in the short term. Studies on chemical composition and heat treatments are continuously conducted to enhance the optimal properties of aluminium alloys. For instance, lithium addition (AA2XXX aluminium alloy series) increases stiffness properties while decreases density, thereby resulting with a much higher specific stiffness. There are some concerns about damage tolerance and fracture toughness, but the third generation of Al-Li alloys has showed comparable or major properties for plane stress fracture toughness than the equivalent conventional aluminium alloys. AA2XXX alloys are going to be one of the candidates to substitute the current aluminium alloys in airframes, competing with carbon fibre composite materials.

Magnesium is a very lightweight element, but its alloys have lower elastic modulus than aluminium alloys and are not interesting for this work. Instead, titanium is a very promising element because of its high strength, relatively low density and exceptional corrosion resistance. Titanium alloys have already been employed in turbo-engines to replace higher-cost nickel-based superalloys thanks to creep resistance up to 600°C, as well as in critical components of airframes. Nevertheless, titanium alloys wide-spreading has been damped by the difficulties in manufacturing and the high cost derived from it.

Titanium has an allotropic transformation at 882°C: α-phase at lower temperature presents a hexagonal close-packed crystal structure, which confers to the metal anisotropic properties and higher stiffness, whereas β-phase at higher temperatures presents a body-centred cubic crystal structure with lower mechanical properties. The inverted jet spoiler is stressed majorly along the chordwise length as a consequence of flexural loads. Thus, when the stiffer axis of the titanium alloy is properly aligned parallel to the chord, in linear hypothesis the spoiler panel should deflect two times less than the aluminium alloy one and reduce vibrational phenomena.

Steels are regularly employed in bearings and landing gears, but rarely in airframes due to the elevated weight. Indeed, there is the tendency to diminish steel presence in aircrafts. However, the spoilers are thin plates and perhaps the advantages of steel great stiffness are worth a trade-off. Ultrahigh-strength low-alloy steels are designed to have remarkable mechanical properties, such as yielding strength and elastic modulus, but the density is much higher than the previously mentioned metals.

The above described metal properties are reported in Table 4.1.

**Table 4.1.** *Properties of common aerospace materials [17,22,23].*

| Material | Density [kg/m$^3$] | Elastic modulus [GPa] | Poisson ratio | Yield strength [MPa] |
|---|---|---|---|---|
| AA7075-T6 | 2800 | 71.0 | 0.33 | 505 |
| AA2090-T83 | 2590 | 76.0 | 0.34 | 520 |
| Ti-8Al-1Mo-1V[1] | 4370 | 145.0 | 0.32 | 910 |
| AISI 4140 | 7850 | 205.0 | 0.29 | 965 |

[1] Values calculated along the axis of maximum properties.

Composite materials are obtained from the union of more materials and offer superior mechanical properties than the single products utilized for its creation. The anisotropic characteristics might be seen as a negative issue for aircraft performances, but many times the aircraft structures are stressed anisotropically as in the case of the inverted jet spoiler and composite materials allow to have the maximum resistance just where it is needed. This means that the material and the product should be symbiotically designed to exploit the incredible composite specific stiffness and strength. Composites are still struggling to find large place in aerospace market because replacing well-known materials with theoretically better materials without many hours of time mission, is highly risky for aircraft companies. Furthermore, automatizing manufacturing processes is very difficult and most of laminates are still fabricated by hand, with variable characteristic from piece to piece. Due to the operator capabilities dependency, non-destructive tests are available to detect undesired porosities or interlaminar cracks [24,25]. The damaged composite can be distinguished also in situ [26], but maintenance on fibre reinforced composites is very expensive and usually substituting the compromised component is preferred. Nevertheless, the reduction in weight could be a “game-changer” for commercial aircrafts, especially thanks to glass and carbon fibres in epoxy resin composite. Long carbon fibres have the highest performances in strength and modulus of elasticity [27], but glass fibres are less expensive. Epoxy resin is a thermoset plastic which incorporates the fibres, transfers loads to the fibres and confers tenacity to the material.

Fibre metal laminates, shown in Figure 4.1, have been studied from the 1970s for the promising mechanical properties. Even though fibre metal laminates lose partially the advantages of a complete fibre reinforced composite, they exhibit at least 20% weight savings compared to conventional aluminium alloys used in airframes. Nonetheless, raw material and manufacturing costs are up to ten times the cost of traditional aluminium alloys

per kilogram [28]. ARALL (Aramidic Reinforced Aluminium Laminates) is a family of composite materials formed by alternating layers of aluminium alloy sheets and unidirectional prepregs of aramid fibres. Similarly, GLARE (GLAss REinforced aluminium laminates) and CARAL (Carbon Reinforced Aluminium Laminate) have an analogous concept by embedding respectively S-glass and carbon fibres in epoxy resin bonded with aluminium alloy sheets. Different GLARE designs are commercially available with diverse mechanical properties depending on the fibres orientation. GLARE materials have been already employed in civil aircrafts, for instance in Airbus A380, thanks to the improved damage tolerance and fatigue resistance. CARAL composites perform better than GLARE, but still studies and tests have to be carried out before they will be employable in aircraft structures.

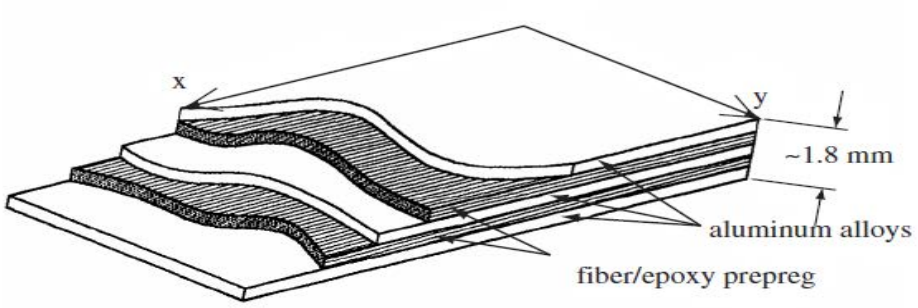


**Figure 4.1.** *Configuration of continuous fibre/metal/epoxy hybrid composite [28].*

In Figures 4.2 and 4.3, the modulus of elasticity among previously mentioned composite materials is compared. The values in Y-coordinate confirm that carbon fibres stiffness is superior to the glass fibres one. The aluminium alloy sheets insertion origins a significant improvement of mechanical properties in GLARE. This is due to the fact that aluminium alloys are stiffer than glass fibre/epoxy composite. Nevertheless, GLARE is still utilized because of weight reduction. On the other hand, CARAL slightly improves the mechanical performances of carbon fibre/epoxy composite in the transverse direction, but aluminium alloy sheets reduce the mechanical properties when the carbon fibres are oriented in the longitudinal direction. Indeed, carbon fibres/epoxy composite has a higher modulus of elasticity when fibres are oriented in the same direction thanks to the elevated modulus of carbon fibres (≈220 GPa). Shear strength of CARAL is considerably augmented given the aluminium isotropic shear modulus contribution and this explains the studies on CARAL application when the elastic properties are worse than the carbon fibre/epoxy composite.

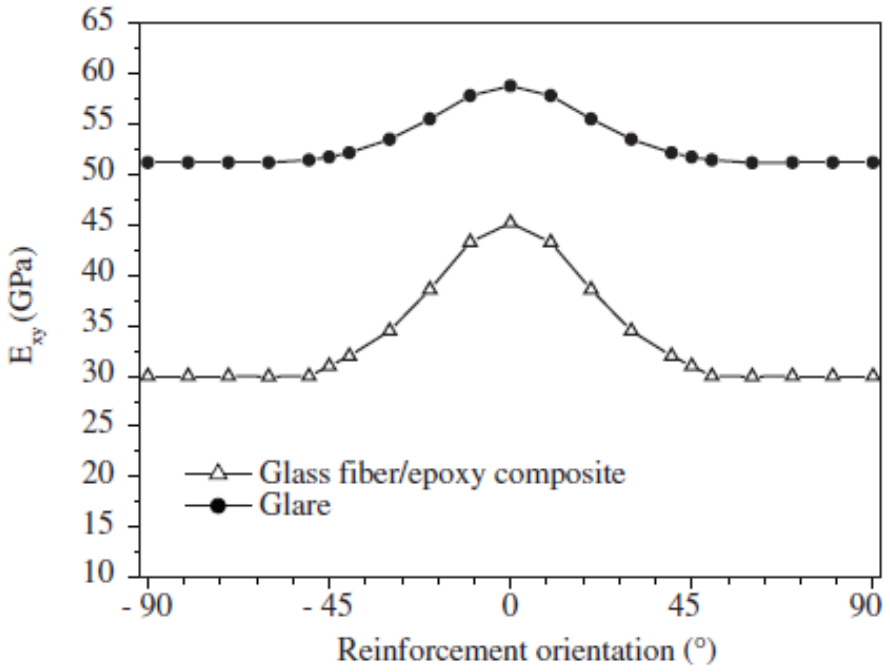


**Figure 4.2.** *Comparison between moduli of elasticity of 2-laminae glass fibre reinforced composite and GLARE depending on reinforcements orientation: the first lamina is oriented of 0° and the orientation of the second one is reported on X coordinate [28].*

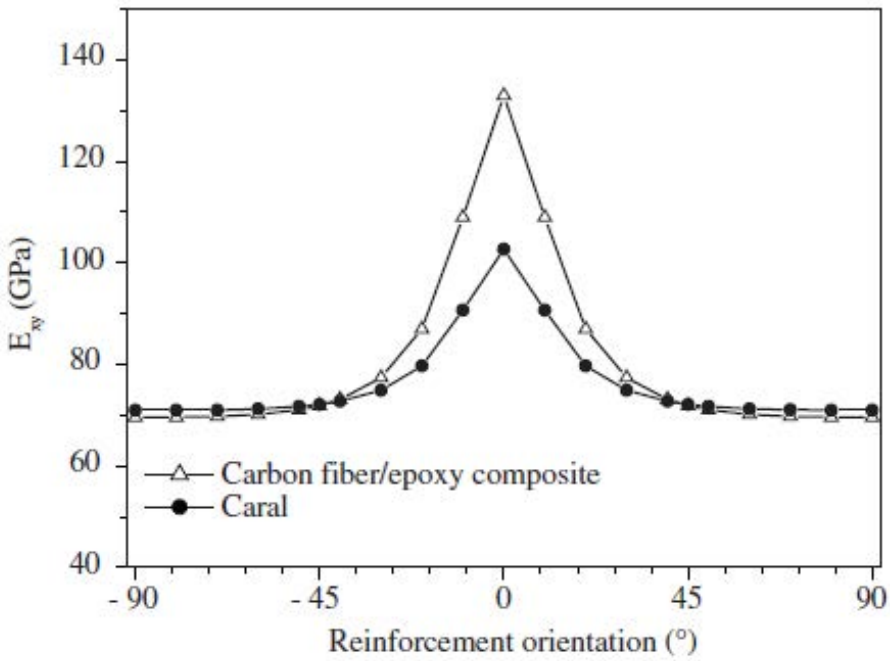


**Figure 4.3.** *Comparison between moduli of elasticity of 2-laminae carbon fibre reinforced composite and CARAL depending on reinforcements orientation: the first lamina is oriented of 0° and the orientation of the second one is reported on X coordinate [28].*

The elastic behaviour and fracture dynamics of composite laminates are extremely more complex than isotropic metals. In Figure 4.4, the tensile behaviour of mentioned laminates is reported. The composite weakness is the fibre/matrix interface bonds and in fibre metal laminates the bond between aluminium alloy and epoxy matrix composite plays a fundamental role as well. Interface bonds transfer stress from matrix to fibres and has usually the lowest strength resistance, which compromises the functional requirements of the whole material. Epoxy matrix composite present a quasi-linear constitutive law up to the ultimate tensile stress (UTS), where the material performance suddenly decays. Even if some fibres could fail before reaching UTS point, the composite keeps working until a major number of fibres is failed. The insertion of aluminium alloy sheets is noticed by the ductility increase and the plastic behaviour typical of metals from 0.4% of strain. Glass fibres/epoxy and especially carbon fibres/epoxy manifest higher ultimate tensile stresses, but GLARE and CARAL have better ductility and impact resistance, essential properties in aerospace applications.

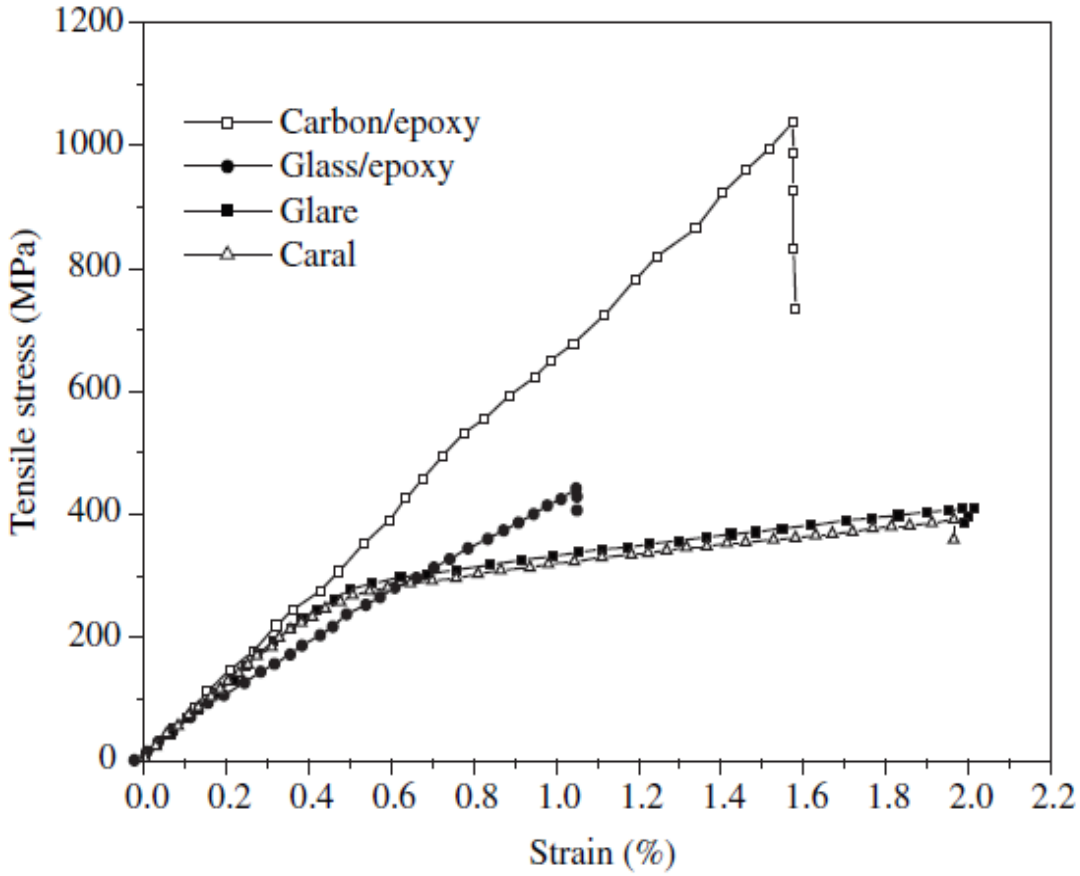


**Figure 4.4.** *Tensile behaviour of reported laminates [28].*

Composite damaging and fracture can occur in a variety of ways: fibres pull-out, fibres buckling, matrix fracture, delamination, interlaminar or intralaminar crack propagation, and so on. A tensile local fracture criterium is not enough to guarantee the safe functioning of the structure. Indeed, for instance, fibre buckling is a phenomenon which occurs only with compression loads. Therefore, compressive strength has to be studied and the tests on the laminate specimens are presented in Figure 4.5. The maximum compressive strength is lower than UTS because fibres generally work better under tension than under compression.

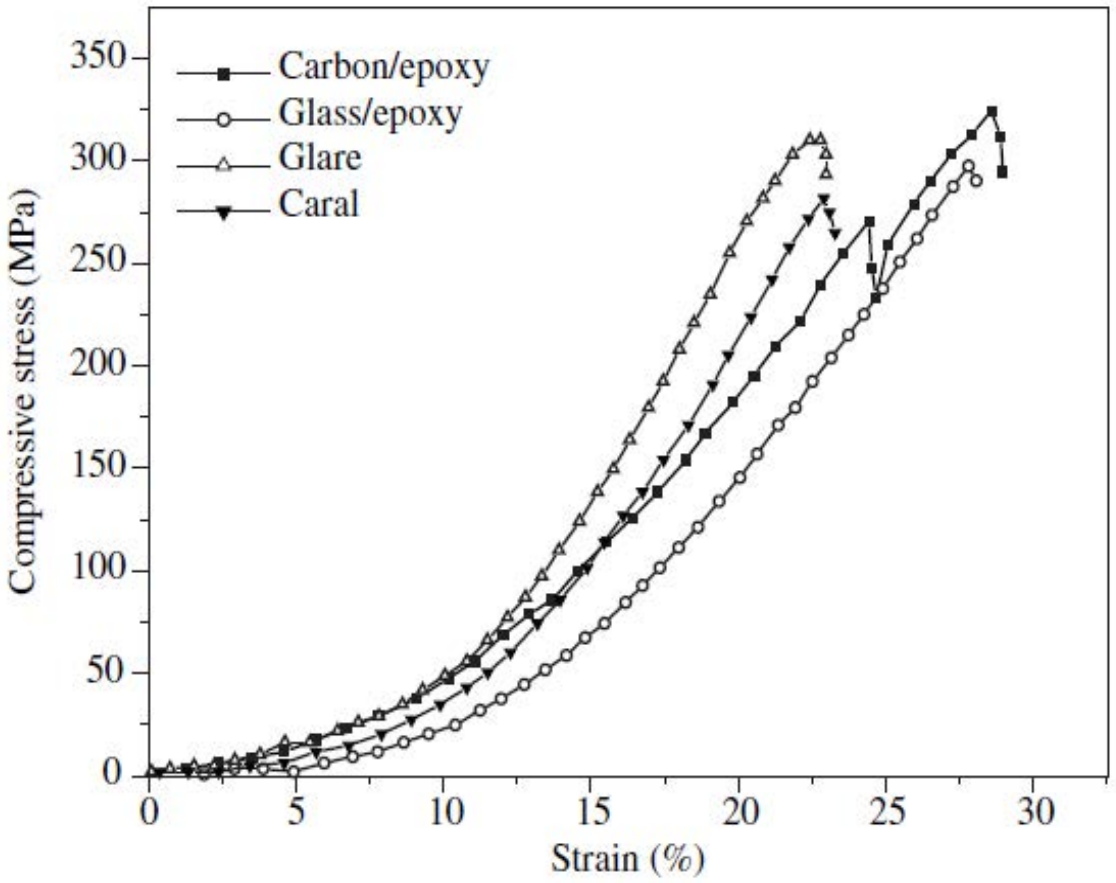


**Figure 4.5.** *Compressive behaviour of reported laminates [28].*

For the inverted jet spoiler, it is convenient that the laminate keeps the fibres aligned to the chord-wise direction, such that the excellent stiffness characteristic of composite materials can be exploited to their maximum, as shown in Table 4.2. The carbon fibre/epoxy composite appears to be the most suitable among the others, increasing the modulus of elasticity while reducing the device weight.

**Table 4.2.** *Properties of laminate materials for aerospace applications when all the laminae have the same orientation [23,28,29].*

| Material | Density [kg/m$^3$] | Elastic modulus [GPa] | Poisson ratio | Ultimate tensile strength [MPa] | Maximum compressive strength [MPa] |
|---|---|---|---|---|---|
| Glass/epoxy | 1790 | 45.0 | 0.15 | 570 | 300 |
| Carbon/epoxy | 1400 | 130.0 | 0.03 | 1160 | 390 |
| GLARE | 2520 | 59.0 | 0.20 | 380 | 310 |
| CARAL | 2320 | 100.0 | 0.25 | 420 | 319 |

If the analysis was linear, the stresses caused by the applied load would be the same regardless the properties of the materials, and the displacements could be calculated without further analyses. Indeed, in linear hypothesis the 2-dimensional model of the inverted jet spoiler can be seen as a 1-dimensional free-fixed beam which undergoes a complex distributed load. The approximation of collapsing the spoiler span dimension brings structurally minimal errors, very little compared to the aerodynamic perturbations due to the spoiler span-wise finite length. From the theory of structural mechanics, applying the system of reference shown in Figure 4.6, the displacements of the isostatic beam elastic line are linked to the distributed loads through the formula:

$$\frac{d^2}{dz^2}\mathrm{v}(z) = -\frac{M_x(z)}{E \cdot I_x}, \tag{4.1}$$

where $z$ is the coordinate running along the beam length (Z axis), v is the vertical displacement in Y direction due to flexural loads, $M_x$ is the bending moment which acts around X axis, $E$ is the material modulus of elasticity and $I_x$ is the beam moment of inertia around X axis.

The equilibrium equation that connects the bending momentum to the distributed load $p$, which in the case of study is the aerodynamic pressure applied to the spoiler panel, is:

$$\frac{d^2}{dz^2}M_x(z) = -p(z)\ . \tag{4.2}$$

$E$ and $I_x$ are supposed to be constant along the spoiler, thus the equation which must be resolved to obtain the displacement v is:

$$\frac{d^4}{dz^4}\mathrm{v}(z) = \frac{p(z)}{E \cdot I_x} \ . \tag{4.3}$$

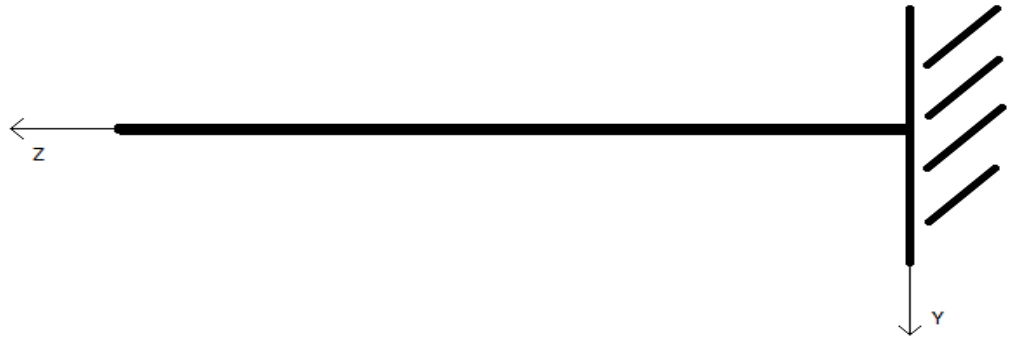


**Figure 4.6.** *Beam reference system, X axis is inward the paper sheet.*

The integration of the aerodynamic pressure on the spoiler in the chord-wise direction is too complex to be resolved by hand, and for this reason the FEM programme ABAQUS was used. However, the solution is always proportional to the same quantities:

$$\mathrm{v}(l) \propto \frac{\bar{p} \cdot l^4}{E \cdot I_x} \ . \tag{4.4}$$

In Equation 4.4, the chord-wise spoiler length is named $l$, therefore the maximum displacement is calculated at the free extreme of the beam. $l$ and $I_x$ are constant along z coordinate as well as $\bar{p}$, which in Equation 4.4 represents the integral average value of the distributed load, does not change in linear model hypothesis. Thereby, when the analysis is intrinsically linear, the material change affects the structural displacement only through the modulus of elasticity in a linear way. This means that doubling material stiffness halves the spoiler displacements.

However, the static analysis cannot be considered linear due to the large displacement. Thus, the different material data is added in ABAQUS and seven more static analyses are run in the simulation of a typical low speed maneuver at low altitude with an angle of attack $\alpha$ = 4°. Table 4.3 shows the spoiler tip displacements and the structural stresses for different implemented materials.

**Table 4.3.** *Results on the upper spoiler obtained with ABAQUS non-linear analyses.*

| Material | Displacement of the upper spoiler tip [mm] | Maximum tensile stress of the upper spoiler [MPa] | Maximum compressive stress of the upper spoiler [MPa] |
|---|---|---|---|
| AA7075-T6 | 2.886 | 32.848 | - |
| AA2090-T83 | 2.700 | 32.849 | - |
| Ti-8Al-1Mo-1V | 1.424 | 32.849 | - |
| AISI 4140 | 1.011 | 32.847 | - |
| Glass/epoxy | 4.523 | 32.853 | 34.292 |
| Carbon/epoxy | 1.576 | 32.848 | 34.284 |
| GLARE | 3.460 | 32.852 | 34.290 |
| CARAL | 2.053 | 32.849 | 34.286 |

The obtained results reflect the fact that the system is very close to be linear. Indeed, structural stresses are practically equal to each other, and the displacements follow the above described theory with very little approximations due to non-linearity effects and spoiler extreme tapering, as shown in Figure 4.7. If all the other parameters in Equation 4.4 remains constant, then the spoiler tip displacement is in inverse proportion to the material modulus of elasticity:

$$\mathrm{v}(l) \propto \frac{1}{E} \ . \tag{4.5}$$

In order to have a preliminary function to evaluate the spoiler tip displacement entity based on the linear hypothesis, a hyperbolic function is implemented in MATLAB:

$$\mathrm{v} = c_1 + \frac{c_2}{E + c_3} \ . \tag{4.6}$$

$c_1$, $c_2$ and $c_3$ are constants that can be calculated by the minimisation of the error *err*:

$$err = norm(\mathrm{v}_i - \mathrm{v}(E_i)) \ , \tag{4.7}$$

where $\mathrm{v}_i$ are the displacements reported in Table 4.3 and $\mathrm{v}(E_i)$ are the displacements computed with the elastic moduli values of the various studied materials through the function

in Equation 4.6. The result of this operation is the black line in Figure 4.7 and, as it can be seen graphically, the theory has an excellent feedback from the numerical simulations. Therefore, the entity of non-linearities are negligible and the spoiler tip displacements can be evaluated without further analyses by the following expression obtained from the error minimisation in MATLAB:

$$\mathrm{v}(l) = 0.006 + \frac{206.167}{E+0.639} \ . \tag{4.8}$$

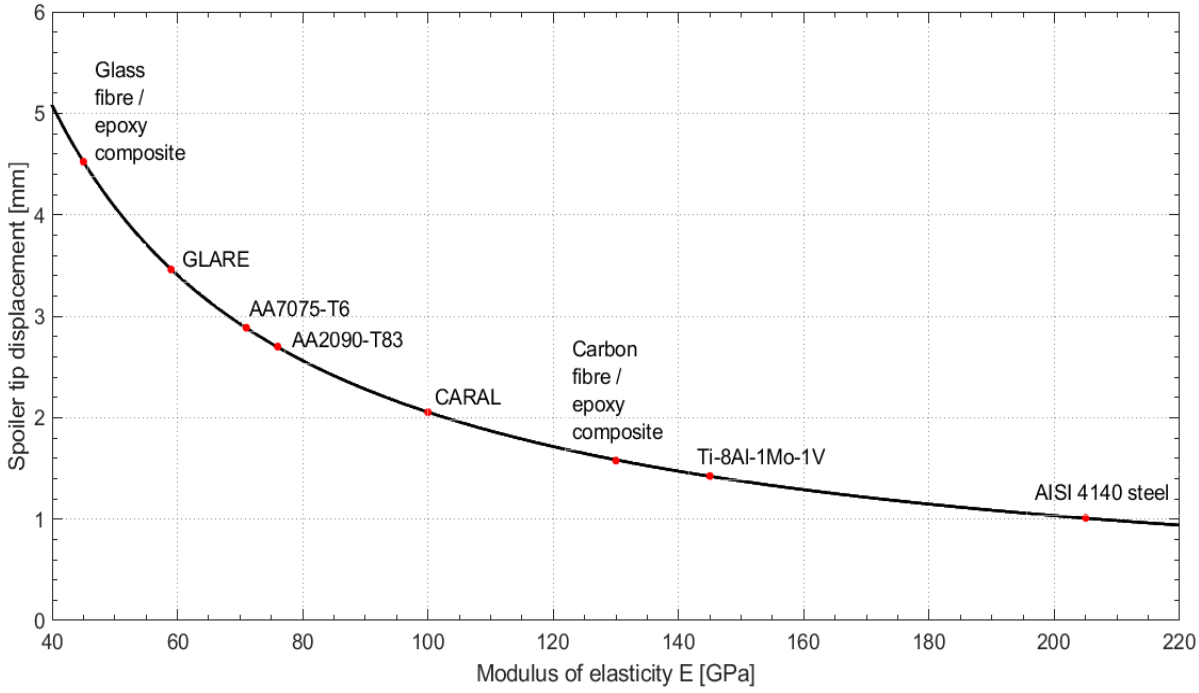


**Figure 4.7.** *Effect of material stiffness on the spoiler tip displacement. Red points represent the simulation solution to the non-linear structural problem, while the black continuous line is obtained from a hyperbolic function through the distance minimisation from the simulation points.*

The maximum stresses in the structure are considerably lower than the yielding tensile stress and the composite maximum sustainable compressive stress. The most effective materials are steel, titanium alloy and carbon fibre/epoxy composite, which can definitely reduce vibration amplitude by increasing the system stiffness. As pointed out before, steel density hinders its utilization in airframes. Titanium alloy Ti-8Al-1Mo-1V is very common in aerospace applications for its excellent specific properties, i.e. strength and stiffness to density ratio, but the composite material with long carbon fibres halves the weight despite performing an incredibly high stiffness. As the research work continues and the

technological tool keep incessantly improving, the composite properties will likely further increase. When all the tests on the feasibility and usability of carbon fibre/epoxy composite will be conducted successfully, this material will bring a breaking-through revolution in airframe industry, as well as in devices like the inverted jet spoiler.

## 4.2 Changing spoiler moment of inertia

Since spoiler thickness determines the quantity of deformed material, it intuitively affects the panel deflection. The thickness $t$ of the panel is included in Equation 4.4 through the moment of inertia $I_x$ of the spoiler rectangular section:

$$I_x = \frac{B \cdot t^3}{12} \ , \tag{4.9}$$

where $B$ is the spoiler span-wise length. Thus, when the system acts linearly and spoiler material and dimensions are maintained constant, the influence of the spoiler thickness is described by:

$$\mathrm{v}(l) \propto \frac{\bar{p}(t)}{t^3} \ . \tag{4.10}$$

The thickness variation inevitably affects the aerodynamic field around the airfoil. Not including the pressure load discrepancy, $t$ appears to have a much greater influence on the spoiler tip displacement than the material property thanks to the cubic exponent. However, thicker spoiler panel causes necessarily the device weight rise and this is significantly inconvenient in aircraft industry.

In order to verify the accuracy of the linear theoretical model, the geometry of the spoiler panel is modified, and the same parameters of Paragraph 3.3 are set up in the aerodynamic and structural analyses. The CFD analysis of a low speed maneuver at low altitude with an angle of attack of 4° is carried out and the static pressures of the airfoil with spoiler different thicknesses are depicted in Figures 4.8 and 4.9. The positive and negative peaks of static pressure ahead and behind the spoiler inlet and outlet are more elevated in comparison with

the case of reference (Figure 3.18). However, the pressure distribution maintains always the same characteristic shape.

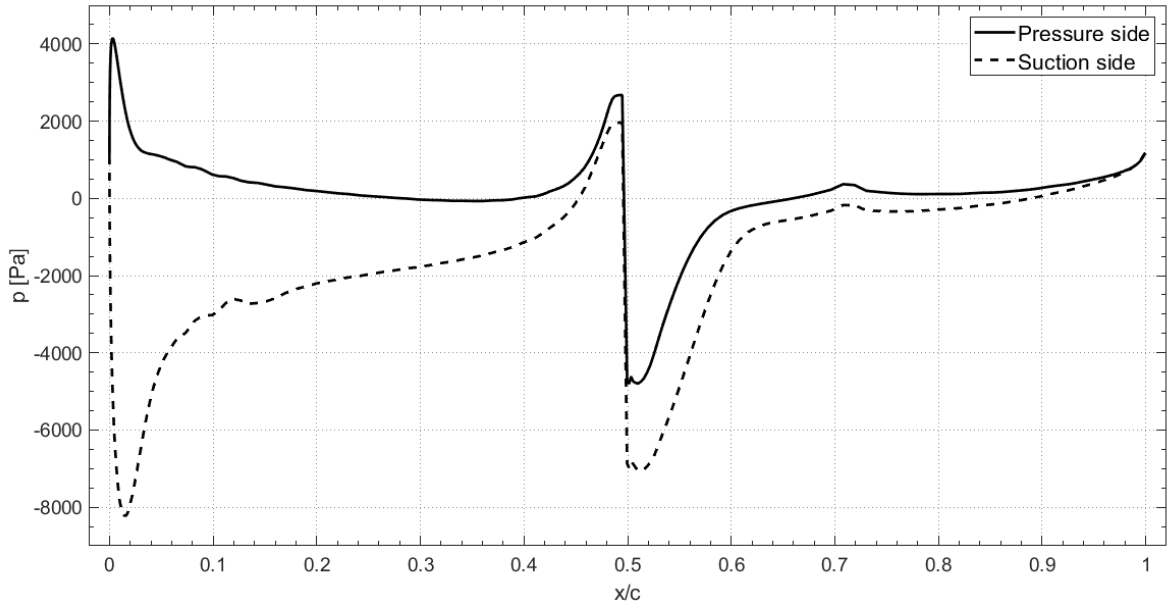


***Figure 4.8.*** *Static pressure obtained from the 2-dimensional analysis with α = 4º and spoiler thickness t = 3 mm.*

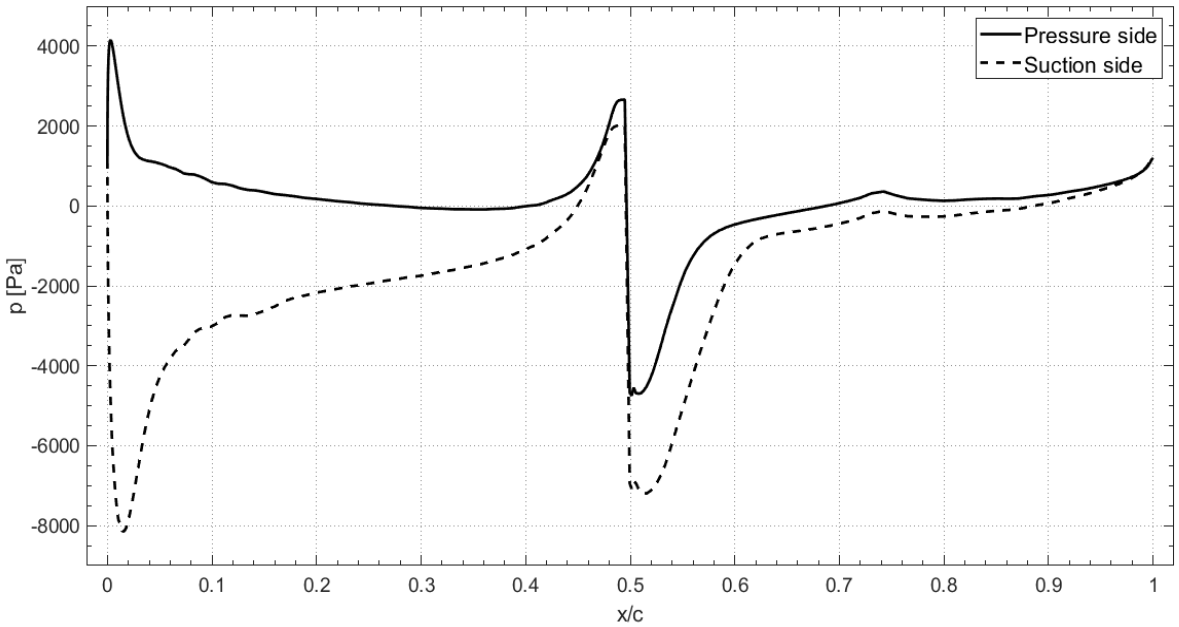


***Figure 4.9.*** *Static pressure obtained from the 2-dimensional analysis with α = 4º and spoiler thickness t = 4 mm.*

Spoiler thickness involves the aerodynamic field modification but lift and drag coefficients are not affected so much, as illustrated in Table 4.4. Therefore, the device performance is not penalised, except for the panel weight increase.

**Table 4.4.** *Aerodynamic coefficients change due to the modification of spoiler thickness.*

| Spoiler thickness [mm] | Lift coefficient $C_l$ | Drag coefficient $C_d$ |
|---|---|---|
| 2.37 | 0.415 | 0.028 |
| 3 | 0.411 | 0.031 |
| 4 | 0.408 | 0.030 |

The results obtained in ABAQUS shown in Table 4.5 highlight two opposed effects of the increase in spoiler thickness: higher pressures near spoiler tips tend to open further the panels, but thicker spoiler deform less thanks to the improved stiffness. Non-linearity due to the aerodynamic field variation is dominant and no expression to approximate the spoiler tip displacement can be extrapolated. Nevertheless, thickness contribution to stiffness is prevailing over aerodynamic pressure variation and thickness augmentation participates in reducing the spoiler stresses and tip displacement, as depicted in Figures 4.10 and 4.11.

**Table 4.5.** *Results from ABAQUS non-linear analyses for different spoiler thicknesses.*

| Spoiler thickness [mm] | Displacement of the upper spoiler tip [mm] | Displacement of the lower spoiler tip [mm] | Maximum tensile stress of the upper spoiler [MPa] | Maximum tensile stress of the lower spoiler [MPa] |
|---|---|---|---|---|
| 2.37 | 2.886 | -2.270 | 32.85 | 26.49 |
| 3 | 2.490 | -1.969 | 30.40 | 25.38 |
| 4 | 1.324 | -0.966 | 21.42 | 16.26 |

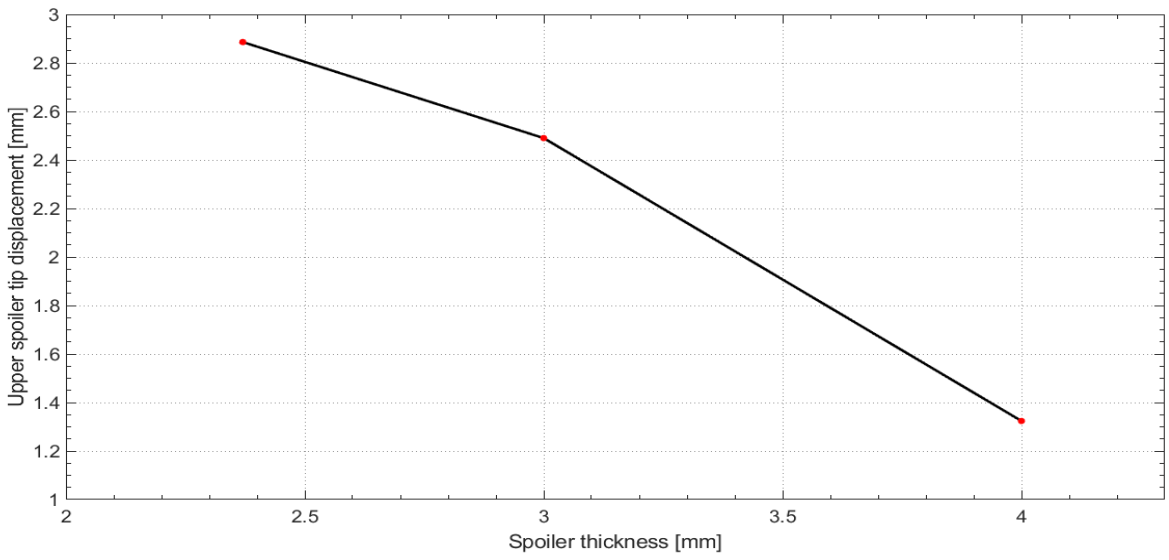


**Figure 4.10.** *Effect of spoiler thickness on the upper tip displacement.*

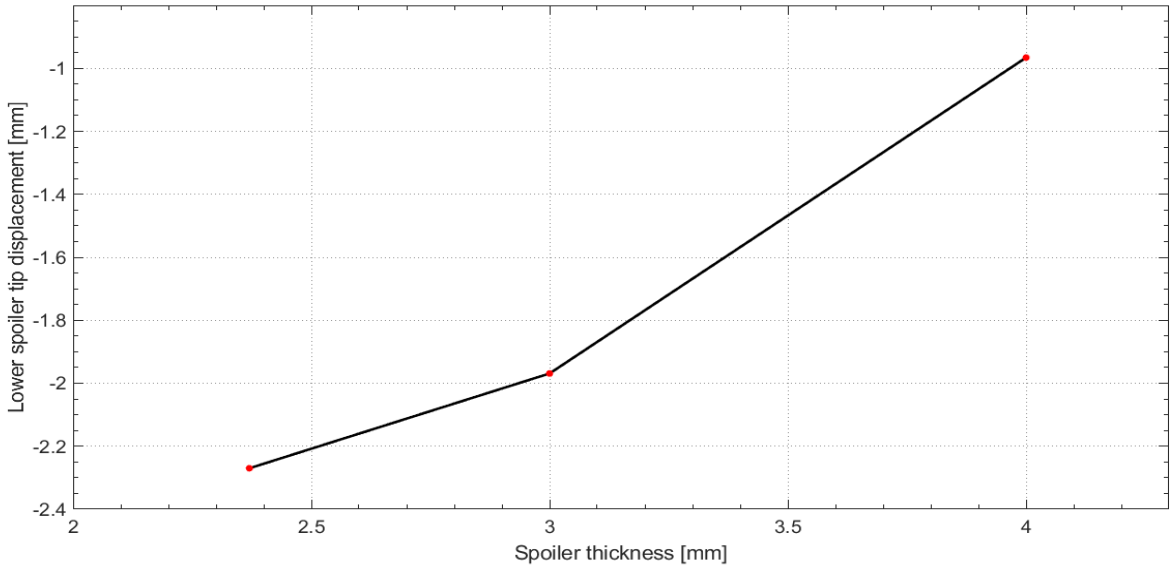


**Figure 4.11.** *Effect of spoiler thickness on the lower tip displacement.*

The spoiler span-wise length $B$ is not involved in the 2-dimensional simulation, but its effect should be similar to the thickness $t$: in linear hypothesis $B$ increases the panel stiffness but it modifies the aerodynamic field around the airfoil. The two contributions should be evaluated in a 3-dimensional analysis, knowing that probably Equation 4.4 loses its validity because of the third dimension, especially if the spoiler span has an elevated length. The comparison with the 3-dimensional case studied in Chapter 2 with respect to the 2-dimensional cases, proves that longer spoiler span is beneficial for the reduction of spoiler deformation, but more analyses should be conducted to evaluate the variation of the aerodynamic field.

## 4.3 Changing hinge position

Spoiler openings is positioned at half of the chord length. In the previous analyses the hinge point was located at 0.7 of the chord because Filippone [12] pointed out that it was the case with the most elevated moment which the opening mechanism must apply. However, as demonstrated by Equation 4.4, the longer the spoiler is, the higher the deflection and the stresses become. Indeed, spoiler length increases the moment arm and the area where the aerodynamic pressures are applied. In order to reduce spoiler deformation, the chord-wise device length should be diminished since the tip displacement in linear case obeys to the following law:

$$v(l) \propto \bar{p}(l) \cdot l^4 \quad . \tag{4.11}$$

Nevertheless, the aerodynamic field is modified because the internal channel length is inevitably shortened. Thus, total viscous losses inside the device are lowered and a more intense jet outward the upper vent can be generated. As Filippone [12] pointed out, the configuration that creates the more intense natural blown jet could not be the configuration in which the most elevated drag force is produced. Therefore, an aerodynamic forces evaluation is conducted to estimate the device performances.

Figures 4.12-14 describe the static pressures around the airfoils with $\alpha$ = 4° and the hinge points located respectively at X/$c$ = 0.65, X/$c$ = 0.6 and X/$c$ = 0.55.

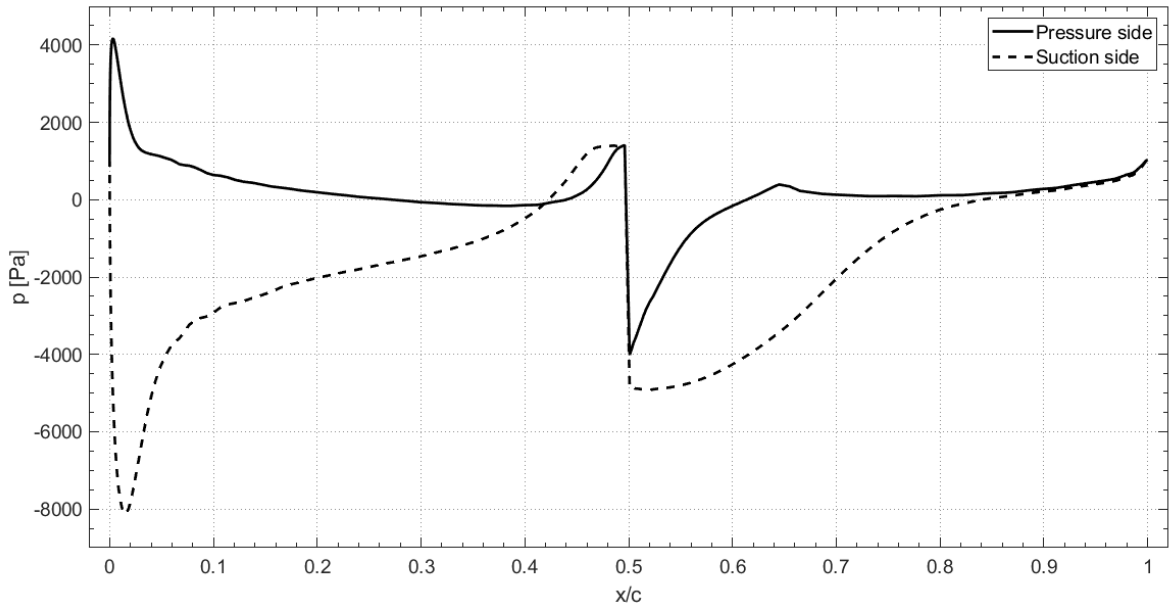


***Figure 4.12.*** *Static pressure obtained from the 2-dimensional analysis with α = 4° and spoiler hinge position at 0.65 of the chord length.*

The first two cases present a distribution similar to the case of reference in Figure 3.18, except for a higher suction peak behind the outlet spoiler vent which improves the wing lift, as shown in Table 4.6. The third case with the hinge situated at 0.55 of the chord length is different from the previous ones. Decreasing spoiler chord-wise length geometrically causes a superior initial inclination of the device panels. Therefore, the lower spoiler acts like an airfoil with a negative angle of attack: there is a stagnation point in the internal channel near the spoiler tip and the fluid accelerate on the external side of the lower spoiler generating a low-pressure zone. Moreover, the jet intensity is augmented over the limit in which the

bubble of the boundary layer separation comprehends the whole part of the airfoil behind the upper spoiler opening. The stall phenomenon deteriorates the aerodynamic properties and the lift decays. Drag force increases with the channel shortening because the more intense jet creates bigger bubbles of fluid recirculation.

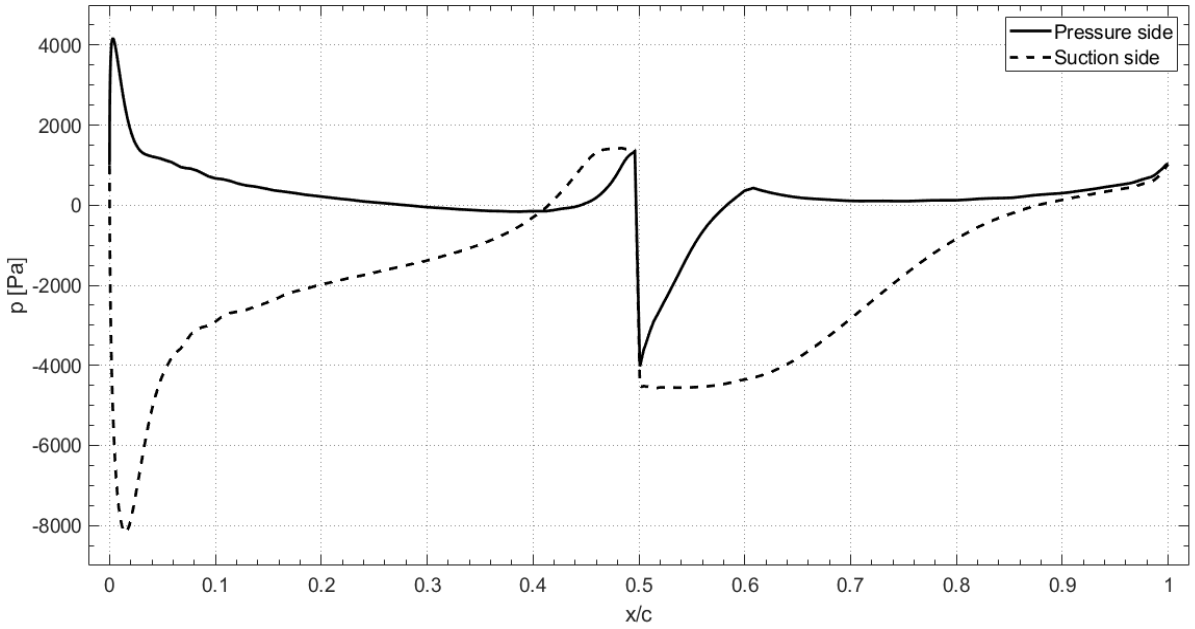


***Figure 4.13.*** *Static pressure obtained from the 2-dimensional analysis with α = 4° and spoiler hinge position at 0.6 of the chord length.*

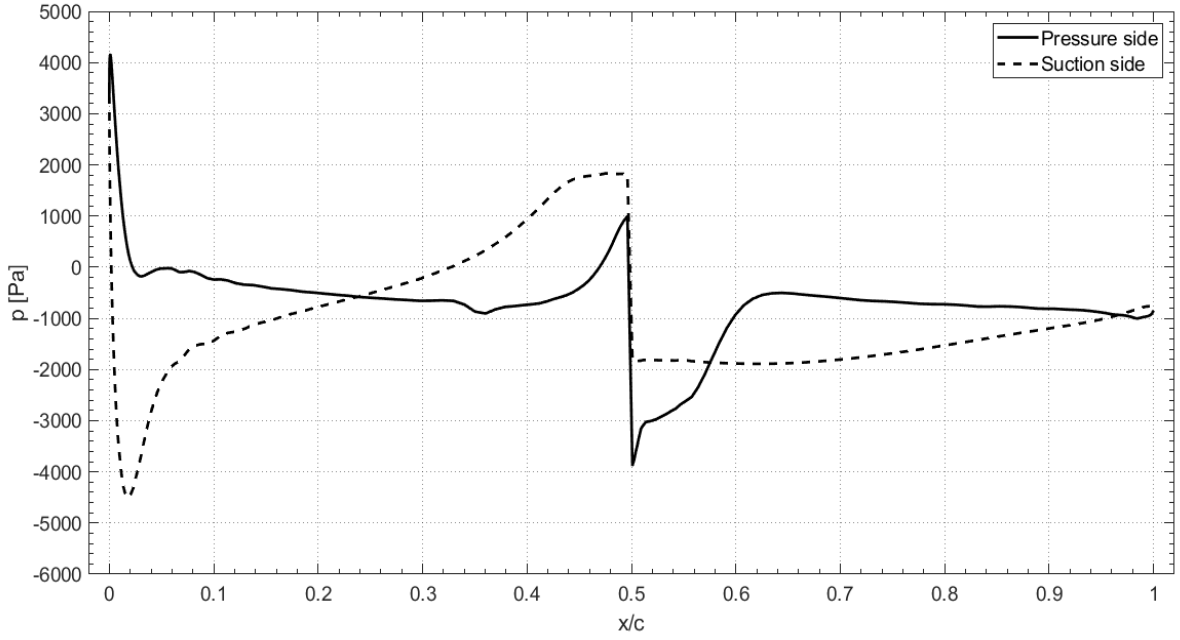


***Figure 4.14.*** *Static pressure obtained from the 2-dimensional analysis with α = 4° and spoiler hinge position at 0.55 of the chord length.*

**Table 4.6.** *Aerodynamic coefficients change due to the modification of spoiler hinge position.*

| Hinge position | Lift coefficient $C_l$ | Drag coefficient $C_d$ |
|---|---|---|
| No spoiler | 0.409 | 0.010 |
| 0.7 | 0.415 | 0.028 |
| 0.65 | 0.458 | 0.053 |
| 0.6 | 0.490 | 0.061 |
| 0.55 | 0.063 | 0.060 |

The comparison with the simple airfoil without spoiler deflection highlights that the lift coefficient is only slightly influenced by the device presence. However, the lift appears to marginally increase up to a hinge position at 0.6 of the adimensionalised chord. Below that value, the lift coefficient manifests a great decay due to the occurrence of wing stall, as shown in Figure 4.15. On the other hand, the drag coefficient is always major with respect to the airfoil with the closed spoiler and the channel shortening increases the drag force by augmenting the dimensions of the boundary layer detachment on the upper side of the airfoil. The inverted jet spoiler effectiveness in the form of drag increment, is illustrated in Figure 4.16.

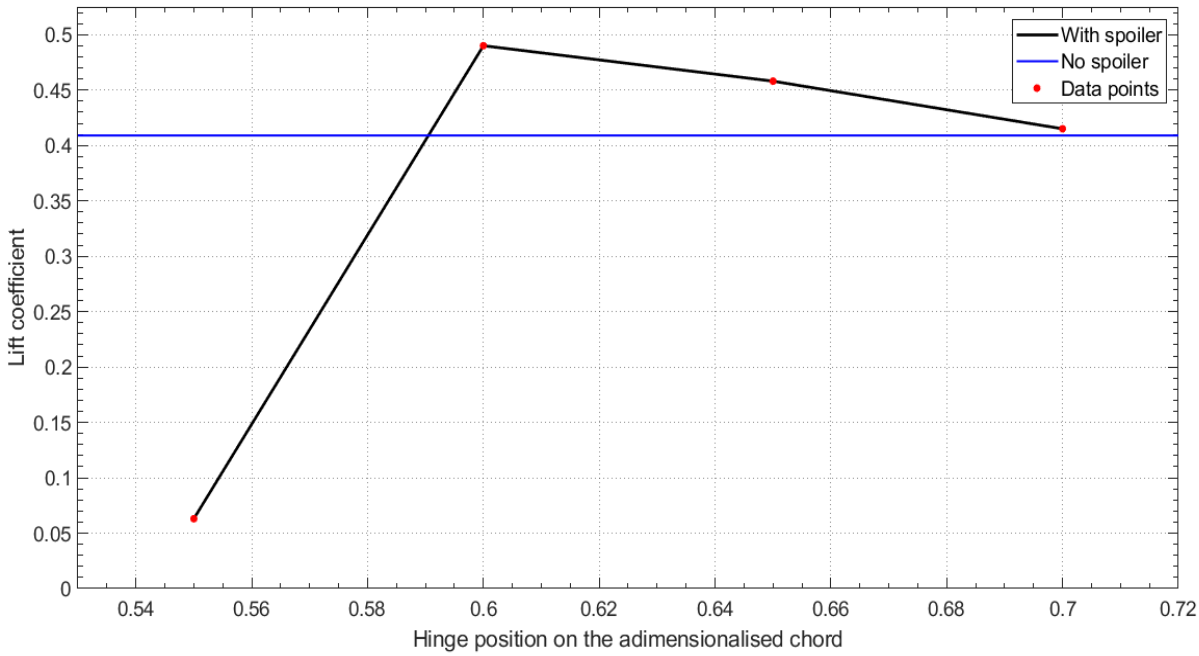


**Figure 4.15.** *Effect of the hinge position on the lift coefficient. It can be noted the great decay for values lower than 0.6.*

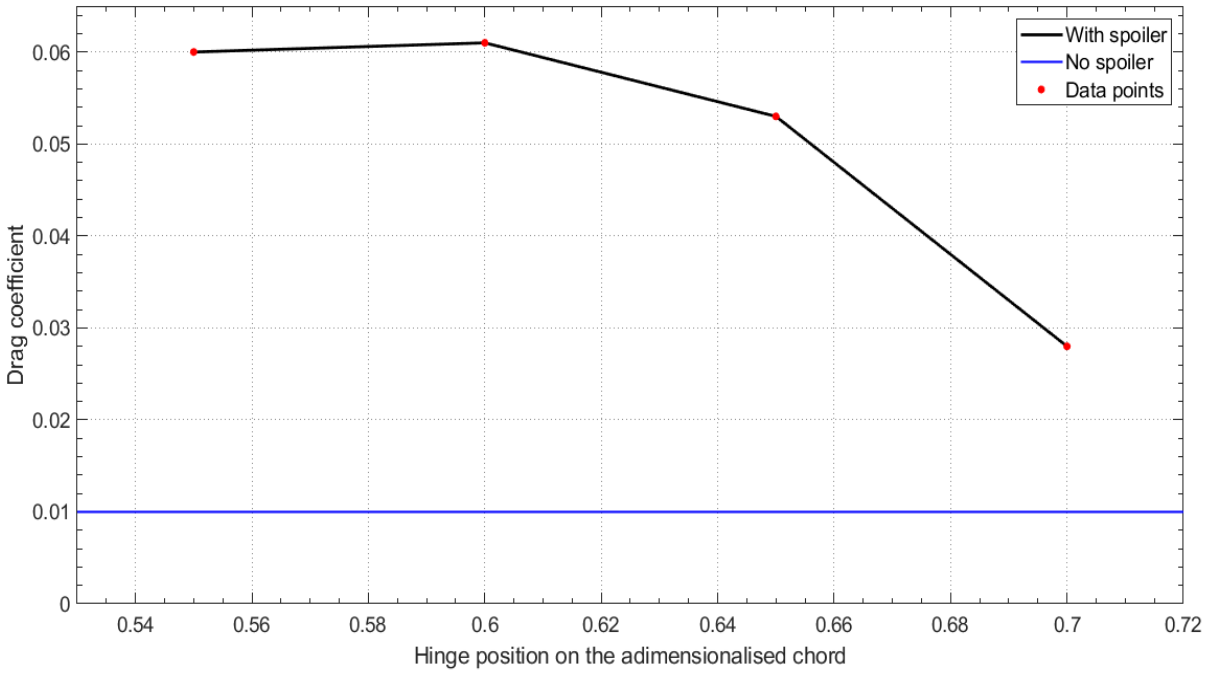


***Figure 4.16.*** *Effect of the hinge position on the drag coefficient. When the spoiler is deflected, the drag force is always greater than the simple airfoil without spoiler.*

As expected, the results obtained with the structural analyses illustrated in Table 4.7 and Figures 4.17 and 4.18, confirm that spoiler panel shortening is the more effective method to reduce the amplitude of displacements. It can be noticed that in the case with X/*c* = 0.55 the aerodynamic field is such different that the lower spoiler is more stressed than the upper one. However, the displacements are so small that can be safely neglected.

**Table 4.7.** *Results from ABAQUS non-linear analyses for different spoiler thicknesses.*

| Hinge position | Displacement of the upper spoiler tip [mm] | Displacement of the lower spoiler tip [mm] | Maximum tensile stress of the upper spoiler [MPa] | Maximum tensile stress of the lower spoiler [MPa] |
|---|---|---|---|---|
| 0.7 | 2.886 | -2.270 | 32.85 | 26.49 |
| 0.65 | 0.378 | -0.302 | 11.42 | 7.65 |
| 0.6 | 0.164 | -0.139 | 8.38 | 5.84 |
| 0.55 | 0.016 | -0.026 | 1.93 | 2.74 |

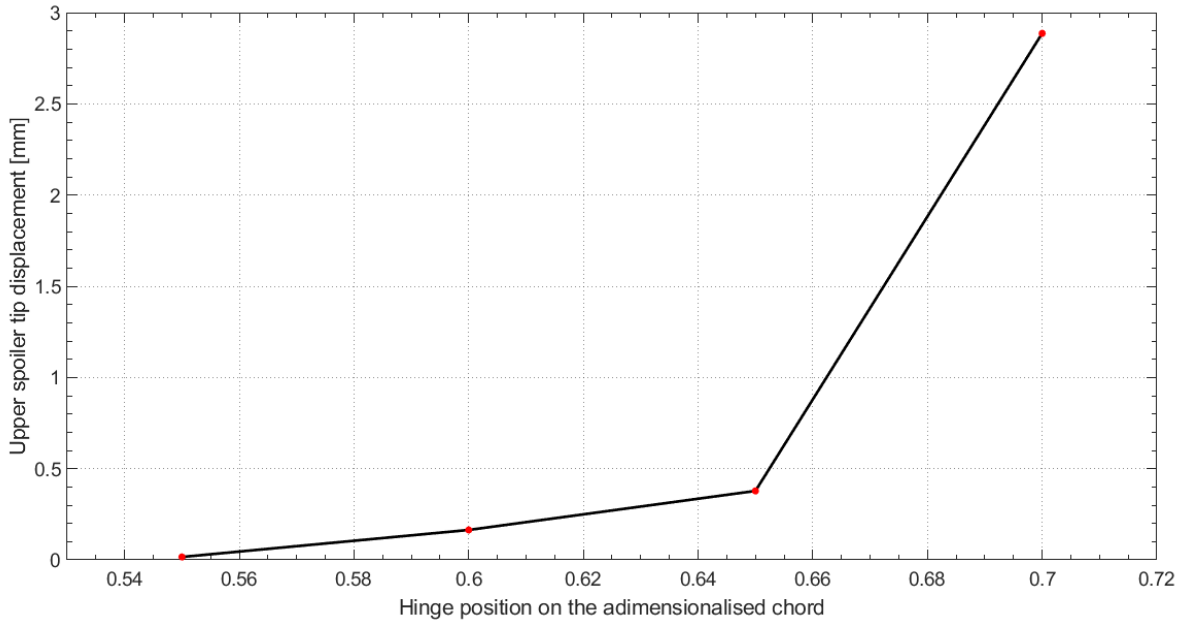


**Figure 4.17.** *Effect of the hinge position on the upper spoiler tip displacement.*

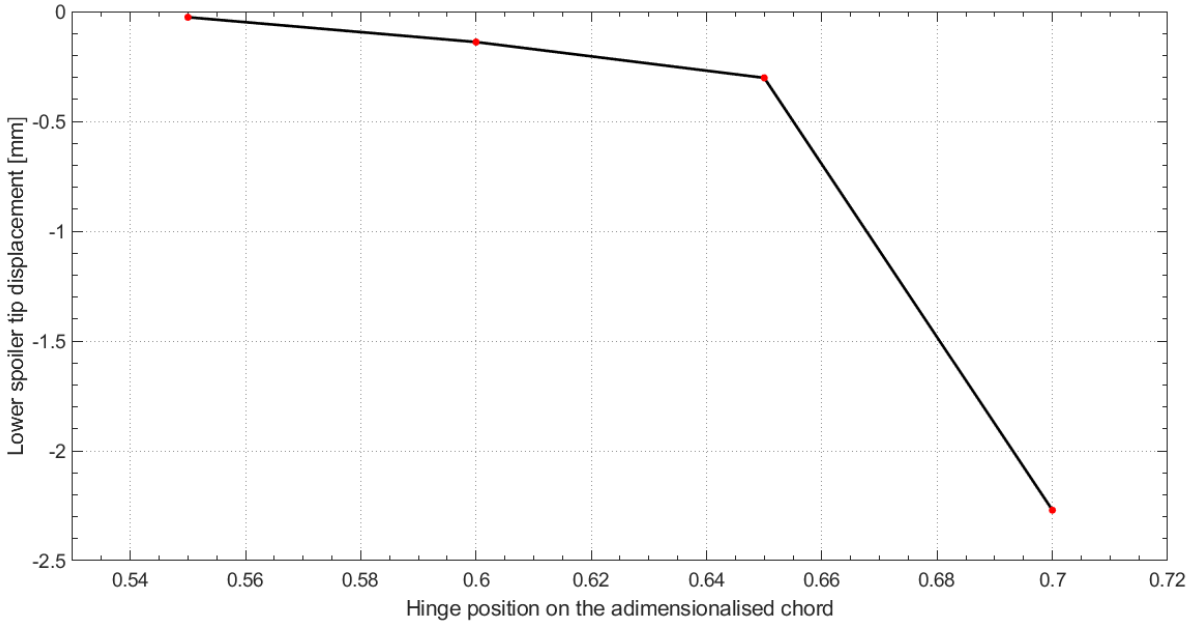


**Figure 4.18.** *Effect of the hinge position on the lower spoiler tip displacement.*

These results seem to be promising, but the risk of the stall, and consequent decay of lift, must be accurately evaluated. The device should be tested experimentally and designed to avoid premature stall, which is even a more dangerous phenomenon than aeroelastic vibrations.

## 4.4 Discussion of the results

In this chapter, the possibility to reduce spoiler deformation has been investigated. The numerical results demonstrated that augmenting the device stiffness is achievable in a variety of ways:

- Shortening spoiler chord-wise length appears to be the most effective, but a risk assessment must be carried out to avoid the stall which causes a dangerous lift decay when the naturally blown jet intensity becomes too elevated.
- Increasing spoiler thickness reduces structural displacements without affecting aerodynamic coefficients, but it increases the device weight.
- Increasing span-wise length increments the spoiler stiffness, but the perturbations of the aerodynamic field should be evaluated with further 3-dimensional analyses.
- High-performance materials, like aluminium-lithium alloys, Ti-8Al-1Mo-1V titanium alloy and carbon fibre/epoxy composite, can provide major stiffness. The accuracy of an inversely proportional relation between spoiler displacements and modulus of elasticity was tested and its validity was proved.

These results can be considered as design guidelines, but the final project should assess the combination of the mentioned aspects with a trade-off among available materials, initial costs, device weight and performances.

# Chapter 5
# Conclusions

In this work a new concept of spoiler was investigated to improve aircraft attitude control: the inverted jet spoiler conceived by Filippone [12]. No structural analyses were carried out to evaluate the device deformation and stresses, although the interaction of the spoiler with the aerodynamic field could cause the initiation of aeroelastic vibrations.

Initially, 3-dimensional structural analyses were conducted extrapolating the aerodynamic pressures of previous works of Filippone. The results highlighted that displacements and stresses could be safely neglected, except for the case in which the loads were synchronized with the first natural frequency of the inverted jet spoiler and the resonance amplifies panel deformation. However, the structural stresses never exceeded the yield strength limit.

The simplification to a 2-dimensional analysis played a fundamental role because of the reduced computational time. Indeed, it made possible the parametric study of the most influencing variables. As intuitively expected, free-stream velocity increases the loads acting on the spoiler. Furthermore, the most critical aerodynamic configuration for the structure includes an angle of attack of 4°. Even if there is still no risk to yield the material, the spoiler deformation is quite large and aeroelastic vibrations could likely occur.

In order to reduce spoiler deformation, stiffer material can be employed since the device displacements stand in inverse proportion to the modulus of elasticity. Despite the high cost, carbon fibre/epoxy composite probably offers the best trade-off between mechanical properties and low weight. On the other hand, it was demonstrated that spoiler stiffness increases by shortening the chord-wise length, thickening the panel and lengthening the span-wise dimension. However, the influence of these geometric features on the aerodynamic field should be studied on a case by case basis.

An inverted jet spoiler 3-dimentional analysis is essential to capture the realistic performances of the device, even if it is numerically considerably expensive. Thus, it is recommended to carry out a complete wing-device simulation in order to assess the aeroelastic performance of the system. Furthermore, experimental tests must be conducted before the device implementation on a real aircraft to verify the aeroelastic vibration amplitude.

# Chapter 6
# Riassunto esteso

## 6.1 Introduzione

Sebbene sia diventato una pratica comune, il controllo d'assetto di un veicolo in volo rimane pur sempre molto complesso e si ricercano continuamente nuovi dispositivi in grado di migliorare le prestazioni attuali. Gli spoiler sono costituiti da pannelli che possono essere estratti da qualsiasi superficie dell'aereo e il loro effetto principale è quello di aumentare considerevolmente la resistenza all'avanzamento per contribuire a generare le forze necessarie per il controllo d'assetto.

Gli spoiler convenzionali sono montati sulla superficie superiore delle ali e possono fornire momenti di rollio, imbardata o beccheggio a seconda della loro posizione e della loro deflessione. In particolare, la deflessione può raggiungere angoli di 90° quando si necessita generare una grande forza di drag durante la fase di atterraggio. Questi dispositivi diminuiscono il consumo di carburante utilizzato durante le manovre e permettono una discesa più ripida per l'atterraggio, riducendo il tempo e lo spazio percorso vicino a terra e diminuendo perciò la fastidiosa emissione rumorosa nelle zone abitate.

Le superfici dei dispositivi tradizionali quali ad esempio gli alettoni ("*split ailerons*", Figura 1.7), richiedono una grande forza per essere mantenuti dispiegati, quindi i meccanismi di apertura possono diventare molto pesanti. Blake [4] propose di invertire il verso del montaggio dell'alettone sulla superficie inferiore dell'ala rispetto alla corrente fluida per fare in modo che i momenti applicati al meccanismo di apertura si compensassero. Questo nuovo sistema, quindi, comprende un "*inverted spoiler*" (Figura 1.8) che permette di diminuire dimensioni e peso del meccanismo di movimentazione interno all'ala. Anche Clark [5] ideò un dispositivo con apertura frontale ("*forward opening inlay spoiler*", Figura 1.9) per generare momenti di imbardata senza compromettere la portanza totale.

Tutti i problemi di danneggiamento e instabilità strutturale sarebbero semplificati se si utilizzassero dei dispositivi a getto d'aria che sostituissero i pannelli mobili, anche se lo

studio dell'aerodinamica dell'ala si complicherebbe ancora di più. Tavella *et al.* [6,7] svilupparono uno spoiler a getto ("*lateral blowing jet spoiler*", Figura 1.10) a forma di un foglio sottile installato sulla punta dell'ala, in grado di modulare la portanza e di generare anche forze laterali e momenti di rollio. Quando gli spoiler a getto sono montati sulle superfici superiore e inferiore dell'ala, vengono chiamati "*jet spoiler*" (Figura 1.11). Questi dispositivi sono in grado di provocare la separazione dello strato limite e lo stallo alare, che aumentano di molto la resistenza all'avanzamento ma penalizzano la portanza. McClure [10] propose una evoluzione dello spoiler a getto, il "*passive jet spoiler*" (Figura 1.13), che non presenta la necessità di fornire l'aria compressa dall'interno dell'ala. Infatti, l'apertura posta nella parte in pressione del profilo permette l'ingresso all'aria che tende a spostarsi verso le uscite posizionate verso la coda del profilo. Inoltre, una valvola permette la regolazione e la modulazione del drag generato. Tuttavia, il canale interno passa attraverso il longherone dell'ala causando considerevoli problemi di fabbricazione e il getto espulso è molto debole a causa delle elevate perdite di pressione.

L'"*inverted jet spoiler*" (Figure 1.14 e 1.15) è un nuovo design di spoiler a getto ideato da Filippone [12, 13]. Durante il volo di crociera gli spoiler sulla superficie superiore e inferiore dell'ala sono chiusi e allineati con il profilo alare. Tuttavia, quando necessario, un meccanismo di apertura (elettrico o basato su un albero a camme) può essere attivato da un sistema di controllo in modo da esporre le cavità all'interno del profilo alla corrente d'aria. Il flusso all'interno del canale viene generato naturalmente per via della differenza di pressione tra estradosso e intradosso del profilo. Il dispositivo con il meccanismo di apertura può essere spostato per lasciare spazio al longherone dell'ala. La portata d'aria all'interno del canale è piccola per la perdita di carico dovuta alla dissipazione per attrito sulle pareti, quindi il getto puntato controcorrente è relativamente debole e viene velocemente ridiretto lungo il profilo dal flusso esterno. Spesso vengono create delle limitate bolle di separazione dello strato limite dietro il getto e all'interno del canale nelle zone di entrata e di uscita del fluido. L'iniziazione dello stallo riduce la portanza, ma l'orientazione dello spoiler inferiore incrementa la pressione e quindi controbilancia la perdita nella portanza. Invece l'aumento della pressione prima dello spoiler e dell'estensione delle superfici aerodinamiche incrementano la forza di drag.

L'ottimizzazione dell'*inverted jet spoiler* è influenzata da diversi parametri: la deflessione dei pannelli, la dimensione della cavità, la lunghezza del canale, la forma del *bypass* piegato a U e la posizione della cerniera determinano l'intensità del getto a seconda delle perdite di

carico e, conseguentemente, le dimensioni della bolla di separazione sulla parte superiore dell'ala, mentre l'estensione e la posizione lungo l'apertura alare e il numero di spoiler definiscono le prestazioni tridimensionali dei dispositivi. L'obiettivo dell'*inverted jet spoiler* è quello di aumentare la forza di resistenza all'avanzamento senza avere effetti sostanziali sulla portanza dell'aereo per generare forze e momenti per il controllo d'assetto e decelerare il velivolo per un atterraggio più veloce. Inoltre, questo dispositivo richiede solamente piccole deflessioni per funzionare correttamente e questo è un vantaggio per la scarsa rilevabilità mediante il radar in ambito militare.

Tuttavia, le superfici dell'*inverted jet spoiler* sono molto sottili e flessibili, rendendole poco rigide nei confronti dei carichi aerodinamici. Pertanto, il sistema si deforma molto e, cambiando la geometria a cui il flusso si deve adattare, anche il campo fluidodinamico viene modificato. Si può instaurare così l'interazione mutevole tra forze inerziali, aerodinamiche ed elastiche, e il rischio di danneggiare o fratturare il materiale per le vibrazioni aeroelastiche è elevato. Se non si arriva a questo limite estremo di rottura catastrofica del dispositivo, in ogni caso le vibrazioni del pannello dello spoiler sono indesiderate perché riducono considerevolmente la vita a fatica del componente e modificano le prestazioni dello stesso. Il nuovo termine "aeroservoelasticità" è stato coniato per le situazioni complesse in cui la teoria dell'aeroelasticità è applicata al sistema del controllo d'assetto. La presente tesi si concentra sul comportamento strutturale dell'*inverted jet spoiler* nell'interazione con la corrente fluida e propone dei metodi per il design che possano ridurre l'eventuale accadimento del fenomeno aeroservoelastico.

## 6.2 Analisi strutturale preliminare

Filippone ha condotto analisi aerodinamiche di modelli bidimensionali e tridimensionali [12,13] e ha dimostrato che la differenza di pressione del flusso interno ed esterno causa la tendenza di ulteriore deflessione del pannello dello spoiler verso l'esterno. Tuttavia, le forze che devono essere applicate dal meccanismo di apertura per contrastare questa tendenza sono minori di quelle che vengono esercitate nei moderni spoiler convenzionali.

Inizialmente, si è implementata una analisi statica in ABAQUS per controllare se la struttura riesca a resistere ai carichi aerodinamici senza superare la tensione di snervamento del materiale e per verificare l'entità delle deformazioni. La geometria è presentata in Figura

2.1, le proprietà di una comune lega di alluminio (Tabella 2.1) per la produzione di ali sono state associate al modello e i carichi sono stati approssimati dagli articoli di Filippone [12,13]. I risultati sono illustrati nelle Figure 2.5-9 e gli spoiler risultano essere i componenti più stressati. Tuttavia, gli spostamenti sono nell'ordine di qualche centesimo di millimetro, trascurabili rispetto alle dimensioni del modello, e le tensioni nell'ordine di qualche MPa, molto lontane dalla tensione di snervamento della lega di alluminio.

Tuttavia, le vibrazioni hanno la capacità di amplificare enormemente il movimento dei componenti, specialmente se i carichi forzano i pannelli a oscillare alla frequenza naturale di questi ultimi. È stata realizzata una analisi modale per conoscere la prima frequenza naturale degli spoiler e il corrispondente modo di vibrare. In seguito, è stata effettuata una analisi dinamica con i carichi che seguivano una legge armonica per porre il dispositivo in risonanza. I risultati (Figure 2.12-14) mostrano spostamenti circa 30 volte e tensioni almeno 15 volte maggiori rispetto all'analisi statica. In ogni caso, le sollecitazioni rimangono entro i limiti di snervamento del materiale anche se i carichi sono pensati non realisticamente per eccitare la struttura nel caso peggiore possibile.

## 6.3 Analisi aeroelastiche bidimensionali

Per evitare gli errori di estrapolazione dei dati dai grafici e avere una accuratezza maggiore, le pressioni aerodinamiche possono essere calcolate tramite delle simulazioni CFD con ANSYS e direttamente trasferite nel modello FEM in ABAQUS. Il modello viene studiato bidimensionalmente per il ridotto tempo computazionale che permette di esplorare più casi per le diverse condizioni ambientali e per l'ottimizzazione del dispositivo.

La geometria è stata ricavata dalla sezione a metà dell'estensione dell'*inverted jet spoiler* lungo l'apertura alare (Figura 3.1). Sono state utilizzate le equazioni del modello SST k-ω che permettono di ottenere una buona accuratezza nella risoluzione del flusso a parete mantenendo l'indipendenza rispetto alle condizioni al contorno. La convergenza dei coefficienti aerodinamici (Figure 3.8 e 3.9) nel caso di raffinamento della mesh conferma la consistenza dei risultati per l'indipendenza dal numero di elementi utilizzati. Inoltre, il parametro $y^+$ non supera mai il valore unitario, come dovrebbe succedere per il modello implementato. La confidenza nei risultati è ulteriormente incrementata anche dalla stretta somiglianza tra i risultati delle analisi di Filippone con quelle svolte. In particolare, per le

condizioni di manovra a bassa velocità a bassa quota con un angolo di attacco a 4°, le differenze sono minime e sono spiegabili attraverso le piccole diversità nella geometria. Le analisi strutturali statiche presentano deformate sempre molto simili tra loro, dato che il pannello si comporta come una mensola incastrata da un lato e libera dall'altro, e le tensioni massime si trovano ad una certa distanza dalla cerniera. Le Figure 3.13-16 illustrano i risultati per un angolo di attacco nullo.

Il parametro esterno che influenza maggiormente la deformazione dello spoiler è la distribuzione di velocità attorno al profilo. Quindi sono state svolte diverse analisi variando l'angolo di attacco e la velocità della corrente indisturbata. Il profilo presenta ovviamente coefficienti di portanza crescenti con l'angolo di attacco. Tuttavia, l'intensificazione del getto comporta un aumento delle dimensioni della bolla di separazione che si genera sull'estradosso e anche il coefficiente di drag cresce con l'angolo di attacco (Figura 3.23). Per la teoria dell'aeroelasticità, l'aumento della velocità del flusso corrisponde a maggiori deformazioni della struttura ed effettivamente i risultati (Figure 3.24-27) calcolati con analisi strutturali non lineari rispecchiano questa affermazione. Infatti, incrementando l'angolo di attacco, la corrente sulla parte superiore del profilo accelera di più e lo spoiler superiore viene più sollecitato. La situazione più critica per lo spoiler superiore prevede un angolo di attacco pari a 4° e la più elevata velocità dell'indisturbato visto che il pannello raccoglie l'energia da quest'ultima per il movimento. Le tensioni rimangono sempre abbondantemente sotto il valore dello snervamento della lega di alluminio, però gli spostamenti della punta dello spoiler superiore sono dell'ordine di qualche millimetro e arrivano anche a superare la decina di millimetri. Questo significa che il rischio di assistere a vibrazioni aeroelastiche sull'*inverted jet spoiler* è molto realistico.

## 6.4 Ridurre l'aeroservoelasticità

Le analisi precedenti hanno evidenziato ampi spostamenti della punta dello spoiler ed esiste il rischio molto elevato che durante gli esperimenti si verifichino vibrazioni aeroelastiche che comprometterebbero il corretto funzionamento del dispositivo. Dunque, si possono adottare delle accortezze sui materiali utilizzati e sulla forma dell'*inverted jet spoiler* in modo da aumentare la rigidezza del pannello e diminuire l'ampiezza delle eventuali vibrazioni aeroelastiche. In ogni caso, anche se queste vibrazioni non venissero riscontrate,

le ampie deformazioni potrebbero alterare le prestazioni dello spoiler e questo avvenimento certamente non è desiderato.

Per le analisi precedenti il materiale scelto è stato la lega di alluminio AA7075-T6, le cui ottime proprietà meccaniche correlate con la bassa densità lo rendono un metallo molto conveniente per l'industria aerospaziale. Grazie anche alla semplicità nella lavorabilità e al basso costo, le leghe di alluminio sono tutt'oggi il materiale più utilizzato nella fusoliera e nelle ali degli aerei. Tuttavia, il maggiore svantaggio di questi metalli è il relativamente scarso modulo di elasticità che causa elevate deflessioni in risposta ai carichi applicati, la deviazione rispetto al campo aerodinamico in condizioni di progetto e il probabile inizio di vibrazioni aeroelastiche. L'aggiunta del litio nelle leghe di alluminio della serie AA2XXX permette di ottenere un incremento del modulo di elasticità rispetto alle leghe della serie AA7XXX con una diminuzione della densità, da cui risulta una rigidezza specifica molto maggiore. Per questo motivo, le leghe di alluminio e litio sono i principali candidati per sostituire le convenzionali leghe di alluminio una volta che tutte le verifiche sulla tolleranza al danno e la tenacità alla frattura saranno state effettuate.

Le leghe di titanio sono principalmente utilizzate nei turboreattori e nei componenti più critici della struttura dei velivoli per via dell'elevata resistenza e della relativamente bassa densità. Tuttavia, l'elevato costo, derivante dalle difficoltà nella lavorazione, ne limita l'utilizzo. La fase α della lega di titanio presenta un reticolo cristallino esagonale compatto che rende le proprietà meccaniche elevate, anche se anisotrope. Tuttavia, l'*inverted jet spoiler* viene sollecitato solo lungo la direzione della corda del profilo, quindi progettando il dispositivo nel modo corretto allineando l'asse di maggiore resistenza alla corda si possono sfruttare al massimo le caratteristiche del materiale.

Gli acciai sono raramente utilizzati nelle ali o nelle fusoliere per la loro densità molto elevata, però in caso di necessità può essere impiegato visto che il pannello dello spoiler è molto sottile. Infatti, gli acciai sono progettati per avere proprietà meccaniche incredibilmente elevate, come la resistenza a snervamento e il modulo elastico. La Tabella 4.1 riporta le caratteristiche dei materiali sopra citati.

I materiali compositi sono ottenuti dall'unione di più materiali e offrono proprietà meccaniche superiori dei prodotti che li compongono. Come notato per le leghe di titanio, l'anisotropia intrinseca dei compositi non costituisce un problema perché le sollecitazioni laterali applicate allo spoiler sono minime, mentre la resistenza è molto importante soprattutto lungo la direzione della corda. Nonostante l'elevato costo e le difficoltà

nell'automatizzare i processi produttivi, i compositi rinforzati a fibre lunghe di carbonio sono destinati a sostituire le leghe di alluminio come materiale principale per la realizzazione delle strutture aerospaziali grazie alle prestazioni maggiori pur dimezzando la densità.
I laminati che alternano fogli di alluminio e di composito con fibre di vetro (GLARE) o di carbonio (CARAL) sono ideati per aumentare l'isotropia e la resistenza all'impatto dei materiali compositi a matrice epossidica rinforzata con fibre. Anche se la densità è maggiore rispetto ai composti puri, il peso diminuisce di almeno il 20% rispetto alle leghe convenzionali di alluminio, però il costo per la produzione è fino a 10 volte maggiore. Le proprietà dei materiali compositi sono riportate in Tabella 4.2.
Se l'analisi fosse lineare, si potrebbe assimilare il modello bidimensionale del pannello ad una trave incastrata-libera che è sottoposta ad un carico distribuito complesso. Dalla teoria della meccanica strutturale, lo spostamento dell'estremità libera della trave è sempre proporzionale alle stesse quantità, ovvero alla media integrale del carico distribuito, alla quarta potenza della lunghezza dello spoiler lungo la direzione della corda, al reciproco del modulo elastico del materiale del pannello e del momento di inerzia della sezione, che a sua volta è proporzionale alla larghezza dello spoiler e alla terza potenza dello spessore dello spoiler:

$$\mathrm{v}(l) \propto \frac{p \cdot l^4}{E \cdot I_x} \propto \frac{p \cdot l^4}{E \cdot B \cdot t^3} \ , \tag{6.1}$$

Da questa equazione si intuisce che impiegando un materiale che abbia un modulo elastico doppio, allora gli spostamenti del pannello saranno dimezzati. Questa relazione tra proprietà dei materiali e deformazione dello spoiler è stata riscontrata anche nelle simulazioni non lineari in ABAQUS (Tabella 4.3), dimostrando che le non linearità del modello possono essere trascurate. Quindi è stato anche possibile ottenere una funzione (Equazione 4.8) che desse il *best fit* dei dati per poter valutare l'influenza del modulo di elasticità dei materiali sulla deformazione dello spoiler senza dover condurre altre simulazioni numeriche. Come mostra la Figura 4.7, i materiali migliori per aumentare la rigidezza sono l'acciaio, la lega di titanio e il composito a matrice epossidica con fibre lunghe di carbonio. Quest'ultimo, nonostante l'elevato costo di produzione, è da preferire per le ottime proprietà pur mantenendo una densità incredibilmente bassa.

L'Equazione 6.1 afferma che, in ipotesi di linearità, tre parametri geometrici possono aumentare la rigidezza dello spoiler: l'incremento dello spessore e della larghezza dello spoiler e la riduzione della sua lunghezza. Ciò nonostante, la modifica della forma del dispositivo ha effetti anche sul campo aerodinamico che circonda il profilo alare, quindi le pressioni che agiscono sul pannello variano.

L'aumento dello spessore del pannello è sconveniente per il peso complessivo del dispositivo, però irrigidisce lo spoiler. I coefficienti aerodinamici di portanza e resistenza non si discostano molto dal caso di riferimento con angolo di attacco a 4° (Tabella 4.4), però i picchi negativi di pressione che agiscono vicino alle estremità dei pannelli sono maggiori e questo provoca una maggiore tendenza di apertura degli spoiler. Ciò nonostante, l'effetto benefico sulla rigidezza prevale e gli spostamenti delle estremità degli spoiler si riduce notevolmente (Figure 4.10 e 4.11).

L'estensione dello spoiler lungo l'apertura alare non viene considerata nelle simulazioni bidimensionali, ma i risultati dell'analisi tridimensionale mostrano deformazioni e tensioni molto minori dimostrando che la larghezza del pannello ha un'influenza positiva per la riduzione delle ampiezze di spostamento strutturale. Tuttavia, l'impatto della larghezza dello spoiler andrebbe calcolata con più accuratezza attraverso delle analisi tridimensionali combinando software CFD e FEM.

Le posizioni della cerniera e delle aperture dello spoiler determinano la lunghezza dei pannelli. Inoltre, se il canale interno è più corto, allora le dissipazioni per attrito diminuiscono e si riesce ad ottenere un getto più intenso sulla parte superiore del profilo. Questo fatto migliora le prestazioni del dispositivo (Figure 4.15 e 4.16) fino ad un certo limite per cui la portanza decade per lo stallo troppo intenso sull'estradosso del profilo. I risultati strutturali (Figure 4.17 e 4.18) confermano che accorciare la lunghezza dello spoiler è molto efficacie per l'aumento della rigidezza. La configurazione con la cerniera posizionata a 0.6 della lunghezza della corda è quella ideale dal punto di vista delle prestazioni aerodinamiche e strutturali.

La combinazione di tutti i parametri presentati dovrebbe fornire al progettista gli strumenti per evitare il dannoso fenomeno delle vibrazioni aeroelastiche.

## 6.5 Conclusioni

In questo lavoro è stato studiato il comportamento aeroelastico di un nuovo design di spoiler per migliorare il controllo d'assetto degli aerei: l'*inverted jet spoiler* ideato da Filippone [12].

Inizialmente, sono state effettuate delle analisi strutturali tridimensionali estrapolando le pressioni aerodinamiche dagli articoli di Filippone. I risultati hanno evidenziato che spostamenti e sollecitazioni potrebbero essere tranquillamente trascurati, ad eccezione del caso in cui i carichi fossero sincronizzati con la prima frequenza naturale dello spoiler poiché la risonanza amplifica la deformazione del pannello. Tuttavia, le sollecitazioni strutturali non superano mai il limite di resistenza allo snervamento.

La semplificazione ad un'analisi bidimensionale ha reso possibile lo studio parametrico delle variabili più influenti grazie al ridotto tempo di calcolo. Come intuitivamente si poteva presumere, la velocità del flusso indisturbato aumenta i carichi che agiscono sullo spoiler. Inoltre, la configurazione aerodinamica più critica per la struttura prevede un angolo di attacco di 4°. Anche se non vi è ancora alcun rischio di frattura del materiale, la deformazione dello spoiler è piuttosto grande e probabilmente potrebbero verificarsi vibrazioni aeroelastiche.

Gli spostamenti dello spoiler sono inversamente proporzionali al modulo di elasticità, quindi è possibile impiegare un materiale più rigido per ridurre la deformazione del pannello. Nonostante l'elevato costo, il materiale composito a matrice epossidica rinforzato con fibre di carbonio offre probabilmente il miglior compromesso tra buone proprietà meccaniche e peso ridotto. D'altra parte, è stato dimostrato che la rigidità dello spoiler aumenta riducendo la lunghezza della corda, aumentando lo spessore il pannello e allungando la dimensione della larghezza.

Un'analisi tridimensionale dell'*inverted jet spoiler* è essenziale per catturare le prestazioni realistiche del dispositivo, anche se è numericamente molto costoso. Pertanto, si raccomanda di eseguire una simulazione completa del dispositivo alare per valutare le prestazioni aeroelastiche del sistema. Inoltre, è necessario condurre test sperimentali prima dell'implementazione reale del dispositivo su un aereo per verificare l'ampiezza di eventuali vibrazioni aeroelastiche.

# Nomenclature

$O^B$ : origin of the body-fixed system of reference

$X^B$ : X-axis of the body-fixed system of reference

$Y^B$ : Y-axis of the body-fixed system of reference

$Z^B$ : Z-axis of the body-fixed system of reference

$O^E$ : origin of the Earth-fixed system of reference

$X^E$ : X-axis of the Earth-fixed system of reference

$Y^E$ : Y-axis of the Earth-fixed system of reference

$Z^E$ : Z-axis of the Earth-fixed system of reference

$\mathbf{R}$ : aircraft position vector

$\mathbf{V}$ : aircraft velocity vector

$u$ : component of $\mathbf{V}$ along $X^B$ axis (m/s)

$v$ : component of $\mathbf{V}$ along $Y^B$ axis (m/s)

$w$ : component of $\mathbf{V}$ along $Z^B$ axis (m/s)

$\boldsymbol{\omega}$ : aircraft angular velocity vector

$p$ : component of $\boldsymbol{\omega}$ along $X^B$ axis or roll rate (rad/s)

$q$ : component of $\boldsymbol{\omega}$ along $Y^B$ axis or pitch rate (rad/s)

$r$ : component of $\boldsymbol{\omega}$ along $Z^B$ axis or yaw rate (rad/s)

$\varphi$ : roll angle (rad)

$\theta$ : pitch angle (rad)

$\psi$ : yaw angle (rad)

$\mathbf{F}$ : aerodynamic force produced by the bypass (N)

$\dot{m}$ : flow mass rate inside the channel (kg/s)

$\mathbf{U}^+$ : mean velocity at the upper spoiler extreme (m/s)

$\mathbf{U}^-$ : mean velocity at the lower spoiler extreme (m/s)

c : generic wing chord length at a certain span distance (m)

b : total wing span (m)

Re : number of Reynolds of undisturbed flow

M : number of Mach of undisturbed flow

h : aircraft altitude (m)

$p_\infty$ : free-stream absolute pressure (Pa)

$\rho_\infty$ : free-stream density (kg/m$^3$)

$T_\infty$ : free-stream temperature (°C)

$U_\infty$ : free-stream velocity (m/s)

$p$ : air absolute pressure (Pa)

$y^+$ : dimensionless wall distance

$y$ : normal distance from the wall (m)

$\delta_v$ : viscous length scale (m)

$\nu$ : fluid kinematic viscosity (m$^2$/s)

$\mu$ : fluid dynamic viscosity (Pa·s)

$\rho$ : fluid density (kg/m$^3$)

$U_\tau$ : shear velocity or friction velocity (m/s)

$\tau_w$ : shear stress at the wall (Pa)

$C_f$ : skin-friction coefficient

$\Delta y_1$: first cell height (m)

$L$ : characteristic length (m)

$C_d$ : airfoil drag coefficient

$C_l$ : airfoil lift coefficient

$\alpha$ : angle of attack (°)

$v$ : displacement in Y direction (m)

$M_x$ : bending moment around X axis (N·m)

$E$ : material modulus of elasticity (Pa)

$I_x$ : beam moment of inertia around X axis (kg·m$^2$)

$l$ : chord-wise spoiler length (m)

$t$ : spoiler thickness (m)

$B$ : spoiler span-wise length (m)

# Bibliographic references


1. Sinha, N. and Ananthkrishnan, N. (2017). *Advanced flight dynamics with elements of flight control*. Boca Raton: CRC Press, pp.1-54.
2. Stengel, R. (2004). *Flight dynamics*. Princeton: Princeton University Press, pp.1-234.
3. Filippone, A. (2007). Steep-Descent Maneuver of Transport Aircraft. *Journal of Aircraft*, 44(5), pp.1727-1739.
4. Blake, W. (2002). *Wing Mounted Aircraft Yaw Control Device*. US 6,491,261 B1.
5. Clark, W. (2005). *Aircraft with Forward Opening Inlay Spoilers for Yaw control*. US 6,892,982 B2.
6. Tavella, D., Wood, N., Lee, C., and Roberts, L. (1986). *Two Blowing Concepts for Roll and Lateral Control of Aircraft*. NASA TR CR-1804478.
7. Tavella, D., Lee, C., Wood, N. and Roberts, L. (1987). Jet spoiler as a yaw control device. *Journal of Aircraft*, 24(9), pp.611-615.
8. Cook, M., Buonanno, A. and Erbslöh, S. (2008). A circulation control actuator for flapless flight control. *The Aeronautical Journal*, 112(1134), pp.483-489.
9. Cyrus, J., Kadlec, E. and Klimas, P. (1985). *Jet Spoiler Arrangements for Wind Turbine*. US 4,504,192.
10. McClure, P. (2006). *Passive Jet Spoiler for Yaw Control of an Aircraft*. US 7,143,983 B2.
11. Olcott, J., Seckel, E. and Ellis, D. (1981). *Analysis and flight evaluation of a small fixed-wing aircraft equipped with hinger-plate spoilers*. Technical Report CR-116247. NASA.
12. Filippone, A. (2009). Inverted Jet Spoilers for Aerodynamic Control. *Journal of Aircraft*, 46(4), pp.1240-1252.
13. Filippone, A. and Ferron, G. Jet-powered Spoiler Concept for Flight Control of a Wing. *Personal communication.*
14. Dai, Y. and Yang, C. (2014). Methods and advances in the study of aeroelasticity with uncertainties. *Chinese Journal of Aeronautics*, 27(3), pp.461-474.

15. Dowell, E., Clark, R., Cox, D., Curtiss, H., Edwards, J., Hall, K., Peters, D., Scanlan, R., Simiu, E., Sisto, F. and Strganac, T. (2005). *A Modern Course in Aeroelasticity*. 4th ed. Dordrecht: Springer Science + Business Media, Inc., pp.1-2.
16. Turbmodels.larc.nasa.gov. (2019). *3D ONERA M6 Wing Validation for Turbulence Model Numerical Analysis*. [online] Available at: https://turbmodels.larc.nasa.gov/onerawingnumerics_val.html [Accessed 11 Mar. 2019].
17. Eswara Prasad, N. and Wanhill, R. (2017). *Aerospace Materials and Material Technologies. Volume 1: Aerospace Materials*. Singapore: Springer, pp.1-367.
18. Colakoglu, M. (2004). Factors effecting internal damping in aluminum. *Journal of theoretical and applied mechanics*, 42(1), pp. 95-105.
19. Athadkar, M. and Desai, S. (2014). Importance of the extent of far-field boundaries and of the grid topology in the CFD simulation of external flows. *International Journal of Mechanical and Production Engineering*, 2(9), pp. 69-72.
20. *ANSYS FLUENT Theory Guide*. Release 14.0 (2011), pp. 68, 119-121.
21. J. D. Anderson (2011). *Fundamentals of Aerodynamics*. 5th ed. New York: McGraw-Hill.
22. Eswara Prasad, N. and Wanhill, R. (2017). *Aerospace Materials and Material Technologies. Volume 2: Aerospace Material Technologies*. Singapore: Springer, pp.143-183.
23. Matweb.com. (2019). *Online Materials Information Resource - MatWeb*. [online] Available at: http://www.matweb.com/ [Accessed 12 Aug. 2019].
24. DeLacy, T. (1985). *Method and Apparatus for Non-Destructive Testing of Composite Materials*. US 4,494,408.
25. Gholizadeh, S. (2016). A review of non-destructive testing methods of composite materials. *Procedia Structural Integrity*, 1, pp.50-57.
26. Garnier, C., Pastor, M., Eyma, F. and Lorrain, B. (2011). The detection of aeronautical defects in situ on composite structures using Non Destructive Testing. *Composite Structures*, 93(5), pp.1328-1336.
27. Nayak, N. V. (2014). Composite Materials in Aerospace Applications. *International Journal of Scientific and Research Publications*, 4(9), pp.1-10.

28. Botelho, E., Silva, R., Pardini, L. and Rezende, M. (2006). A review on the development and properties of continuous fiber/epoxy/aluminum hybrid composites for aircraft structures. *Materials Research*, 9(3), pp.247-256.
29. Wu, G. and Yang, J. (2005). The mechanical behavior of GLARE laminates for aircraft structures. *JOM*, 57(1), pp.72-79.